

CHALMERS

Chalmers University of Technology, Sweden



Lafarge Research Center
Microstructuration Group



<< **Materials and Nanotechnology Master Program** >>

2009-2011

Master Thesis

Formulation, Deposition and Characterization of surface properties of organic coatings

Author : I. Sotiriou

Supervisor: Matthieu Horgnies
Examiner: Professor Anders Palmqvist

Abstract

In this study, an attempt was made to deposit coatings consisting of organics and carbonates/minerals, on a substrate of Ultra High Performance Concrete (UHPC) with different deposition methods in order to find the appropriate one. The methods used were dip coating, spin coating, and storage in bath. Beyond chitosan, various other organics were used, like alginate, carrageenan, fatty acids, and carboxymethylcellulose. The insoluble organic molecules were used as a substrate for CaCO_3 crystallization under a choice of conditions correlated with the control of the reaction. Na_2CO_3 and CaCl_2 were provided as inorganic soluble carbonates to induce crystallization. Different characterization methods were used to analyze the microstructure, mechanical and surface properties of the coatings. Concerning the surface properties, the properties of hydrophobicity or superhydrophobicity were especially researched. The combination of SEM observation and investigations by XRD on the precipitated crystals showed that the deposition of organo/mineral coatings on the UHPC substrate could form a homogeneous layer, with remarkable surface properties.

Key words: CaCO_3 polymorphs; crystallization; organic coatings; microstructure surface

CONTENTS

	List of Figures.....	5
	List of Tables.....	9
1	Introduction.....	10
2	Bibliographic Review: super-hydrophobic performances induced by different techniques of surface functionalization.....	11
	2.1. Introduction: from biomimetic to artificial functionalization.....	11
	2.2. Theory of super-hydrophobicity.....	13
	2.3. Techniques and Examples.....	14
	2.3.1. Lithography.....	14
	2.3.2. Electro-deposition.....	17
	2.3.3. Chemical deposition.....	19
	2.3.4. Layer-by-Layer.....	21
	2.3.5. Plasma deposition.....	26
	2.3.6. UV-curing.....	28
	2.4. Superhydrophobicity according to the texture.....	30
	2.5. Durable superhydrophobic surfaces.....	32
	2.6. Conclusions.....	33
	2.7. References.....	34
3	Materials and Models.....	37
	3.1. Organics.....	37
	3.2. Carbonates used in this study.....	42
	3.3. Substrate – Ultra High Performance Concrete (UHPC).....	42
	3.4. Solutions made of organics and carbonates.....	43
	3.5. Models of natural resistant microstructures based on CaCO₃.	
	Mussels-Nacre.....	44
4	Methodologies of deposition of organic coatings.....	46
	4.1. Deposition of layers made of organics and additives.....	46
	4.1.1. Dip-coating method.....	46
	4.1.2. Spin-coating method.....	48
	4.1.3. Storage in bath.....	49

	4.2. Control of crystallization of CaCO₃.....	49
	4.2.1. Dip-coating of organic/carbonate layers.....	50
5	Characterization of the microstructure and surface properties of the coatings (SEM, WCA, XRD, Scratching, Sorptivity).....	53
	5.1. Deposition of layers made of organics and additives.....	53
	5.1.1. Dip-coating method.....	53
	5.1.2. Spin-coating method.....	68
	5.1.3. Storage in bath.....	70
	5.2. Control of the crystallization of CaCO₃.....	77
	5.2.1. Dip-coating of organic/carbonate layers.....	77
	5.3. Use of substrate made of ordinary concrete and plaster.....	87
6	Discussion.....	88
7	Conclusions.....	90
8	References.....	91

List of Figures

2.1.1 (a) SEM micrographs (shown at three magnifications) of lotus (*N. nucifera*) leaf surface, which consists of microstructure formed by papillose epidermal cells covered with epicuticular and nanostructured wax tubules (Bhushan et al.) and (b) image of water droplet sitting on the lotus leaf.

2.2.1 Experimental results of the Kao group (from [1]). The cosine of the effective contact angle of a water drop is measured as a function of the cosine of the Young angle (determined on a flat surface of the same material and varied using different liquids). The results are obtained on hydrophobic ($\cos \theta$) and hydrophilic ($\cos \theta$) situations. In both cases, the roughness is found to affect dramatically the contact angle, but differently.

2.2.2 The two superhydrophobic states: in the Wenzel state (a), the liquid follows the solid surface. In the Cassie state (b), it only contacts the top of the asperities, leaving air below.

2.3.1 SEM images (60°) of the size-reduced polystyrene beads and the water contact angle measurement on the corresponding modified surfaces (insets). The diameters of polystyrene beads and water contact angles on these surfaces were measured to be (a) 400 nm, 135° , (b) 360 nm, 144° , (c) 330 nm, 152° , and (d) 190 nm, 168° . Bar: $1 \mu\text{m}$.

2.3.2 SEM image of a 440-nm-diameter double-layer polystyrene surface after 120 s of oxygen plasma treatment. Bar: $1 \mu\text{m}$. (Left inset). The side-view illustration of the shape modification for double layer arrays before and after the oxygen plasma treatment (Right inset). The water contact angle on the corresponding modified surface was measured to be 170° .

2.3.3 Diagram calculated with the data of Jau-Ye Shiu et al.

2.3.4 (a-h) SEM photographs of micro-structured water repellent surfaces: (a, b) silicon chips with regular patterns of spikes, (c) copper foil Cu-1, (d) copper foil Cu-2, (e) aluminum foil Al-1, (f) replicate of *Alocasia*, (g) replicate of *Rosa*, and replicate of *Nelumbo*.

2.3.5 Scanning electron micrographs of combination rough-smooth-textured surfaces. A) Smooth photo-resist pillars on smooth copper base surfaces. B) Rough copper pillars on smooth copper base surfaces. C) Smooth photo-resist pillars on rough copper base surfaces. C) Smooth SU-8 pillars on rough copper, the water contact angle on these combined surfaces was increased for $136 (\pm 3)^\circ$ on the copper, $130 (\pm 3)^\circ$ on the SU-8 to $146 (\pm 3)^\circ$, close to the angle where very high pillars of this size and separation reach a maximum contact angle. The electron micrographs were taken at an angle of 45° to emphasize roughness.

2.3.6 A) Scanning electron micrograph of electrodeposited copper. B) Drop of water on surface A, contact angle $136 (\pm 3)^\circ$. C) Scanning electron micrograph of electrodeposited copper ‘chocolate chip cookies’. D) Drop of water on surface C, contact angle $160 (\pm 3)^\circ$. The electron micrographs were taken at an angle of 45° to emphasize roughness.

2.3.7 Preparation of superhydrophobic films based on raspberry-like particles.

2.3.8 Rhodorsil-particle films deposited on glass. The concentrations (w/v) of the SiO_2 nanoparticles in the dispersions (deposited on the glass surfaces) are shown in the upper right corner of each image.

2.3.9 SEM micrographs taken at 45° tilt angle, show three magnifications of (a) nano and hierarchical structures fabricated with CNTs after 3 h at 120°C .

2.3.10 (A) SEM image of the fully treated structure B with silica nanoparticles. (B) Water droplet on this superhydrophobic surface.

2.3.11 Schematic illustration for creating microsphere-patterned polyimide films.

2.3.12 SEM images of hierarchical structures composed of microspheres and $[(\text{PAH}/\text{PAA})(\text{PAH}/\text{SiO}_2)_3]_n$ films: (a, b) $n = 1$, (c) $n = 3$, and (d) $n = 5$.

2.3.13 SEM images of carbon nanotube forests. (a) As-grown forest prepared by PECVD with nanotube diameter of 50 nm and a height of 2 μm , (b) PTFE-coated forest after HFCVD treatment, and (c) an essentially spherical water droplet suspended on PTFE-coated forest.

2.3.14 ESEM image of an as-grown forest without PTFE treatment, after exposure to water, showing the nanotubes bundling together because of the attractive capillary forces that arise during evaporative drying.

2.3.15 SEM images of the PET surfaces treated with oxygen plasma at various RF powers: (a) untreated, (b) 50 W, (c) 100 W and (d) 200 W (the treatment time was fixed at 10 min).

2.3.16 A schematic illustration of the procedure for creating a lotus-leaf-like PFPE-SS structure.

2.3.17 (A) Top view and (B) 30° angle oblique view FE-SEM images of a p-AAO membrane template anodized for 20 min at 180 V. (C) FE-SEM images of a PFPE-SS nanopillar film peeled from the p-AAO membrane. The inset is a water droplet, with an extremely high static contact angle, sitting on the PFPE-SS nanopillars.

3.1.1 Chitosan structure.

3.1.2 Alginate monomer (a) and chain (b) conformation.

3.1.3 Structural unit of carrageenan.

3.1.4 Structural unit of stearic acid.

3.1.5 Na-CMC structure.

3.5.1 Morphology of Abalone Nacre consisting of aragonite crystals (Wang et al. (2001) and combines with organic interlayer to induce high mechanical strength (Aksay et al.)

3.5.2 Structure of a mussel from Isère Lake.

4.1.1 Different steps followed during the dip-coating method: (a) pour the organic solution in a Tupperware, (b) soak a few seconds the substrate and (c) dry horizontally.

4.2.1 Methodology of coating the UHPC substrate with the aim to control the crystallization, either by direct dip-coating of the organics/carbonates and or by dip-coating of organic/carbonates followed by placement in carbonated aqueous solution.

5.1.1 View of UHPC surface after deposition of coating.

5.1.2 View of UHPC surface after deposition of coating.

5.1.3 View of UHPC surface after deposition of coating.

5.1.4 View of UHPC surface after deposition of coating.

5.1.5 SEM images of the surface of coating (a) and (b) and cross-section (c) and (d) of a 7% chitosan 652 + 2% citric acid + 4% CR₂ + 4% additive MN.

5.1.6 View of UHPC surface after deposition of coating.

5.1.7 SEM images of the surface of coating and of a 7% chitosan 652 + 2% citric acid + 4% CR₃ + 4% additive MN in H₂O deposited solution.

5.1.8 View of UHPC surface after deposition of coating.

5.1.9 SEM images of the surface of coating and of a 7% chitosan 652 + 2% citric acid + 4% CR₂ + 4% additive MN₁ in H₂O.

5.1.10 Virtual description of the sorptivity measurement process.

5.1.11 Surface absorption of UHPC sample with 7% chitosan 652 + 2% citric acid + 4% CR₂ + 4% additive MN coating film as a function of time.

5.1.12 Surface absorption of UHPC sample with 7% chitosan 652 + 2% citric acid + 2% CR₃ + 4% additive MN coating film as a function of time.

5.1.13 Three balls test on disk (integral in the graph image) of a reference UHPC (left up), a treated with chitosan 652, CR₂ and additive MN UHPC substrate (left middle) and a treated with chitosan 652, CR₃ and additive MN (left down). The graph shows the behaviour of each coated UHPC substrate in comparison with the reference one.

5.1.14 Scratching tests that were applied in the best of our samples 7% chitosan 652 + 2% citric acid + 2% CR₃ + 4% additive MN in water (a) and in 7% chitosan 652 + 2% citric acid + 4% CR₂ + 4% additive MN in water (b).

5.1.15 SEM images of the surface of coating and of a 7% chitosan 652 + 2% citric acid + 5% CR₂ in H₂O spin coated solution.

5.1.16 SEM images of the surface of coating and of a 7% chitosan 652 + 2% citric acid + 2% CR₃ + 4% additives MN in H₂O spin-coated solution.

5.1.17 SEM images of the surface of coating and of a 7% chitosan 652 + 2% citric acid + 5% CR₁ in H₂O spin-coated solution.

5.1.18 View of UHPC surface after deposition of coating.

5.1.19 View of UHPC surface after deposition of coating (a) and after drying for 24h (b).

5.1.20 View of UHPC surface after deposition of coating (a) and after drying for 24h (b).

5.1.21 View of UHPC surface after deposition of coating.

5.1.22 View of UHPC surface after deposition of coating (a) and after drying for 24h (b).

5.1.23 SEM images of the surface of coating (a) and (b) and cross-section (c) and (d) of a 7% chitosan 652 + 2% citric acid + 4% CR₂ + 4% additive MN in H₂O.

5.1.24 View of UHPC surface after deposition of coating (a) and after drying for 24h (b).

5.1.25 SEM images of the surface of coating (a) and (b) and cross-section (c) and (d) of a 7% chitosan 652 + 2% citric acid + 2% CR₃ + 4% additive MN in H₂O.

5.1.26 View of UHPC surface after deposition of coating (a) and after drying for 24h (b).

5.1.27 View of UHPC surface after deposition of coating (a) and after drying for 24h (b).

5.2.1 SEM images of the surface of coating (a) and (b), and cross-section (c) and (d) of a 1% chitosan 652 + 1% citric acid + (10% CaCl₂ + 10% Na₂CO₃) in H₂O.

5.2.2 SEM images of the surface of coating (a) and (b) and cross-section (c) and (d) of a 1% chitosan 652 + 1% citric acid + (10% CaCl₂ + 10% Na₂CO₃) (*2) in H₂O.

5.2.3 SEM image of cross-section of the coating from 7% chitosan 652 + 1% acetic acid.

5.2.4 SEM images of the surface of coating (a) and (b) and cross-section (c) and (d) of a 1% alginate in H₂O + (10% Na₂CO₃ + 10% CaCl₂) in H₂O.

5.2.5 XRD results of the coating made by 1% alginate in H₂O + (10% Na₂CO₃ + 10% CaCl₂).

5.2.6 SEM images of the surface of coating (a) and (b) and cross-section (c) and (d) of a 1% carrageenan in H₂O + (10% Na₂CO₃ + 10% CaCl₂) in H₂O.

5.2.7 XRD results of the coating made by 1% carrageenan in H₂O + (10% Na₂CO₃ + 10% CaCl₂).

5.2.8 SEM images of the surface of coating (a) and (b) and cross-section (c) and (d) of a 1% stearic acid in hexane + (10% CaCl₂ + 10% Na₂CO₃) in H₂O deposited solution.

5.2.9 SEM images of the surface of coating (a) and (b) and cross-section (c) and (d) of a 1% carboxymethylcellulose in H₂O + (10% CaCl₂ + 10% Na₂CO₃) in H₂O.

5.3.1 Dip-coating of chitosan 652 + 1% acetic acid on plaster and ordinary concrete in different chitosan 652 concentrations: (a) and (c) 1% chitosan while (b) and (d) 7% chitosan .

List of Tables

2.4.1 Summary of the water contact angles measured in the reports according to the texture of the surfaces for the variety of the techniques applied.

4.1.1 Summary of the solutions prepared for dip-coating method which consist of chitosan 652, citric acid and carbonates individually or in combination with additives MN.

4.1.2 Summary of the solutions prepared for spin-coating method, which consist of chitosan 652, citric acid, and carbonates individually, or in combination with additives MN.

4.1.3 Summary of the solutions prepared for storage in bath which consist of chitosan 652, citric acid and carbonates individually or in combination with additives MN.

5.1.1 Mass measurements after each dip-coating and percentage of average mass uptake.

5.1.2 Results of the surface absorption measurements for the UHPC sample with 7% chitosan 652 + 2% citric acid + 4% CR₂ + 4% additives MN coating film.

5.1.3 Results of the surface absorption measurements of the UHPC sample with 7% chitosan 652 + 2% citric acid + 2% CR₃ + 4% additives MN coating film.

5.1.4 Results of the WCA measurements of the UHPC sample with 7% chitosan 652 + 2% citric acid + 2% CR₃ + 4% additives MN coating film.

5.2.1 Summary of the properties of each coating related with the WCA results.



1 Introduction

Natural biomineralization products have been the focus of materials scientists because of their unique properties. Many experiments have been designed and carried out to achieve possible mechanisms for the formation of natural biominerals (mussel, sea-urchin, abalone, etc.). These biological organisms produce organic-inorganic materials such as shell, bone, and pearl. Moreover, the biological materials have organic macromolecules, which influence the nucleation and growth of inorganic compounds such as CaCO_3 because of their reactive functional groups, such as carboxylate groups ^[1-6]. CaCO_3 can exist in six different forms, of which the three major, in order of decreasing stability, are calcite, aragonite, and vaterite ^[7]. Two hydrated crystalline forms and an amorphous form of CaCO_3 (ACC) also exist, but they are generally unstable and they are transformed into the calcite, aragonite, or vaterite polymorphs. The inorganic-organic interface is usually the precursor of the biomineralization process where the organic part provides the information for the inorganic nucleation ^[8-12].

The layered structures, as the one of nacre, depend on the interaction between insoluble organic matrixes as substrates and soluble inorganic matrixes, which can promote heterogeneous nucleation. Natural organic materials such as chitosan ^[13-15], carboxymethyl chitosan ^[16], xanthan ^[17], sodium stearate ^[18] and even polymers such as polymethyl methacrylate (PMMA) ^[19] used as insoluble organic matrixes and acidic macromolecules such as polyacrylic acid (PAA) ^[20] or polyglutamic acid (PGA) ^[21] were used as soluble inorganic matrixes.

Some natural biomaterials are known for their noticeable mechanical properties, difficult to reproduce in a conventional way. Nacre, as mentioned, is a layer composite consisting of highly organized aragonite platelet layers, with a thickness from 0.2 to 0.8 μm , separated by layers of organic molecules like proteins and polysaccharides ^[22].

A bibliographic review related to superhydrophobicity and the techniques for its induction has been pursued. It involves a brief description of a series of publications associated with different techniques of artificial surface functionalization, with the aim to mimic natural surfaces and to future introduction of them to our project. In the case of the organic coatings, the report comprises the explanation of the materials that were used and the natural models that this project is based on. Additionally, the methodologies that followed for the deposition of the coatings were depicted as well as the characterization of the microstructure and the surface properties of the coatings.

2 Bibliographic review: super-hydrophobic performances induced by different techniques of surface functionalization

2.1 Introduction: from biomimetic to artificial functionalization

During the last decades, there has been a rapid increase in research for superhydrophobic surfaces, based on imitation of already known surfaces from the nature. Micro- nanomaterials and devices can be manufactured by mimicking objects and processes found in nature with specific functions and properties. The advantage of mimicking the biomaterials is that they can be highly organized from the molecular to the nano-, micro- and the macro-scale. Furthermore, such surfaces can be combined to form hierarchical structures resulting in millions of different elements. Additionally, a combination of physico-chemical properties with the morphology can lead to high performance surfaces. As a result, properties like superhydrophobicity, self-cleaning, high adhesion, drag reduction in fluid flow, energy conversion, biologically self-assembly and self-healing can be achieved.

A very well known term related with superhydrophobicity is the “lotus effect”. This term refers to the water repellent leaves of the lotus plant (*Nelumbo nucifera*). Due to their diversity in the structure and morphology, the leaves provide multifunctional properties. They consist of three-dimensional epicuticular waxes and cuticular folding which are able to create a double structure, like hierarchical structures such as tubules. The papillose epidermal cells form asperities that will provide roughness on the surface. They are covered by the three-dimensional epicuticular waxes, which will finally lead to the formation of the hierarchical structures with hydrophobic properties. The main concept is that the water droplets sit on the apex of the wax asperities nanostructures due to the air, which is trapped in the valley between the water bubble and the surface. This means that the plants finally exhibit superhydrophobicity (Figure 2.1.1(a)) ^[23].

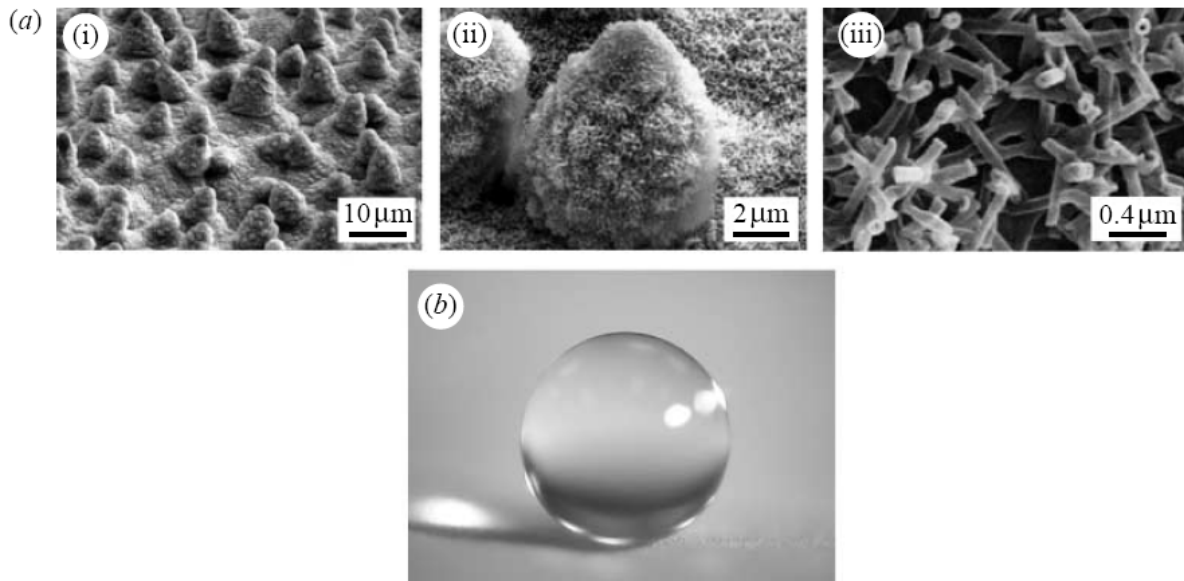


Figure 2.1.1 (a) SEM micrographs (shown at three magnifications) of lotus (*N. nucifera*) leaf surface, which consists of microstructure formed by papillose epidermal cells covered with epicuticular and nanostructured wax tubules (Bhushan et al.) and (b) image of water droplet sitting on the lotus leaf. ^[23]

In the case of the lotus leaf, the water contact angle reaches a value of 164° contact angle (WCA) and 3° water contact angle hysteresis (WCAH) (Figure 2.1.1(b)) ^[23]. As a result, when the water droplets roll off the surface of the leaves, they remove any contaminants from them, leading to self-cleaning. Roughness induced superhydrophobic and self-cleaning surfaces are important in various applications such as self-cleaning windows, exterior paints for buildings, textiles, solar panels and applications requiring antifouling and reduction of drag in fluid flow.

To achieve superhydrophobic surfaces, it is necessary to use already known techniques that have been used for the fabrication of micro- and nano-structure. Techniques such as etching, nanolithography, self-assembly, and deposition give the opportunity to enhance the superhydrophobic properties (maximum water contact angle $> 140^\circ$, hysteresis $< 10^\circ$).

There are two main requirements to obtain a superhydrophobic surface. First, the surface must be homogeneously structured, and, second, it should be covered by chemicals intrinsically hydrophobic (low surface energy, water contact angle $\geq 90^\circ$). Furthermore, different ways exist to achieve such properties individually or by combining two techniques. The goal in the future, which correlates the bibliographic review with the project, is the introduction of a series of organics (ex. chitosan) to enhance the hydrophobic/superhydrophobic effect.

2.2 Theory of super-hydrophobicity

As mentioned above, a surface could become superhydrophobic either by increasing its roughness if it is already hydrophobic ($\theta > 90^\circ$) or by lowering the surface energy. Shibushi et al. from the Kao Corporation made a series of experiments showing how texturing a surface modifies the contact angle, as a function of the chemical wettability of the solid (Figure 2.2.1) [24]. The effect of roughness is determined by comparing the apparent contact angle θ^* on a rough surface, with the Young contact angle on a flat surface of the same chemical composition.

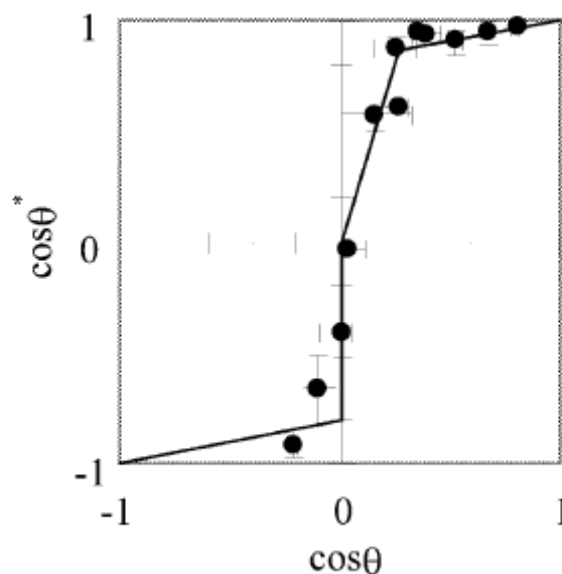


Figure 2.2.1 Experimental results of the Kao group (from [1]). The cosine of the effective contact angle of a water drop is measured as a function of the cosine of the Young angle (determined on a flat surface of the same material and varied using different liquids). The results are obtained on hydrophobic and hydrophilic situations. In both cases, the roughness is found to affect dramatically the contact angle, but differently. [24]

As obtained from the diagram, when the contact angle on a flat surface has a value of less than 90° , it is hydrophilic, the increase of the roughness induces a decrease in the apparent contact angle. On the other hand, the area, which we are focusing on in this report, is the area with an apparent contact angle higher than 140° induced by an increase in the roughness of a hydrophobic surface ($\theta > 90^\circ$).

There are two possible origins for the effect of superhydrophobicity: either the liquid follows the solid surface, or air flows inside the texture. In the first case (Wenzel state) (Figure 2.2.2(a)) [25] the solid roughness r , defined as the ratio between the true surface area over the apparent one, ($r > 1$), is responsible for the contact angle value θ^* and improves the

natural hydrophobicity of the material. Thus, the solid surface energy can be seen as multiplied by the factor r , which yields:

$$\cos \theta^* = r \cos \theta,$$

where θ is the Young contact angle, fixed by the chemical nature of the solid, liquid and vapor. Thus, the contact angle of hydrophobic materials will increase with increasing surface roughness.

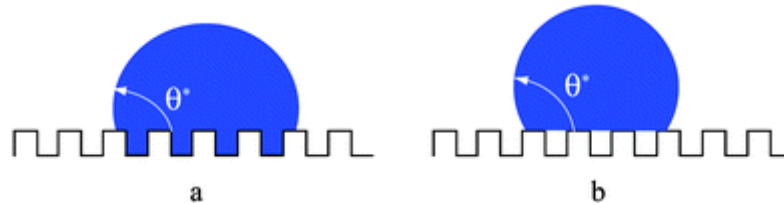


Figure 2.2.2 The two superhydrophobic states: in the Wenzel state (a), the liquid follows the solid surface. In the Cassie state (b), it only contacts the top of the asperities, leaving air below. ^[25]

In the case of Cassie state (as we mentioned above for the lotus leaf) (Figure 2.2.2(b)) ^[25] the only area of the solid, which meets the water droplet, is the top of the asperities, on a fraction that is denoted by ϕ_s . The area between the water droplet and the surface, which is not in contact with it, is filled by air. As a result, the smaller the ϕ_s , the closer the contact angle is to the value of 180° , thus the higher the hydrophobicity. The equation showing this condition is:

$$\cos \theta^* = -1 + \phi_s (\cos \theta + 1)$$

The conclusion that emerges from the above is that the surface energy can be lowered if air can be trapped below the drop.

2.3 Techniques and Examples

2.3.1 Lithography

Lithography is a well-known technique for the formation of superhydrophobic surfaces. It can be used to form one level structures (nano- or microstructure) or hierarchical structures. It includes several branched techniques like X-ray, nanosphere lithography, E-beam and soft lithography. Jau-Ye Shiu et al. ^[26] fabricated well-ordered tunable superhydrophobic surfaces by nanosphere lithography. First, by spin-coating mono-dispersed polystyrene beads solution on substrate surfaces, self-organized closed-packed nanostructures can be easily achieved. By oxygen plasma etching, the nano-structured

surfaces can change their liquid-solid fraction and reduce the diameter of the polystyrene beads. The size reduced polystyrene beads are then coated with a 20-nm-thick gold film and modified with octadecanethiol. The contact angles of the surface measured, changed from 132° to 168° with a beads diameter of 190 nm. The time of the oxygen plasma treatment affects the water contact angle. The highest contact angle measured was 170° with a 440-nm beads diameter in a double layer polystyrene surface. Figures 2.3.1 and 2.3.2 show the SEM observations of both the one layer and the double layer samples. Figure 2.3.3 summarizes the contact angles measured as a function of the beads diameter.

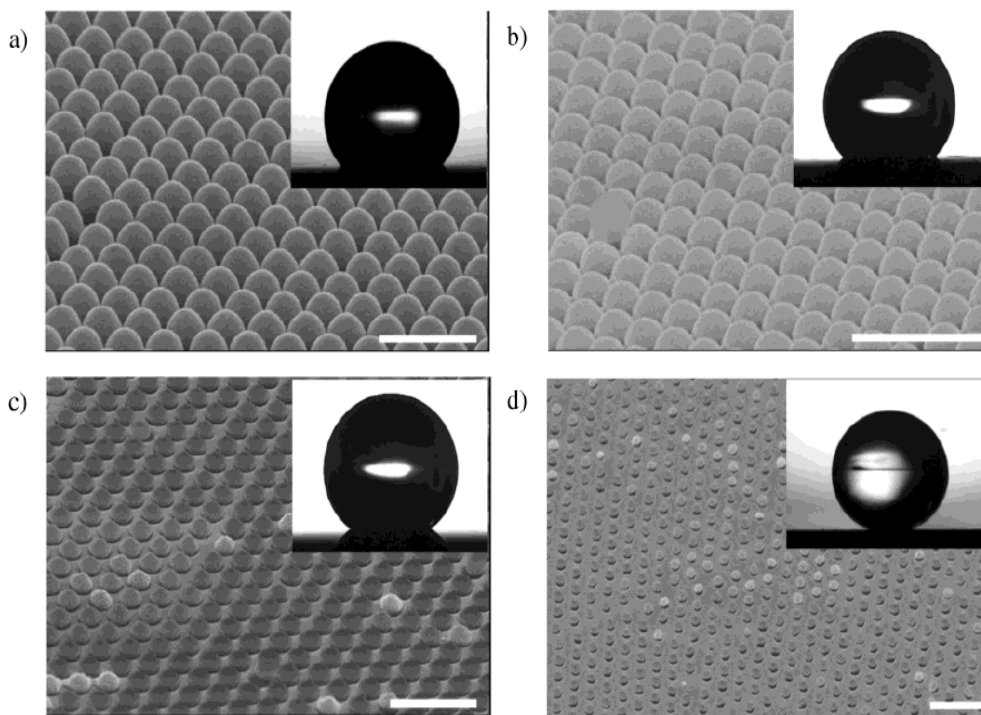


Figure 2.3.1 SEM images (60°) of the size-reduced polystyrene beads and the water contact angle measurement on the corresponding modified surfaces (insets). The diameters of polystyrene beads and water contact angles on these surfaces were measured to be (a) 400 nm, 135°, (b) 360 nm, 144°, (c) 330 nm, 152°, and (d) 190 nm, 168°. Bar: 1 μm .^[26]

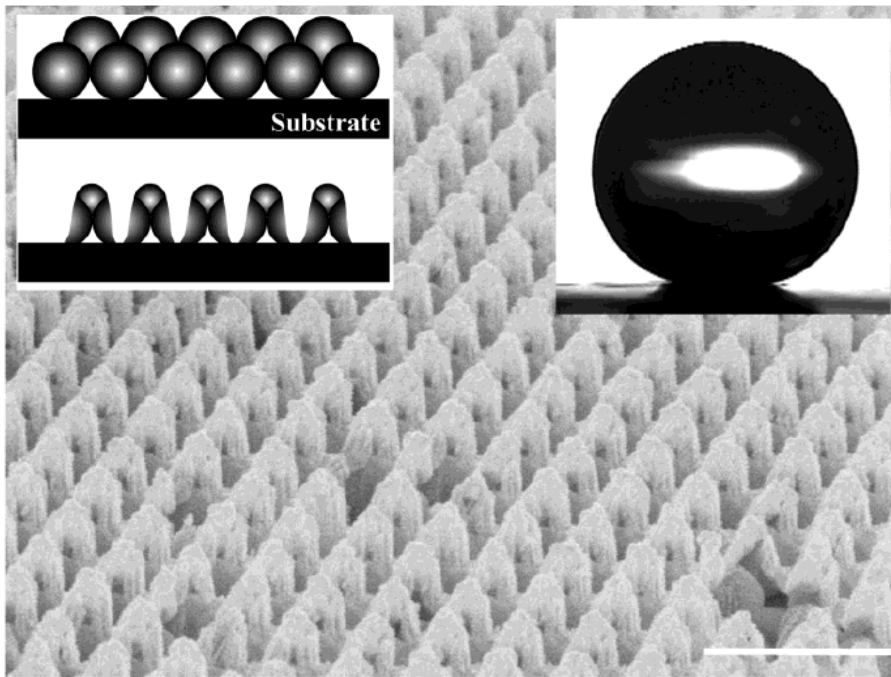


Figure 2.3.2 SEM image of a 440-nm-diameter double-layer polystyrene surface after 120 s of oxygen plasma treatment. Bar: 1 μm . (Left inset) The side-view illustration of the shape modification for double layer arrays before and after the oxygen plasma treatment. (Right inset) The water contact angle on the corresponding modified surface was measured to be 170°. [26]

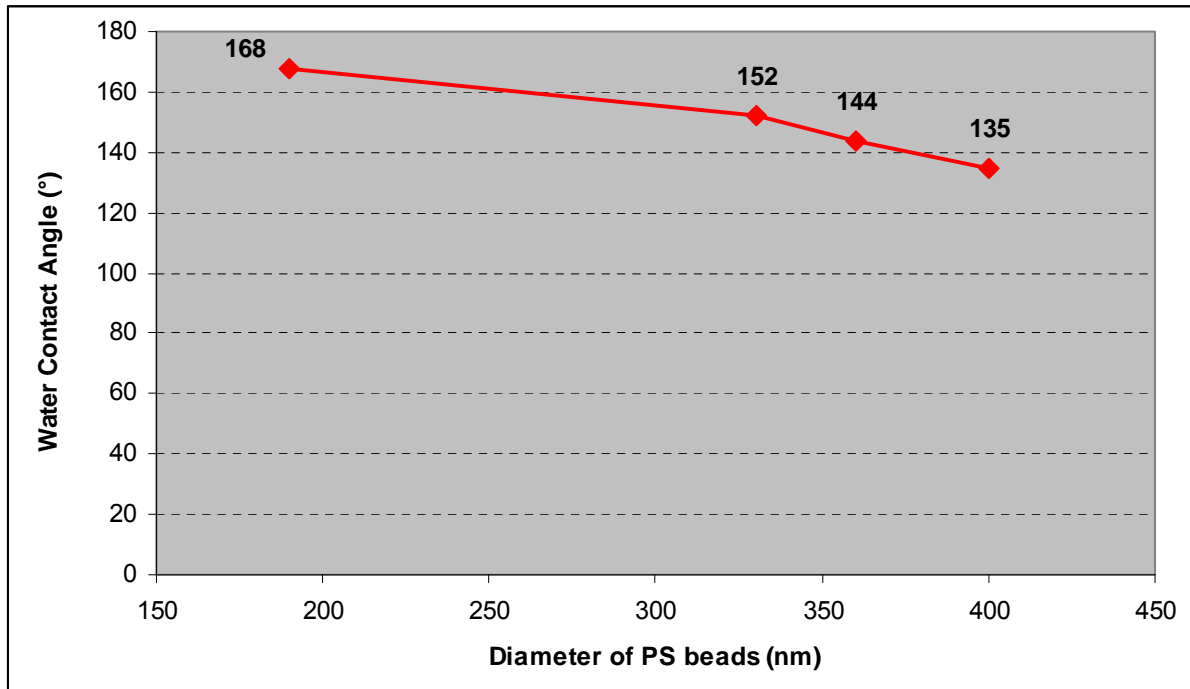


Figure 2.3.3 Diagram calculated with the data of Jau-Ye Shiu et al. [26].

In a second case of lithography technique, Furstner et al. [27] tried to define the wetting and self-cleaning properties of artificial superhydrophobic surfaces by texturing 3 types of

surfaces with different chemical composition. Such surfaces are silicon wafer specimens with different regular arrays of spikes, replicates of water-repellent leaves and commercially available metal foils normally used for printed electronic circuits or condensers. In the case of silicon wafers, pillars with 1 μm diameter, 4 μm pillar high and 3 μm pitches were fabricated and further modified by chemical treatment. The contact angle measured 166° and the contact angle hysteresis 3°. The replicates of Alocasia, Rosa and Nelumbo leaves manufactured with a scale-like roughness (in the range of 1-3 μm) and modified chemically by two-component silicon moulding mass were applied onto them.

The highest contact angle measured in the case of Nelumbo replicate was 157.8° and the contact angle hysteresis was 7.9°. Finally, the metal foils with a surface structure of 3 μm (designated with Cu-2) showed a contact angle of 168° and contact angle hysteresis equal to 0.5°. Figure 2.3.4 shows the SEM observation of the 3 different types of surfaces.

As obtained in both of the above experiments, the lithography technique can be used as the primary technique and combined with another one, either with oxygen plasma etching or with chemical treatment (deposition), to obtain the best result. Thus, both the roughness and the chemical modification are important factors to obtain superhydrophobic surfaces.

2.3.2 *Electro-deposition*

The deposition is also an important technique, which leads to superhydrophobic surfaces and includes for example the electro-deposition and the immersion into solutions. Shirtcliffe et al. [28] fabricated a dual scale roughness surface, which produces unusually water-repellent surfaces. The surface structure comprised of pillars with 15 μm diameter, 2 μm height and 15 μm pitch. The process includes electro-deposition of copper from acidic copper sulfate solution onto flat copper to create surfaces of varying levels of roughness. The deposited layers of copper were coated with a fluorocarbon hydrophobic layer. The contact angle measured 165°. Surfaces with different structures can be created (Figure 2.3.5) until they reach the best one, which is that of rough copper pillars on rough copper surfaces (Figure 2.3.6).

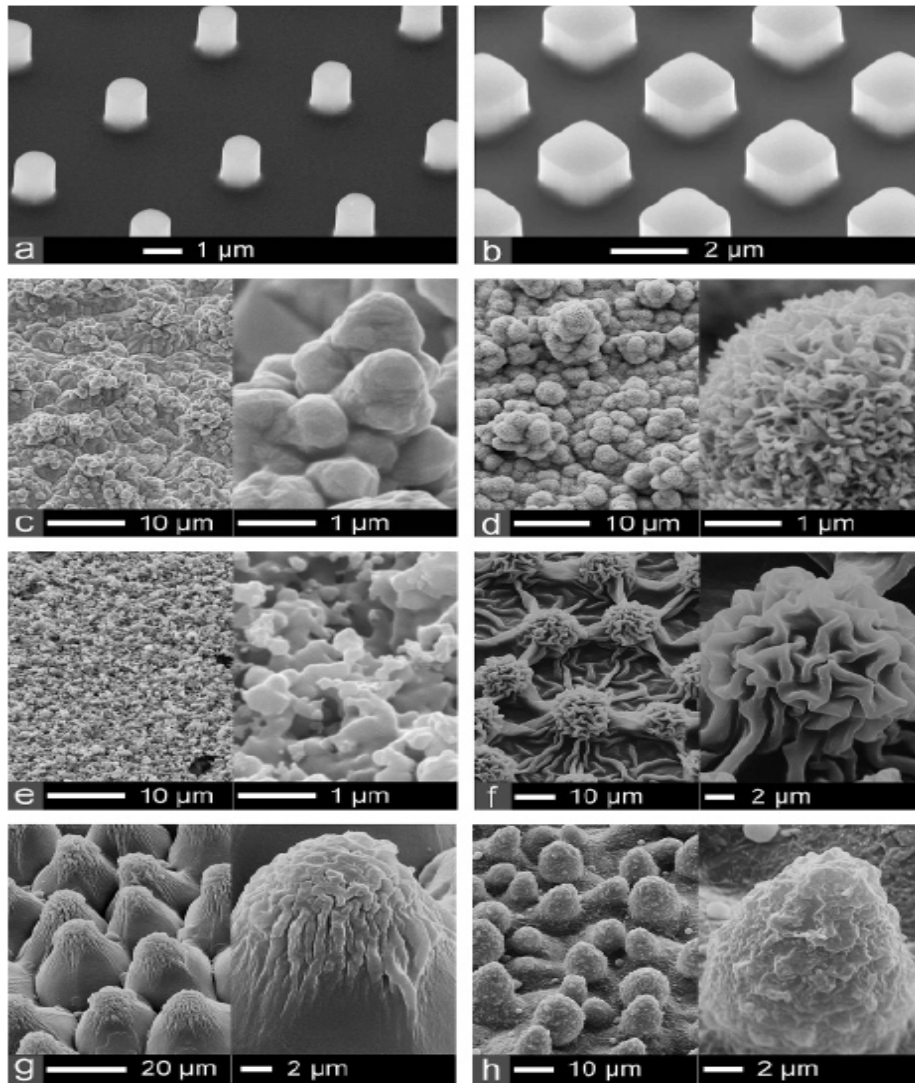


Figure 2.3.4 (a-h) SEM photographs of micro-structured water repellent surfaces: (a, b) silicon wafers with regular patterns of spikes, (c) copper foil Cu-1, (d) copper foil Cu-2, (e) aluminum foil Al-1, (f) replicate of Alocasia, (g) replicate of Rosa, and replicate of Nelumbo. ^[27]

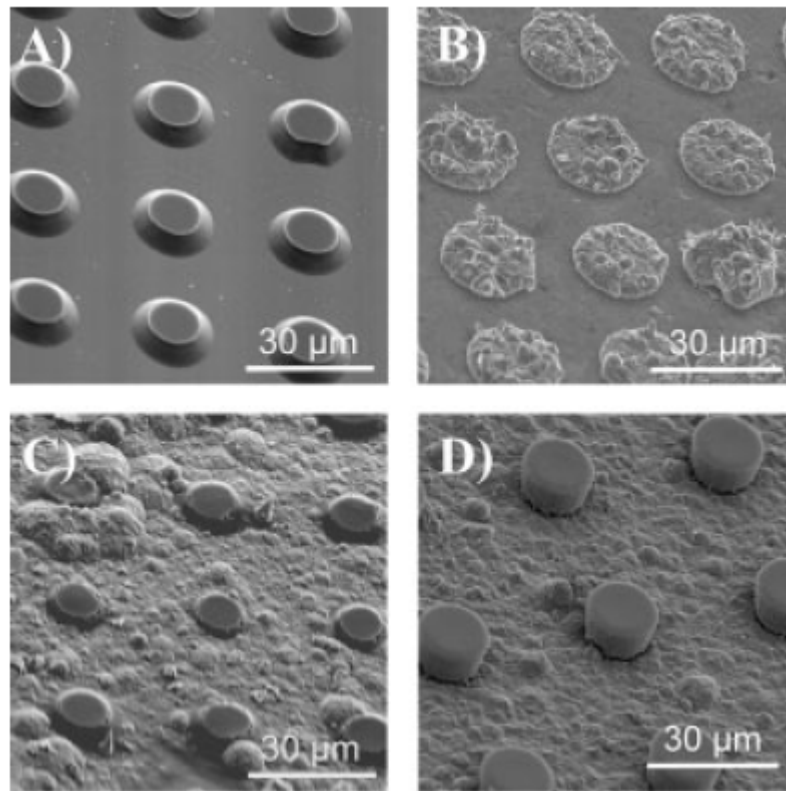


Figure 2.3.5 Scanning electron micrographs of combination of rough-smooth-textured surfaces. A) Smooth photo-resist pillars on smooth copper base surfaces. B) Rough copper pillars on smooth copper base surfaces. C) Smooth photo-resist pillars on rough copper base surfaces. C) Smooth SU-8 pillars on rough copper, the water contact angle on these combined surfaces was increased for $136 (\pm 3)^\circ$ on the copper, $130 (\pm 3)^\circ$ on the SU-8 to $146 (\pm 3)^\circ$, close to the angle where very high pillars of this size and separation reach a maximum contact angle. The electron micrographs were taken at an angle of 45° to emphasize roughness. ^[28]

2.3.3 Chemical deposition

W. Ming et al. ^[29] mimicked the raspberry structure of particles to form superhydrophobic surfaces. A cross-linked film based on an epoxy-amine system was prepared with unreacted epoxy groups, which were then grafted by amine-surface-functionalized raspberry-like silica particles (Figure 2.3.7). At the end, a layer of monoepoxy-end-capped PDMS (Poly-DiMethylSiloxane) was grafted onto the particles to induce hydrophobicity with a contact angle of 165° and contact angle hysteresis of 2° .

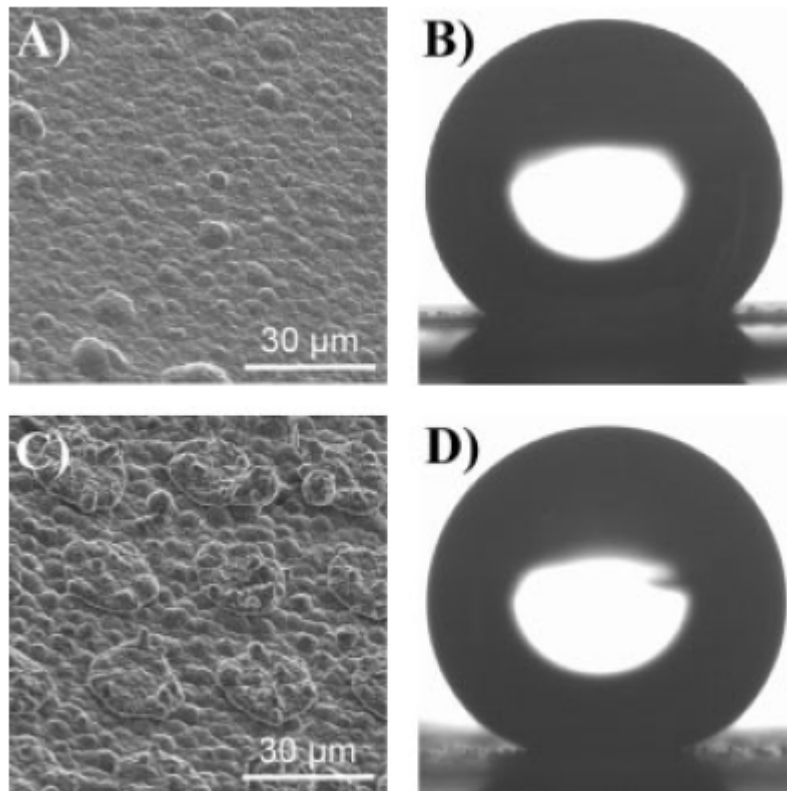


Figure 2.3.6 A) Scanning electron micrograph of electrodeposited copper. B) Drop of water on surface A, contact angle $136 (\pm 3)^\circ$. C) Scanning electron micrograph of electrodeposited copper "chocolate chip cookies". D) Drop of water on surface C, contact angle $160 (\pm 3)^\circ$. The electron micrographs were taken at an angle of 45° to emphasize roughness. [28]

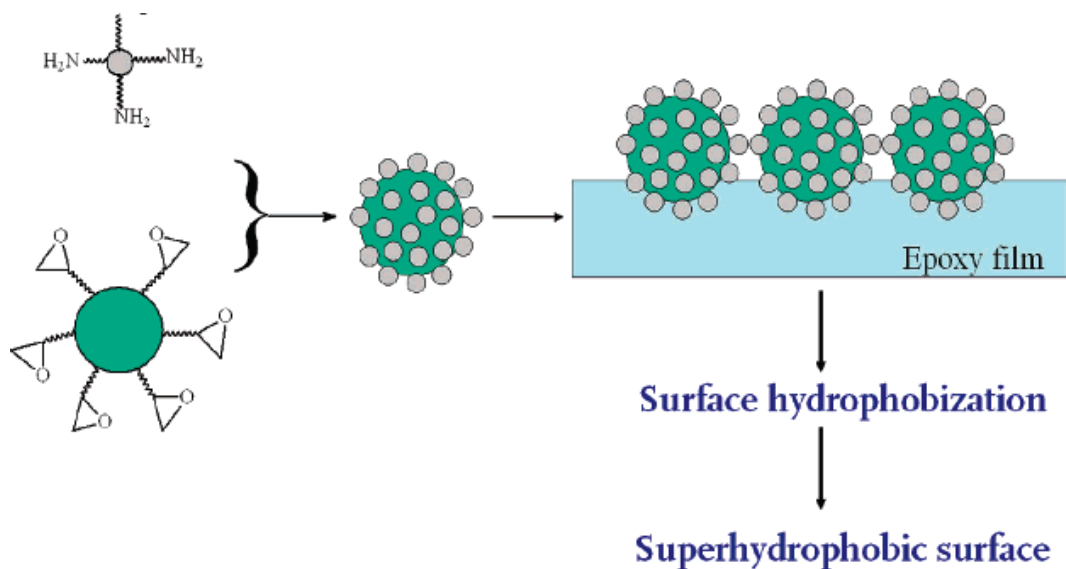


Figure 2.3.7 Preparation of superhydrophobic films based on raspberry-like particles. [29]

Another example of chemical deposition technique to induce repellent surfaces is the work of Manoudis et al. ^[30] who manufactured composite superhydrophobic films in various substrates. Hydrophilic silica nanoparticles were dispersed in solution of poly (methyl methacrylate) (PMMA) and in solutions of a commercial poly (alkyl siloxane) (Rhodorsil 224). The suspensions were sprayed on various substrates and induced superhydrophobic surfaces with a roughness of 0.8 nm. The effect of particle concentration was significant with a suitable value of 2 % (Figure 2.3.8). In the case of PMMA – SiO₂, the contact angle reached a value of 154°, contact angle hysteresis was 5°, and in that of Siloxane – SiO₂, the contact angle increased to 164° and the contact angle hysteresis decreased to 3°.

This work has been extended a bit more by using the Siloxane – SiO₂ composite film for the protection of Opuka substrate, a fine-grained argillite used for the restoration of the Prague castle ^[31]. Same conclusion came up in that case, where the particle concentration is the important factor, which affects the performance of the film on the substrate. Thus, a particle concentration of ≥0.5 % leads to contact angle of 160° and contact angle hysteresis of 3°. Opuka substrate is the only paper found to be close to the concrete substrate.

2.3.4 Layer-by-Layer

Sili Ren et al. ^[32] prepared and characterized an ultra-hydrophobic surface based on a stearic acid (STA) self-assembly monolayer over polyethyleneimine (PEI) thin films. The fabrication was based on Layer-by-Layer self-assembly monolayer. The first step involves immersion of aluminum substrates (polished aluminum wafer and evaporated aluminum film on glass plates) into a dilute aqueous solution of PEI. A thin layer of PEI formed and then the PEI-coated aluminum substrates were placed into a dilute solution of STA to form a second layer.

The significant part of this work was the high roughness reached equal to 21.3 nm. The contact angle measured was 166° but the contact angle hysteresis was 10° which was considered being high enough to consider it as a superhydrophobic surface and compare to others presented in this review.

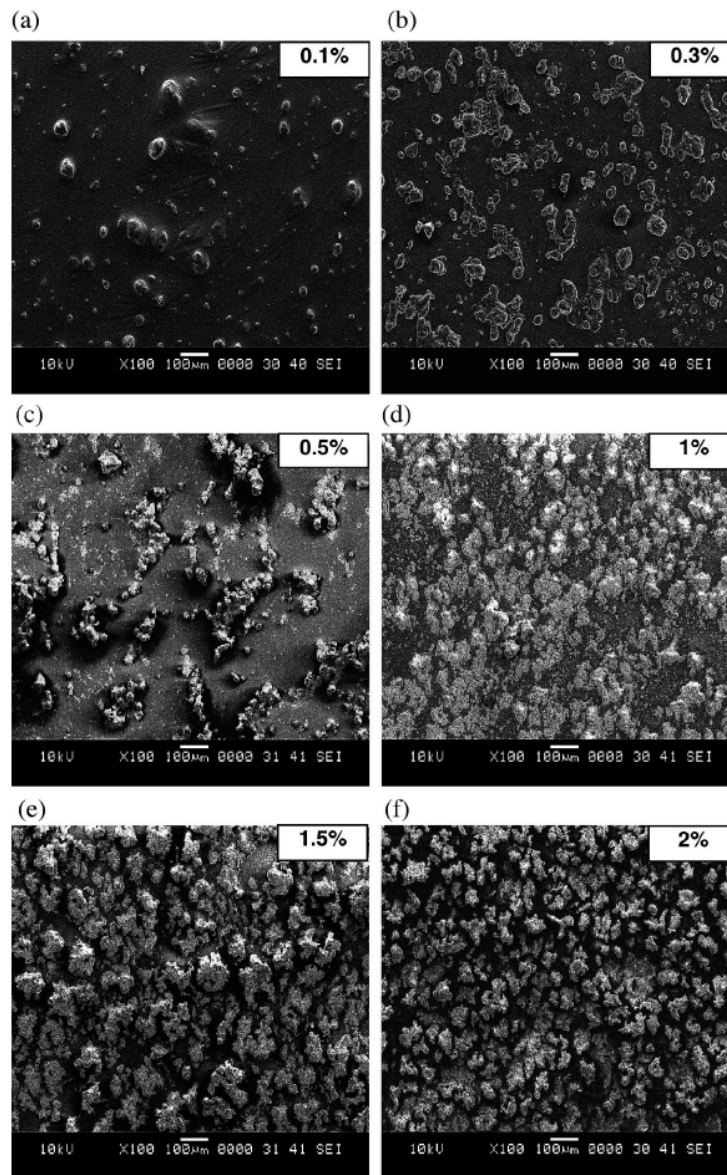
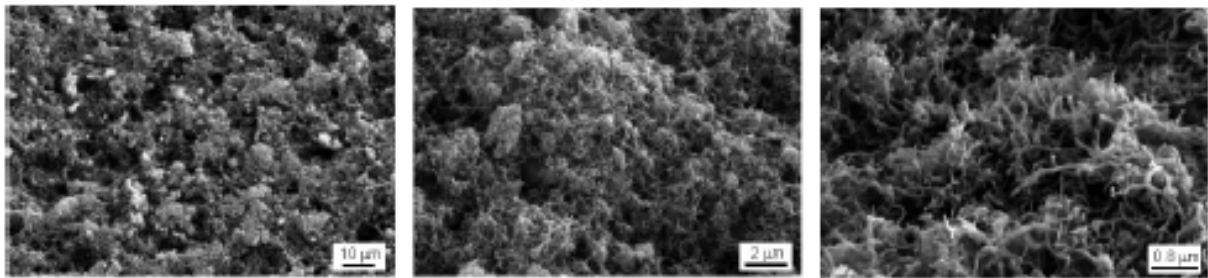


Figure 2.3.8 Rhodorsil-particle films deposited on glass. The concentrations (w/v) of the SiO₂ nanoparticles in the dispersions (deposited on the glass surfaces) are shown in the upper right corner of each image. ^[30]

Carbon nanotubes (CNTs) also play a very important role in the formation of superhydrophobic surfaces and many different techniques have been applied with their use. Yong Chae Jung and Bharat Bhushan ^[33] manufactured mechanically durable CNT composite hierarchical structures showing superhydrophobicity, self-cleaning properties and low-drag. They fabricated multi-walled CNTs with catalyst-assisted chemical vapor deposition (CCVD) which was used to initiate their growth. With the use of soft lithography, they created replications with pillars of 14 µm diameter, 30 µm high and 23 µm pitch. They finally managed to form a very durable hierarchical structure with a contact angle of 170° and contact angle hysteresis of 2° (Figure 2.3.9).

Carbon nanotubes (CNT) composite after three hours (120° C)

Nanostructure with CNT



Hierarchical structure with CNT

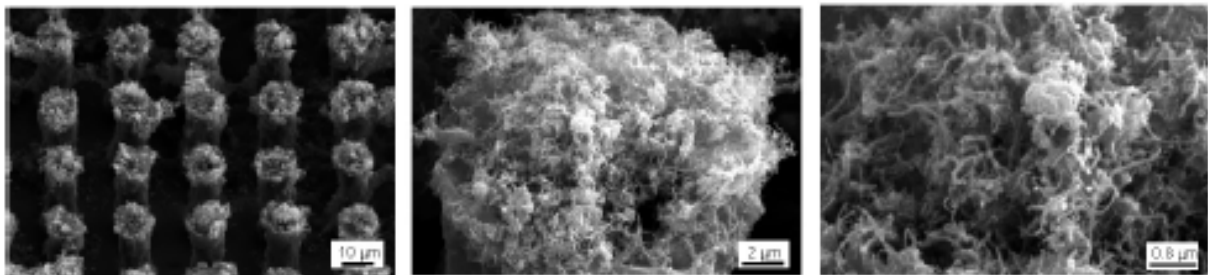


Figure 2.3.9 SEM micrographs taken at 45° tilt angle, show three magnifications of (a) nano and hierarchical structures fabricated with CNTs after 3 h at 120 °C. [33]

The layer-by-layer (LBL) technique is one of the most well-known techniques for the production of superhydrophobic surfaces. Lei Zhai et al. [34] mimicked the honeycomb-like structure and manufactured stable superhydrophobic surfaces with the use of polyelectrolyte multilayer. The multilayers were assembled from poly (allylamine hydrochloride) (PAH) and poly(acrylic acid) (PAA) which by acidic treatment were made porous of 400 nm where SiO₂ nanoparticles deposited. These processes were followed by chemical vapor deposition (CVD) of semifluorinated silane and post thermal treatment. They managed to reach a very high static contact angle of 172° and low contact angle hysteresis of 2° (Figure 2.3.10).

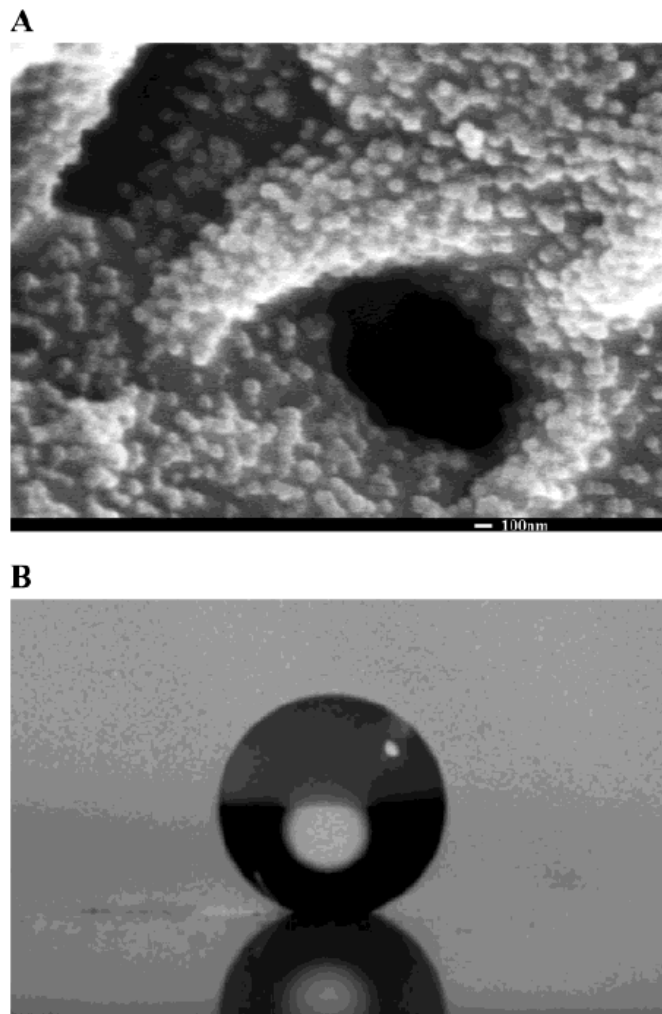


Figure 2.3.10 (A) SEM image of the fully treated structure B with silica nanoparticles. (B) Water droplet on this superhydrophobic surface. ^[34]

A similar work made by Yan Zhao et al. ^[35] proposed the LBL technique in combination with replica molding. They made polyimide films with a hierarchical topography. Firstly, they prepared microsphere-patterned polyimide precursor film by replica molding (Figure 2.3.11) and then multilayer of polyelectrolytes with SiO₂ nanoparticles (film of [(PAH/PAA)(PAH/SiO₂)₃]_n). This procedure was followed by thermal and fluoroalkylsilane treatment. The final pattern was a hierarchical structure with three assembly cycles of SiO₂ nanoparticles with roughness of 59.5 nm (Figure 2.3.12). The static contact angle measured 160.2° and the contact angle hysteresis was too high with a value of 17.5°. The final film showed very good mechanical and chemical stability.

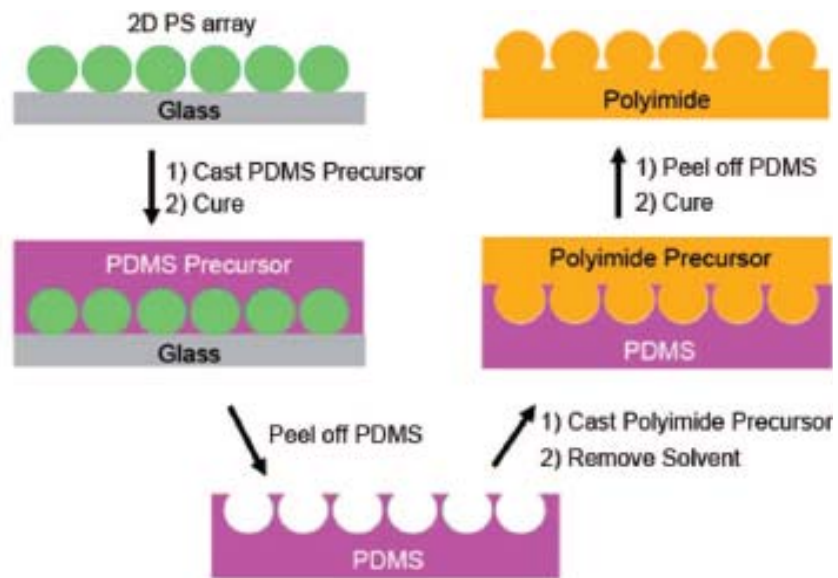


Figure 2.3.11 Schematic illustration for creating microsphere-patterned polyimide films. [35]

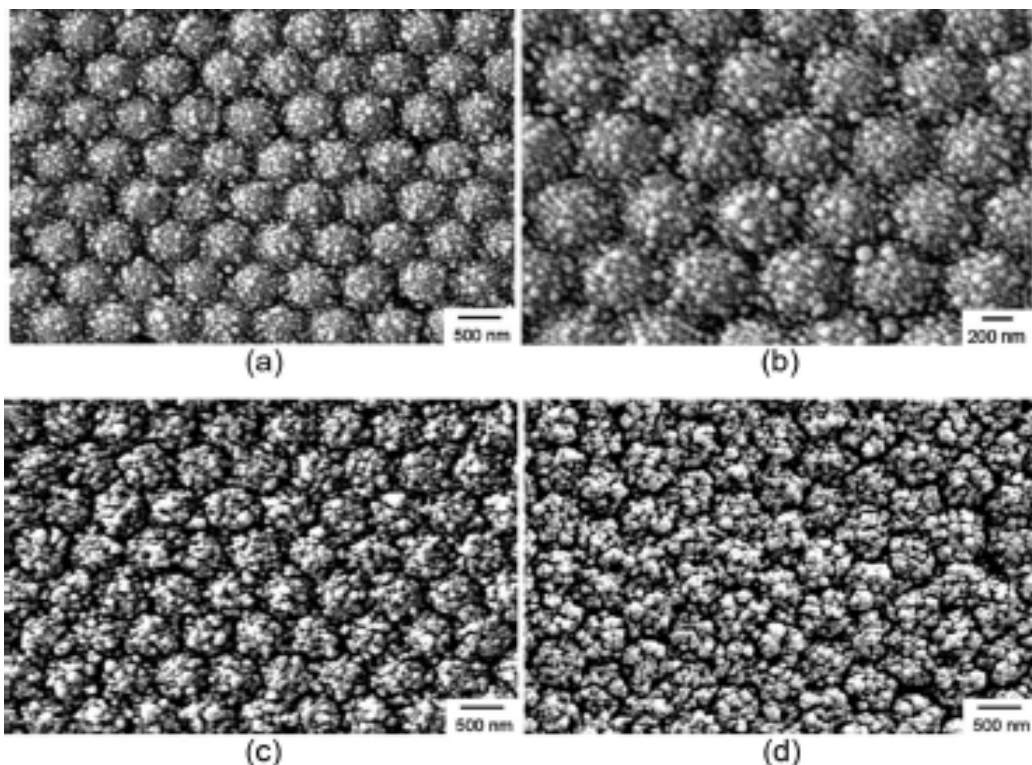


Figure 2.3.12 SEM images of hierarchical structures composed of microspheres and $[(\text{PAH}/\text{PAA})(\text{PAH}/\text{SiO}_2)_3]_n$ films: (a, b) $n = 1$, (c) $n = 3$, and (d) $n = 5$. [35]

2.3.5 Plasma deposition

Another technique is the plasma enhanced chemical vapour deposition (PECVD). Lau et al. [36] combined this technique with hot filament chemical vapour deposition (HFCVD) and with the use of CNTs. They managed to mimic the lotus leaf structure by producing a superhydrophobic carbon nanotube forest. PECVD was used for the deposition of vertically aligned carbon nanotube forest. The CNTs were coated with PTFE by HFCVD. They had a diameter of 50 nm and 1.1 μm high with a density of 10 nanotubes per μm^2 (Figure 2.3.13). The advancing and the receding contact angles measured 170° and 160°, respectively. The final durable properties were good enough with the consideration that upon wetting volatile liquid exposure, untreated forests were found to bundle together under surface tension forces during drying (Figure 2.3.14).

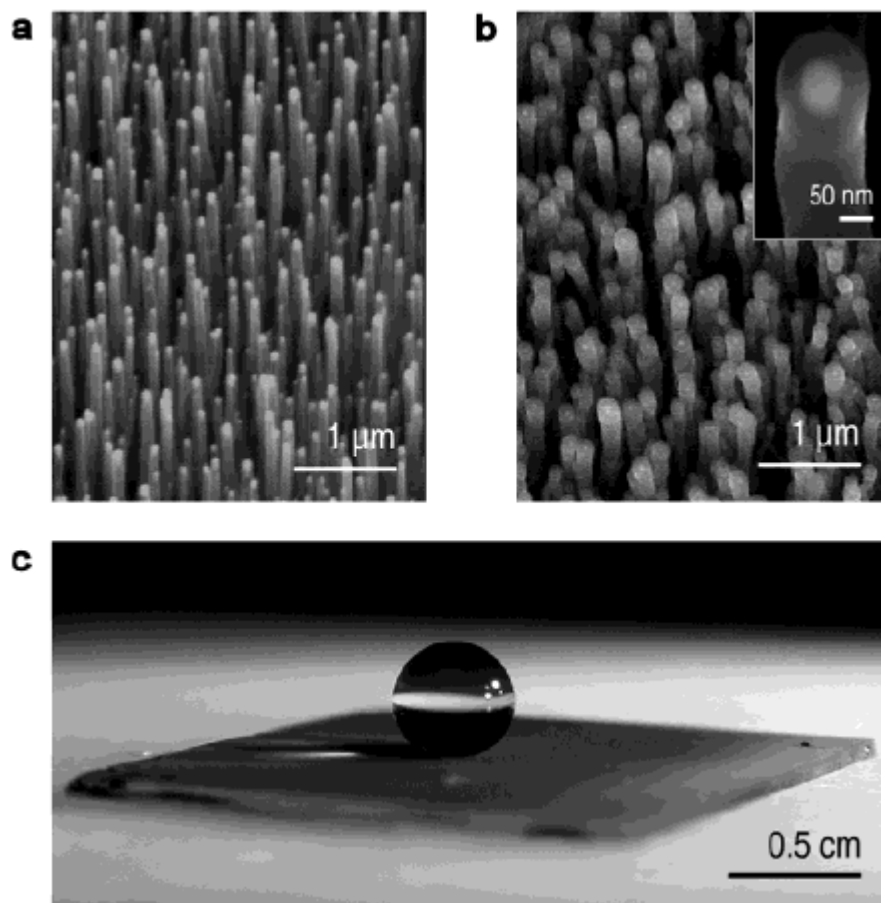


Figure 2.3.13 SEM images of carbon nanotube forests. (a) As-grown forest prepared by PECVD with nanotube diameter of 50 nm and a height of 2 μm , (b) PTFE-coated forest after HFCVD treatment, and (c) an essentially spherical water droplet suspended on PTFE-coated forest. [36]

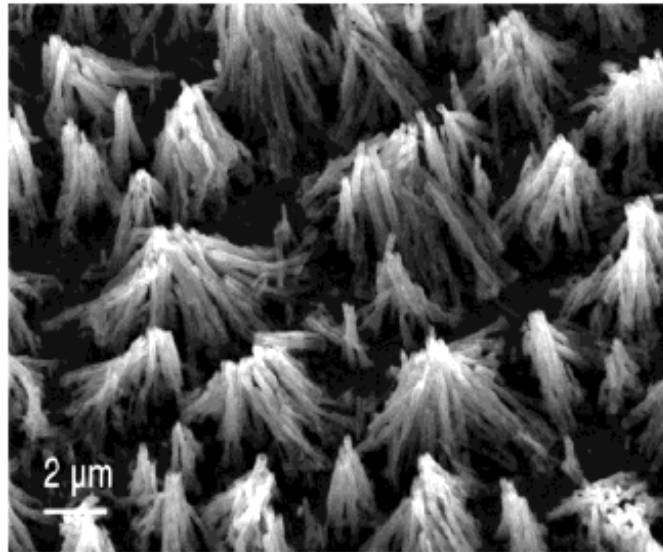


Figure 2.3.14 ESEM image of an as-grown forest without PTFE treatment, after exposure to water, showing the nanotubes bundling together because of the attractive capillary forces that arise during evaporative drying. ^[36]

Oxygen plasma treatment has been used as a technique from Teshima et al. ^[37] for the fabrication of transparent ultra water-repellent poly(ethylene terephthalate) (PET) nano-textured substrates and subsequent hydrophobic coating of layers of a) fluoroalkylsilane (FAS) with CVD and b) tetramethylsilane [TMS], $\text{Si}(\text{CH}_3)_4$ with PECVD. In the case of FAS-coated, the roughness measured 6.5 nm and in the case of TMS-coated 15.3 nm. During oxygen plasma treatment, a range of 50-200 Watts radio frequency power (RF) was used, where 100 Watts was found to be the best radio frequency power (Figure 2.3.15). The height of the pillars on the PET substrates after oxygen plasma treatment was greater than 5nm. In both cases, the water contact angle was higher than 150° and the film showed more than 90 % transparency.

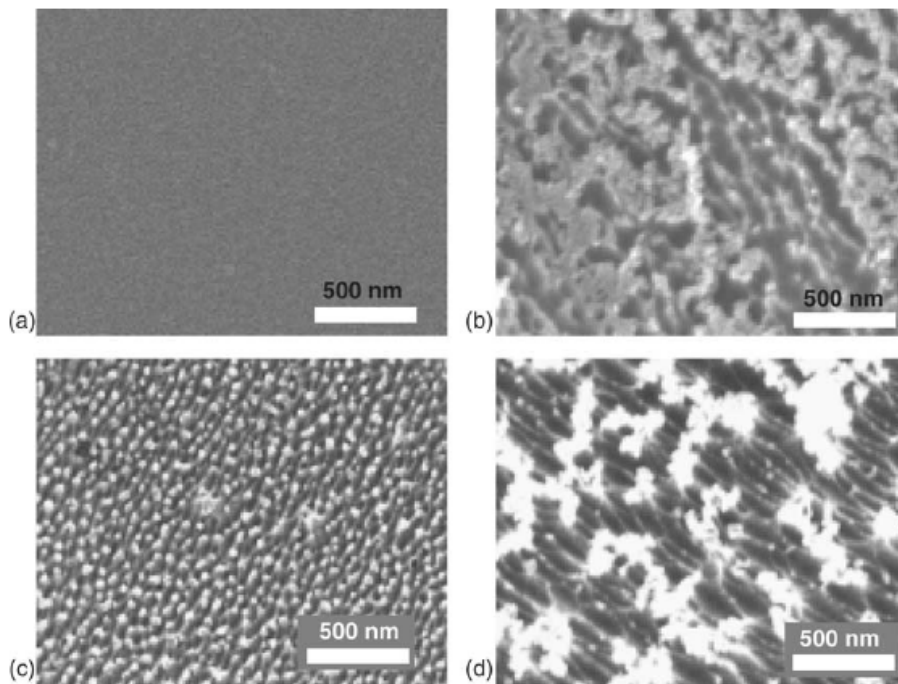


Figure 2.3.15 SEM images of the PET surfaces treated with oxygen plasma at various RF powers: (a) untreated, (b) 50 W, (c) 100 W and (d) 200 W (the treatment time was fixed at 10 min).^[37]

2.3.6 UV-curing

The last technique that will be mentioned in this report is the use of solvent-resistant photocurable perfluoropolyethers. Lei Zhang et al.^[38] prepared flexible, translucent, and stable superhydrophobic films made of crosslinked styrene end-functionalized perfluoropolyether (PFPE) and a highly fluorinated styrene sulfonate ester (SS) that has a nanopillar structure or a lotus-leaf-like topography. UV radiation of the prepolymer took place with the use of a textured porous anodized aluminum oxide p-AAO, in order to obtain a multiscale topography. The entire procedure is illustrated in Figure 2.3.16. The final pattern observed, had pore diameter of 140 nm and pillar length of 3 μm (Figure 2.3.17). The water contact angle and the contact angle hysteresis measured were 171° and 3°, respectively. An important role in this procedure, for the texturation of the substrate, is the anodization of the aluminum foil to produce p-AAO.

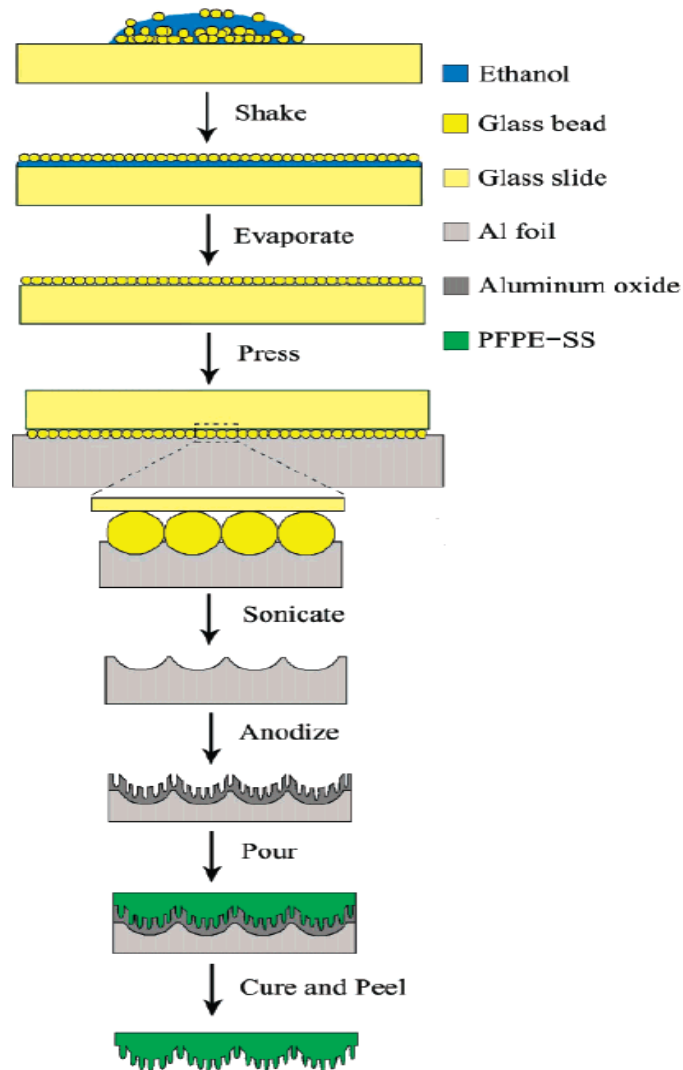


Figure 2.3.16 A schematic illustration of the procedure for creating a lotus-leaf-like PFPE-SS structure. [38]

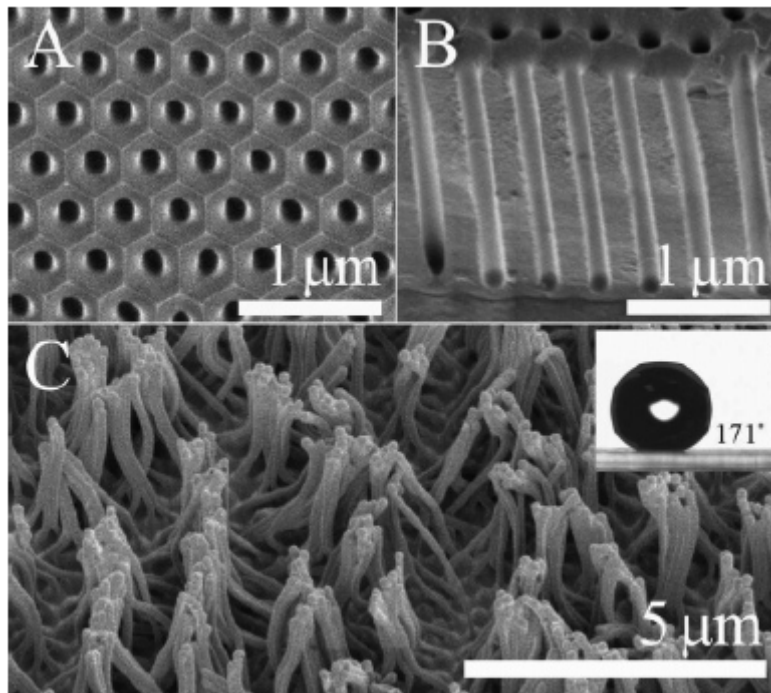


Figure 2.3.17 (A) Top view and (B) 30° angle oblique view FE-SEM images of a p-AAO membrane template anodized for 20 min at 180 V. (C) FE-SEM images of a PFPE-SS nanopillar film peeled from the p-AAO membrane. The inset is a water droplet, with an extremely high static contact angle, sitting on the PFPE-SS nanopillars. ^[38]

2.4 Superhydrophobicity according to the texture

Different techniques that induced superhydrophobicity were mentioned. The techniques which role is to texture the surfaces, can lead to high contact angles, higher than 140°, and low contact angles hysteresis, less than 10°. The table below (Table 2.4.1) summarizes the values of the contact angle in relation to the texture of the surfaces and according to the various techniques used.

Technique the report based on	Main Technique	Secondary Technique	Water Contact Angle	Contact Angle Hysterisis	Texture of the surface
Lithography	Nanosphere lithography	Oxygen plasma etching	170°	-	440-nm beads diameter in a double layer polystyrene surface
	X-ray Lithography	Chemical Treatment	1)Silicon wafers:166° 2)Plant's replicates:157.8° 3)Metal foils:164.8°	1)Silicon wafers:3° 2)Plant's replicates:7.9° 3)Metal foils: 0.5°.	1)silicon wafer's pillars: d:1 µm, h:4 µm, p: 3 µm 2) plants replicates: scale like roughness in the range of 1-3 µm. 3) metal foils: surface structure of 3 µm
Electrodeposition		Chemical Treatment	165°	-	Copper from acidic copper sulfate solution onto flat copper. Pillars:15 µm, h:2 µm, p: 15 µm
Chemical Deposition			165°	2°	Raspberry like particles
			Siloxane:164°, PMMA:154°	Siloxane:3° PMMA:5°	Silica Nanoparticles (SiO ₂) dispersed in solutions of Siloxane and PMMA and deposited on the substrates
Layer-by-Layer		Chemical Treatment	166°	10°	Films made by STA chemically adsorbed onto the PEI coated aluminum wafer. Roughness of 21.3 nm
	Catalyst-assisted chemical vapor deposition (CCVD)	Soft Lithography	170°	2°	Micropatterned silicon surface modified by CNT composite. Pillars: d:14 µm, h:30 µm, p: 23 µm
		1) CVD of Semifluorinated silane 2) Post-Thermal treatment.	172°	2°	Bilayer of PAH/PAA films with SiO ₂ nanoparticles and semifluorinated silane.
		Replica Molding	160.2°	17.5°	Polyelectrolytes/SiO ₂ Nanoparticles Multilayers on Microsphere-Patterned Polyimide Precursor Films. Hierarchical structure with 59.5 nm roughness.
Plasma Deposition	Plasma enhanced chemical vapour composition (PECVD)	Hot filament chemical vapour deposition (HFCVD)	170°	10°	PTFE-coated carbon nanotube forests of 50 nm in diameter and 1.1 µm height.
	Oxygen plasma treatment	1) CVD 2) PECVD	Higher than 150°	-	PET substrates coated with hydrophobic layers of a) FAS and b) TMS
UV-curing			171°	3°	Films of crosslinked styrene end-functionalized PFPE and a highly fluorinated styrene SS. Hexagonally close-packed pores with uniform diameters (140 nm) with a channel length of about 1-3 µm.

Table 2.4.1 Summary of the water contact angles measured in the reports according to the texture of the surfaces for the variety of the techniques applied.

2.5 Durable Superhydrophobic Surfaces

The bibliographic review leads us to conclusions regarding the durability of the superhydrophobic surfaces. For some of the papers described, the work was extended into mechanical tests to determine the performance of the surfaces over time and after exposure under specific conditions. The results from these studies can help us in the selection of the appropriate technique, which could be combined with significant final durable surfaces.

Carbon nanotubes (CNTs) are known for their high performance in strength and hardness. They also exhibit very good stability of wetting properties for long-term exposure to water and high water pressure ^[33]. When forests of CNTs, treated with PTFE, were exposed in repeating cycles of condensation and evaporation, no effects were observed on their structure. On the other hand, upon water or wetting volatile liquid exposure, untreated forests were found to bundle together under surface tension forces during drying ^[36].

For polyelectrolyte bilayers of PAH/PAA derivatives with silica nanoparticles, the surfaces remained superhydrophobic after being immersed in water for at least a week or in a high humidity environment for at least a month ^[34]. The layers also show very good chemical durability. By inserting and removing the sample vertically into and out of a beaker filled with sand for fire fighting, and followed by cleaning with an air flow, no changes in the water contact angle were found ^[35].

Super-liquid-repellent surfaces, prepared by colloidal silica nanoparticles covered with fluoroalkyl groups ^[39], did not alter their surface roughness after tests within experimental accuracy, implying that the durability of the layer coated was acceptable for practical use as well. Fluoroalkyl groups also affected poly (ethylene terephthalate) substrates ^[37] and their transparency, which remained high enough in the range of 90%.

A final example of durable surfaces is the post-treatment of solid surfaces with aliphatic and fluorinated aliphatic amines to produce surfaces that retained their superhydrophobic properties for six weeks of complete submersion in water ^[40].

2.6 Conclusions

From the works analyzed, we can conclude that both roughening the surface and lowering its energy are important and necessary parameters to obtain superhydrophobicity with specific properties such as self-cleaning and anti-icing. There are different techniques to achieve rough surfaces like template methods, chemical etching, polymer solution evaporation, electro-spinning, chemical vapor deposition, plasma, reactive ion, electro-deposition, nanorod array growth and textured block copolymer morphologies. Furthermore, techniques concern the decrease of surface energy are aliphatic thiols, fluorinated copolymers, semifluorinated silanes and poly(tetrafluoroethylene). A broad description of the most important and well-known techniques have been given in this report. As a result, the combination of them is the best way to create surfaces with high static contact angle and low contact angle hysteresis properties.

The question comes up now, is it possible to link the techniques for the induction of superhydrophobicity with the organic coatings and the correlation with CaCO_3 crystal growth. The primary attempt that we should focus on is the growth and control of the crystallization on a substrate, in terms of the orientation of the crystals and the generation of a film capable of covering the entire surface. By that way, we will be able to manipulate and chemically modify the organic coating, in order to achieve superhydrophobic surface properties. This could be done in a first step by soft lithography and in a second one by introduction of activated sites on the crystal surface to form carbonated nanopillars. Thus, the replication of carbonated natural structures, with a carbonated surface could be achieved.

2.7 References

- [23] Bharat Bhushan. **Biomimetics: lessons from nature-an overview**. Philosophical Transactions of the Royal Society A, 2009, 367, 1445-1486.
- [24] José Bico, Uwe Thiele, David Quéré. **Wetting of textured surfaces**. Colloids and Surfaces-Physicochemical and Engineering Aspects, 2002, 206, 41-46.
- [25] Mathilde Callies, David Quéré. **On Water Repelency**. Soft Matter, 2005, 1, 55-61.
- [26] Jau-Ye Shiu, Chun-Wen Kuo, Peilin Chen and Chung-Yuan Mou. **Fabrication of Tunable Superhydrophobic Surfaces by Nanosphere Lithography**. Chemistry of Materials, 2004, 16 (4), 561-564.
- [27] Reiner Furstner and Wilhelm Barthlott, Christoph Neinhuis, Peter Walzel. **Wetting and Self-Cleaning Properties of Artificial Superhydrophobic Surfaces**. Langmuir, 2005, 21, 956-961.
- [28] Neil J. Shirtcliffe, Glen McHalle, Michael Newton, Gregoire Shebrol, Carole Perry. **Dual scale roughnes produces unusually water-repellent surfaces**. Advanced Materials, 2004, 16 (21), 1929-1932.
- [29] W. Ming, D. Wu, R. van Benthem, and G. de With. **Superhydrophobic Films from Raspberry-like Particles**. Nano Letters, 2005, 5 (11), 2298-2301.
- [30] Panagiotis N. Manoudis, Ioannis Karapanagiotis, Andreas Tsakalof, Ioannis Zuburtikudis and Costas Panayiotou. **Superhydrophobic Composite Films Produced on Various Substrates**. Langmuir, 2008, 24, 11225-11232.
- [31] P.N Manoudis, I. Karapanagiotis, A. Tsakalof, I. Zuburtikoudis, B. Kolinkeova and C. Panagiotou. **Surface Properties of Superhydrophobic Coatings for Stone Protection**. Journal of Nano Research, 2009, 8, 23-33.
- [32] Sili Ren, Shengrong Yang, Yapu Zhao, Tongxi Yu, Xudong Xiao. **Preparation and characterization of an ultrahydrophobic surface based on a stearic acid self-assembled monolayer over polyethyleneimine thin films**. Surface Science, 2003, 546, 64-74.
- [33] Yong Chae Jung and Bharat Bhushan. **Mechanically Durable Carbon Nanotube Composite Hierarchical Structures with Superhydrophobicity, Self-Cleaning, and Low-Drag**. ACS Nano, 2009, 3 (12), 4155-4163.
- [34] Lei Zhai, Fevzi Cü . Cebeci, Robert E. Cohen, and Michael F. Rubner. **Stable Superhydrophobic Coatings from Polyelectrolyte Multilayers**. Nano Letters, 2004, 4 (7), 1349-1353.
- [35] Yan Zhao, Mei Li, Qinghua Lu, and Zhengyu Shi. **Superhydrophobic Polyimide Films with a Hierarchical Topography: Combined Replica Molding and Layer-by-Layer Assembly**. Langmuir, 2008, 24, 12651-12657.

- [36] Kenneth K. S. Lau, Jose Bico, Kenneth B. K. Teo, Manish Chhowalla, Gehan A. J. Amaratunga, William I. Milne, Gareth H. McKinley and Karen K. Gleason. **Superhydrophobic Carbon Nanotube Forests**. Nano Letters, 2003, 3 (12), 1701-1705.
- [37] Katsuya Teshimaa, Hiroyuki Sugimurab, Yasushi Inouec, Osamu Takaic, Atsushi Takano. **Transparent ultra water-repellent poly (ethylene terephthalate) substrates fabricated by oxygen plasma treatment and subsequent hydrophobic coating**. Applied Surface Science, 2005, 244, 619-622.
- [38] Lei Zhang, Zhilian Zhou, Bin Cheng, Joseph M. DeSimone and Edward T. Samulsk. **Superhydrophobic Behavior of a Perfluoropolyether Lotus-Leaf-like Topography**. Langmuir, 2006, 22, 8576-8580.
- [39] Masaya Hikita, Keiji Tanaka, Tetsuya Nakamura, Tisato Kajiyama and Atsushi Takahara. **Super-Liquid-Repellent Surfaces Prepared by Colloidal Silica Nanoparticles Covered with Fluoroalkyl Groups**. Langmuir 2005, 21, 7299-7302.
- [40] Maren E. Buck, Sarina C. Schwartz, and David M. Lynn. **Superhydrophobic Thin Films Fabricated by Reactive Layer-by-Layer Assembly of Azlactone-Functionalized Polymers**. Chemistry of Materials, 2010, 22, 6319–6327.

Additional References studied during the Bibliographic Review

- 1) Bharat Bhushan, Yong Chae Jung. **Natural and biomimetic artificial surfaces for superhydrophobicity, self-cleaning, low adhesion and drag reduction**. Progress in Materials Science, 2011, 56, 1–108.
- 2) L. Huang, S. P. Lau, H. Y. Yang, E. S. P. Leong, and S. F. Yu - S. Praver. **Stable Superhydrophobic Surface via Carbon Nanotubes Coated with a ZnO Thin Film**. The Journal of Physical Chemistry B, 2005, 109, 7746-7748.
- 3) Bharat Bhushan, Kerstin Koch and Yong Chae Jung. **Biomimetic hierarchical structure for self-cleaning**. Applied Physics Letters, 2008, 93, 93-101.
- 4) Bharat Bhushan, Yong Chae Jung, Adrian Niemietz, and Kerstin Koch. **Lotus-Like Biomimetic Hierarchical Structures Developed by the Self-Assembly of Tubular Plant Waxes**. Langmuir, 2009, 25, 1659-1666.

- 5) Woo Lee, Mi-Kyoung Jin, Won-Cheol Yoo, and Jin-Kyu Lee. **Nanostructuring of a Polymeric Substrate with Well-Defined Nanometer-Scale Topography and Tailored Surface Wettability.** Langmuir, 2004, 20, 7665-7669.
- 6) H.M. Shang, Y. Wang, S.J. Limmer, T.P. Chou, K. Takahashi, G.Z. Cao. **Optically transparent superhydrophobic silica-based films.** Thin Solid Films, 2005, 472, 37– 43.
- 7) Xi Zhang, Feng Shi, Xi Yu, Huan Liu, Yu Fu, Zhiqiang Wang, Lei Jiang and Xiaoyuan Li. **Polyelectrolyte Multilayer as Matrix for Electrochemical Deposition of Gold Clusters: Toward Super-Hydrophobic Surface.** Journal of the American Chemical Society, 2004, 126, 3064-3065.
- 8) Rob J. Klein, P. Maarten Biesheuvel, Ben C. Yu, Carl D. Meinhart and Fred F. Lange. **Producing Super-Hydrophobic Surfaces with Nano-Silica Spheres.** Zeitschrift fur Metallkunde, 2003, 94 (4), 377-380.
- 9) Jilin Zhang, Jian Li, Yanchun Han. **Superhydrophobic PTFE Surfaces by Extension.** Macromol. Rapid Commun. 2004, 25, 1105-1108.
- 10) Masaya Hikita, Keiji Tanaka, Tetsuya Nakamura, Tisato Kajiyama and Atsushi Takahara. **Super-Liquid-Repellent Surfaces Prepared by Colloidal Silica Nanoparticles Covered with Fluoroalkyl Groups.** Langmuir, 2005, 21, 7299-7302.
- 11) M.T. Khorasani, H. Mirzadeh, Z. Kerman. **Wettability of porous polydimethylsiloxane surface: morphology study.** Applied Surface Science, 2005, 242, 339-345.
- 12) Edward Bormashenko, Tamir Stein, Gene Whyman, Yelena Bormashenko and Roman Pogreb. **Wetting Properties of the Multiscaled Nanostructured Polymer and Metallic Superhydrophobic Surfaces.** Langmuir, 2006, 22, 9982-9985.
- 13) Tae Oh Yoon, Hyun Joo Shin, Sae Chae Jeoung and Youn-I Park. **Formation of superhydrophobic poly(dimethylsiloxane) by ultrafast laser-induced surface modification.** Optics Express, 2008, 16 (17), 12716.
- 14) Fan Xia, Lin Feng, Shutao Wang, Taolei Sun, Wenlong Song, Wuhui Jiang, and Lei Jiang. **Dual-Responsive Surfaces That Switch between Superhydrophilicity and Superhydrophobicity.** Advanced Materials, 2006, 18, 432–436.
- 15) Wenjie Zhao, Liping Wang and Qunji Xue. **Design and Fabrication of Nanopillar Patterned Au Textures for Improving Nanotribological Performance.** Applied Materials and Interfaces, 2010, 2 (3), 788-794.
- 16) Maren E. Buck, Sarina C. Schwartz, and David M. Lynn. **Superhydrophobic Thin Films Fabricated by Reactive Layer-by-Layer Assembly of Azlactone-Functionalized Polymers.** Chemistry of Materials, 2010, 22, 6319–6327.

3 Materials and Models

Recently, the crystallization of inorganic compounds on solid organic templates has attracted a great deal of attention. Organic biomolecules such as collagen^[41], cholesterol^[42], elastin^[43], and chitin^[44] showed significant effects on the control of CaCO₃ crystallization^[45]. Synthetic compounds such as self-assembled monolayers^[46], polyamide^[47], lyotropic liquid crystals^[48] were also employed as organic templates for the deposition of inorganic compounds.

Our approach has been to obtain new organo-mineral/carbonate coatings on the surface of UHPC followed by the optimization, growth, and control of different forms of CaCO₃ crystals.

3.1 Organics

The organics used in this study and described below are:

- a. chitosan
- b. alginate
- c. carrageenan
- d. stearic acid
- e. CarboxyMethylCellulose (CMC)

a. Chitosan

Chitosan (Figure 3.1.1), poly- β (1,4)-2-deoxy-D-glucose, is the deacetylated product of chitin, poly(N-acetyl-D-glucosamine), a natural polysaccharide found in the exoskeletons of crustaceans and insects and in the cell wall of fungi and microorganisms.

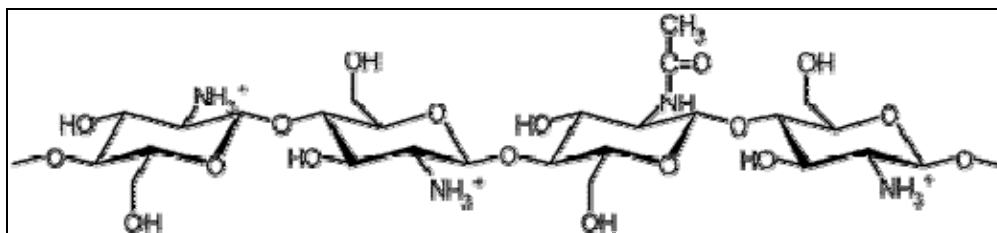


Figure 3.1.1 Chitosan structure.

Chitin with a degree of deacetylation (DA) of 75% or above is generally known as chitosan, which can be considered a copolymer composed of glucosamine and N-acetylglucosamine units and dissolves readily in dilute organic acids, providing clear, homogeneous and viscous solutions. Thus, the chemically active groups in the chitosan structure are the free amine groups, located in the C2 position of the glucose residue in the polysaccharide chain, and the hydroxyl groups, with both being susceptible to modifications.^[49]

Due to the same chemical structure between chitin and chitosan, the DA, which reflects the balance between the two kinds of residues, plays an important role. It also allows us to define the two terms chitin and chitosan according to their respective solubilities in dilute acidic media (except the case of sulphuric acid). Then, chitosan is the only derivative to be soluble in these conditions and corresponds approximately to DA's below 60%.^[50]

The conformations in solution, the physical, physicochemical, and biological properties of chitosan depend on structural parameters such as the molecular weight, DA, and the distribution of the two kinds of residues constituting the chain. Thanks to the presence of the primary amine groups born by the glucosamine residues, they necessarily depend on its ionization state and then external parameters including pH, ionic strength, and time. Therefore, the relation between parameters such as pK_a , DA, and α , the degree of dissociation, must be quite well-known to interpret the properties mentioned above.^[51-52]

The type of chitosan used in this study is called chitosan "652", provided by France Chitine, and is a chitosan powder produced by the shrimp shell with particles of 100 mesh and density of 0.6 g/cm^3 , with intrinsic viscosity between 5 to 20 cps and DA of 90%.

b. Alginate

Alginate is a naturally occurring polysaccharide which must be regarded as a family of copolymers since the fraction and sequence of the two monomers, α -L-guluronic acid (G)

and β -D-mannuronic acid (M) (Figure 3.1.2a) varies over a wide range. The fact that G and M are C5 epimers results in switch-over of the monomer chair conformation, giving rise to all four possible glycosidic linkages and at the molecular level (Figure 3.1.2b), large effects like cavity formations between G residues are observed. [53]

The affinity of alginates towards certain ions and the ability to bind these ions selectively and cooperatively leads to gelation of alginates [54-55]. The length of the G blocks depends on the selective ion binding, which parallel affects the mechanical rigidity when it increases. Acid gels can also be formed at pH below the pK α value of the uronic acid residues. [53, 56]

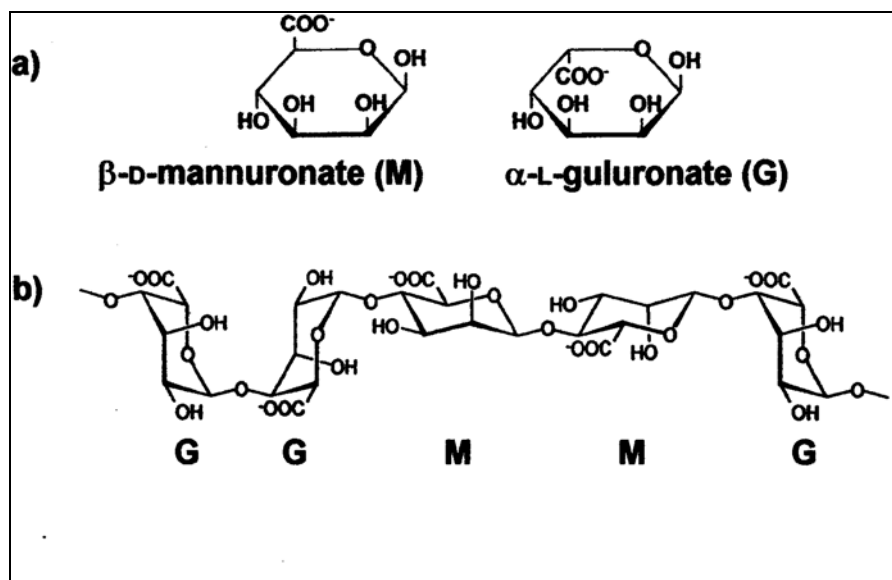


Figure 3.1.2 Alginate monomer (a) and chain (b) conformation.

The type of alginate used in this study was alginic acid sodium salt, provided by Sigma-Aldrich, with viscosity of 15-20 cp when 1% in H₂O and MW of 120,000-190,000 g/mol.

c. Carrageenan

Carrageenan is prepared by alkaline extraction and modification from seaweed. It is a linear polysaccharide of about 25,000 galactose derivatives with regular structure, depending on the source and extraction conditions. There are three different types of carrageenan that dominate known as kappa, iota and lambda. The differences between them are the degree of sulfation, the solubility, the ability to form gels under different conditions, the extent of

branching, and the cation binding. What links them together are the similar d-galactose backbones (alternating α -1.3 to β -1.4 linkages) (Figure 3.1.3).

Carrageenan is used mainly as a food additive as well as in cosmetics, pharmaceuticals, in toothpastes and room deodorizer. Other applications refer to liquid petrolatum while it has been used also as an emulsifier in mineral oil laxatives. [57]

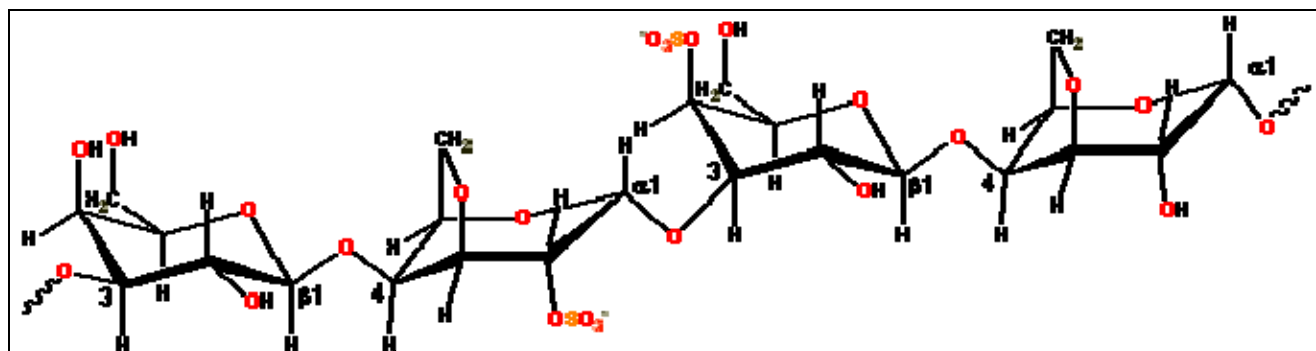


Figure 3.1.3 Structural unit of carrageenan

The type of carrageenan used was Santiago MM 30, provided by Cargill Haubourdin SAS, with a viscosity, in a 1% aqueous solution, of 500-600 cps, pH of 8-11 and particle size of 250 μm .

d. Stearic acid

Stearic acid (octadecanoic acid) is a saturated fatty acid derived from animals and vegetable fats and oils [58]. It has been used in the manufacturing of pharmaceutical products and especially due to its inertness, incompatibility and low toxicity, it has been used in the development of drug delivery systems. [59]

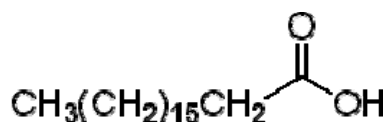


Figure 3.1.4 Structural unit of stearic acid

As a fatty acid, stearic acid is a relatively non-polar compound. Therefore, it will be more soluble in non-polar solvents and less soluble in polar solvents [60]. Additionally, the effect of the hydrogen bonding properties of a stearic acid – solvent system could affect its solubility with the most hydrogen bonding characteristics leading to the most favourable dissolution of stearic acid [61]. The stearic acid used in this study, provided by Sigma-Aldrich, had a MW of 285.49 g/mol.

e. CarboxyMethylCellulose (CMC)

CarboxyMethylCellulose (CMC) is an anionic polysaccharide that is obtained through the reaction of a cellulose alkali with monochloroacetate of sodium. Many applications of CMC exist in the pharmacy, cosmetics, and food industries. It is used as a thickener, stabilizer, water binder, and film to improve the consistency and flow properties [62]. In addition, due to its inertness and noncaloricity, cellulose gum is used in dietetic foods [63]. It is compatible with a wide range of other food ingredients like proteins, sugars, and other hydrocolloids where synergistic interaction can occur. When it reacts with liquids, CMC represents a complex rheological system, due to the formation of aggregates and thus higher-level structures [64]. Furthermore, studies showed already that CMC exhibits a pseudoplastic and thixotropic behavior.

A CMC derivative is purified sodium CMC with the following structure:

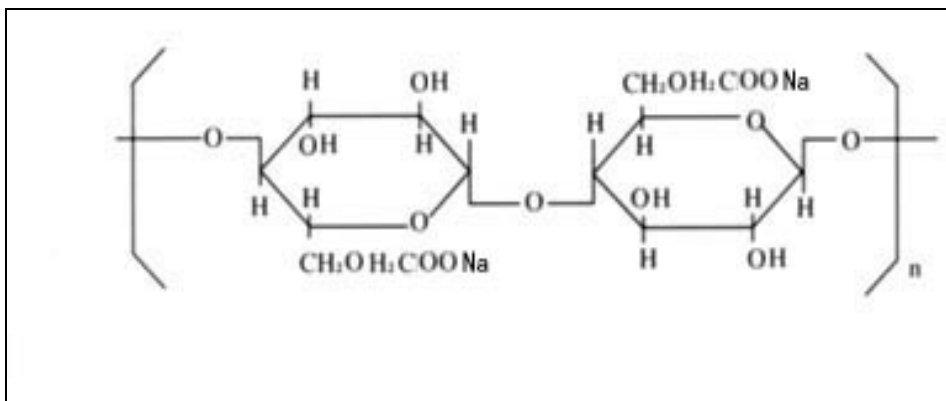


Figure 3.1.5 Na-CMC structure

Na-CMC is a weak polyacid with a white or slightly yellowish powder or fibrous product. It is odorless with a bulk weight of 400–800 kg/m³ and density of 1.59 g/cm³. The softening temperature of Na-CMC is 170 °C and at a higher temperature, it decomposes. Na-CMC is soluble in cold and hot water and it forms highly viscous aqueous solutions. In aqueous solutions, it is a polyelectrolyte. Na-CMC is approved for widespread use in medicine and pharmacy [65].

The carboxymethylcellulose used, in its specific type of Blanose 7H9, provided by Hercules, has a viscosity, when 1% diluted in aqueous solution, of 4000-9000 mPa.s and a bulk density of 0.55 to 1 g/ml.

3.2 Carbonates used in this study

Calcium carbonate has become an important mineral material due to its abundant existence in nature. There is a wide range of applications such as in paper-making, medicines, detergents, ceramics, rubber, paint, etc.... In living organisms, the control and modulation of organic additives can form calcium carbonate with unusual properties. The process is called biomineralization and results in pearls and mollusc shells, etc. The formation of kidney and gallstones is the negative aspect of a biomineralization process ^[66].

CaCO₃ exists mainly in six different polymorphs: amorphous calcium carbonate (ACC), calcium carbonate hexahydrate, calcium carbonate monohydrate, vaterite, aragonite, and calcite, where the thermodynamic stability increases from ACC to calcite. ACC plays an important role in biological calcium carbonates and usually contains 15% water. This property in combination with the fact that ACC is considered the precursor of more thermodynamically stable CaCO₃ makes the formation, control, and stabilization of ACC a challenging process. ^[7]

The most commonly found polymorphs in nature are aragonite and calcite. The chemical purity, morphology, specific area, and particle size determine the properties of CaCO₃ and, as a result, its applications. Therefore, controllable synthesis of CaCO₃ in the presence of additives, such as amino acids ^[67], surfactants ^[66], biodegradable polymers ^[68], double hydrophilic block polymers ^[69], and inorganic ions ^[70] has attracted much interest.

3.3 Substrate – Ultra High Performance Concrete (UHPC)

A mix-design based on ultrahigh-performance concrete (UHPC) was used to prepare the samples. However, no fibers were introduced in the final mix that was made of white Portland cement, limestone filler, silica fumes, sand, and admixture. The UHPC samples presented a small overall porosity.

The samples (UHPC) were prepared by pouring the fresh concrete mixture into horizontal and rectangular formwork (15 cm length, 12 cm width and 1 cm thick) made of polyvinylchloride (PVC).

During the cast of the concrete samples, no demolding agent and no steps of agitation or densification were used. All the UHPC samples were removed from their formworks after 18h. They were cured during 7 days under ambient conditions (20°C; 50% relative humidity) to complete the hydration.

3.4 Solutions made of organics and carbonates

A variety of solutions has been prepared during this study in order to achieve the best concentration between the organics and the minerals/carbonates (additives) and to define the best organics that could induce CaCO_3 crystallization on the UHPC surface. Moreover, the adhesion between the organic coating and the substrate was a challenge, which refers additionally to the process of deposition that will be discussed in the following chapters.

The preparation of a first series of solutions focused mainly on the use of chitosan as an organic material. Chitosan is mainly found in natural shell and is supposed to induce CaCO_3 crystallization. Chitosan, due to its complicated structure and manufacturing process (deacetylation of chitin), has a specific dissolution process, which is followed in every solution preparation. The solubility of chitosan is dependent on the protonisation of the free amine group of D-glucosamine unit present in the polymer, meaning the solubility will depend on the degree of acetylation and on the pH of the solution. Most of current chitosan, with DA in the range of 30% to 10%, are soluble at 1% concentration in diluted acid media (1 to 2%) and at pH below 5,6. In this study, the organic acids that have been used were the citric acid and the acetic acid. In order to achieve easy solution, the chitosan powder was never dropped directly in acidic solution, because chitosan is difficult to dissolve. Instead, first, re-hydration of chitosan powder took place in water for 15-20 minutes, and then it was added to the acid.

To start this study, a series of additives were used, with the code name CR, individually or with another series of additives, with the code name MN, in combination with different concentrations of chitosan to optimize the best composition. The chitosan concentration varied from 1% to 20% with the best of them ranging around 7% and those of the additives around 2-4%. The concentration of citric acid varied from 1%-5% to be balanced with that of chitosan. Finally, a dispersive agent was used in some of the solutions to avoid precipitation.

A second series of solutions was prepared, where acetic acid was used instead of citric acid to reduce the precipitation, to increase the Water Contact Angle, and to reduce the hydration of concrete that emerges from the distribution when citric acid is used. The acetic acid was always mixed with chitosan as an organic material.

The final series focused on the use of inorganics salts such as Na_2CO_3 and CaCl_2 , which react to induce crystallization of the different forms of CaCO_3 crystals. The salts were mixed with chitosan and with the rest of the organic materials (alginate, carrageen, CMC, stearate,...).

3.5 Models of natural resistant microstructures based on CaCO_3 . *Mussels-Nacre.*

A three-level hierarchical architecture that is composed of CaCO_3 crystals of different morphologies is the structural design of nacreous layer. The inorganic crystals form plate units that link together and are covered by organic molecules. This well-designed construction and hierarchical structures has attracted the interest of researchers from different chemistry disciplines, in addition to its attention-grabbing mechanical properties, incorporation of macromolecules, mineral bridges, and manufacturing process [71].

In recent times, many investigations have been focused on the nanoscale properties of nacre. As Wang et al. [72] showed (Figure 3.5.1), the connection and orientation of aragonite plates of 200 to 600 nm thickness in the nacreous layer have been well examined. Flat crystals of CaCO_3 and organic molecules, such as biopolymers, proteins and chitin, could assemble to form a layered composite structure, which corresponds to that of nacreous layer.

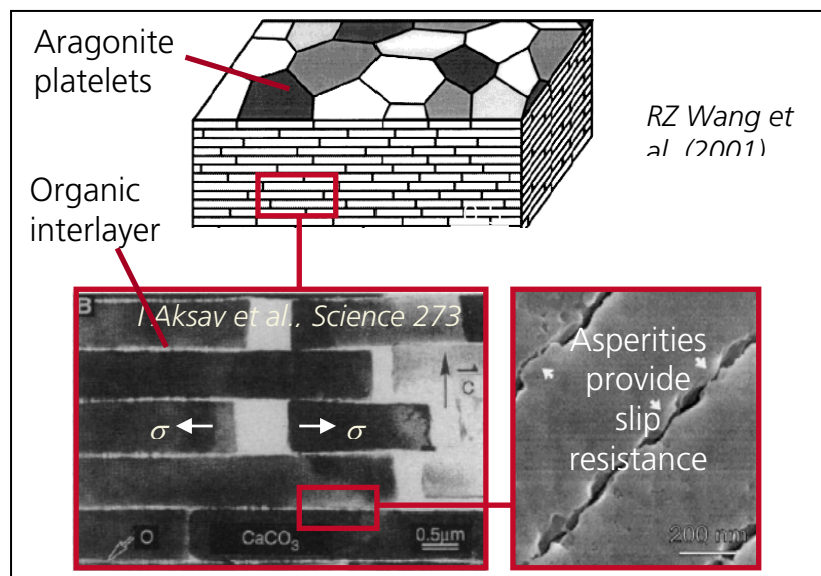


Figure 3.5.1 Morphology of Abalone Nacre consisting of aragonite crystals (Wang et al. (2001)) and combines with organic interlayer to induce high mechanical strength (Aksay et al.)

Aksay et al. [73] showed that the layer-by-layer assembly of aragonite crystals and the organic molecules provide slip resistance and as a result, high mechanical strength which when combined can be compared to bricks and mortar, respectively.

Same configuration was seen in a mussel from Isère Lake where two different structures were observed in the same examined sample. The first one refers to the arrangement closer to the surface (Figure 3.5.2 upper right) which consists of CaCO_3

columns. The second located in a lower level closer to the bulk and responds to the previous configuration of Abalone nacre (Figure 3.5.2 lower right).

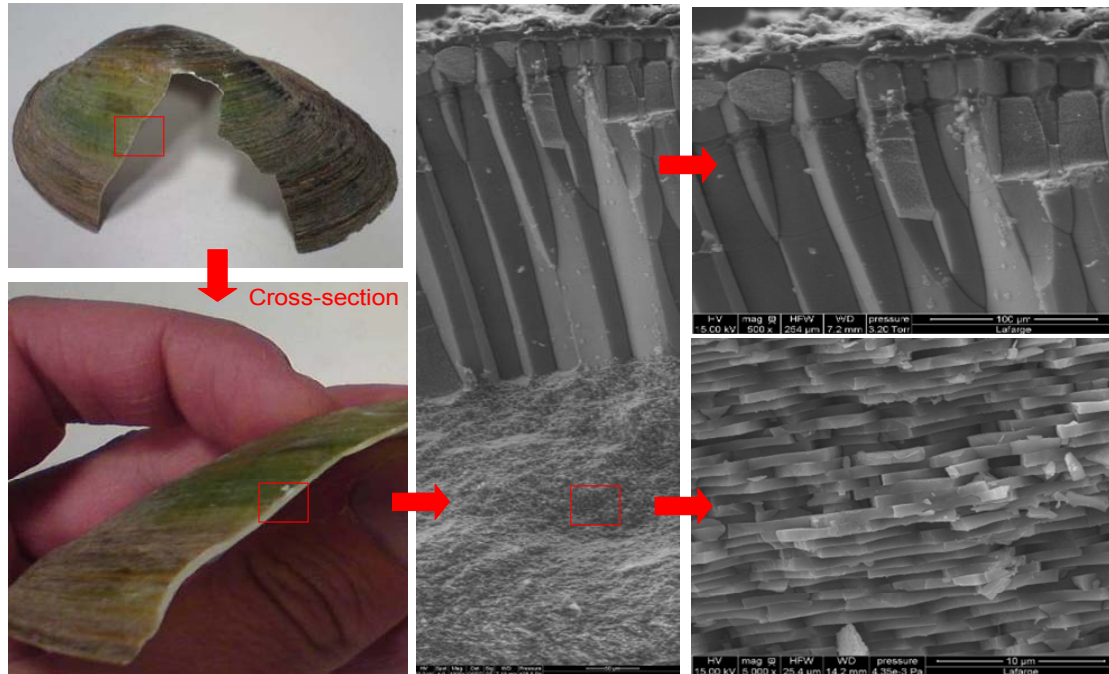


Figure 3.5.2 Structure of a mussel from Isère Lake

4 Methodologies of deposition of organic coatings

4.1 Deposition of layers made of organics and additives

For the depositions of the organic/additives of chitosan and additives MN or CR coatings on the UHPC substrate, three different methods were used:

1. Dip-coating
2. Spin-coating
3. Storage in bath

All the solutions were prepared according to the best composition between additive MN and the organic solution. The aim of the use of three different deposition methods is to find the most effective way to achieve a homogeneous distributed layer, which will cover the entire UHPC substrate and will not form cracks and agglomerations.

For the preparation of the solutions, the same procedure took place for all the samples independent of the coating method. The dissolution of chitosan with citric acid in H₂O, mentioned in chapter 3.4, followed the addition of additive CR₁ and the stirring of the solutions for 20min. Thereinafter, the additive MN was added in the solution, which was stirred for 30min. until complete mixing of the reactants was achieved. The high viscosity observed at the end was significant for the choice of the coating method and the good adhesion of the coating on the substrate.

4.1.1 Dip-coating method

During the dip-coating method, three different steps were taken and performed in all the samples irrespectively of the solutions. The three steps are illustrated in Figure 4.1.1. The first step includes pouring of the organic/additives solution in a Tupperware container followed by soaking for few seconds of the UHPC substrate in the solution (Figure 4.1.1(a, b)). The last step involves the horizontal drying of the sample under lab conditions (Figure 4.1.1(c)). This process was repeated 5 times in order to achieve a thick layer on the substrate. During the preparation of a few of the first samples and the mass measurement after each dip-coating, it was concluded to be beneficial to reduce the dip-coating to 2 times and to increase the time of dip-coating to 10 sec. After each cycle, mass measurements

were done to define the mass uptake and as a result the percentage and contribution of the coating on the substrate.

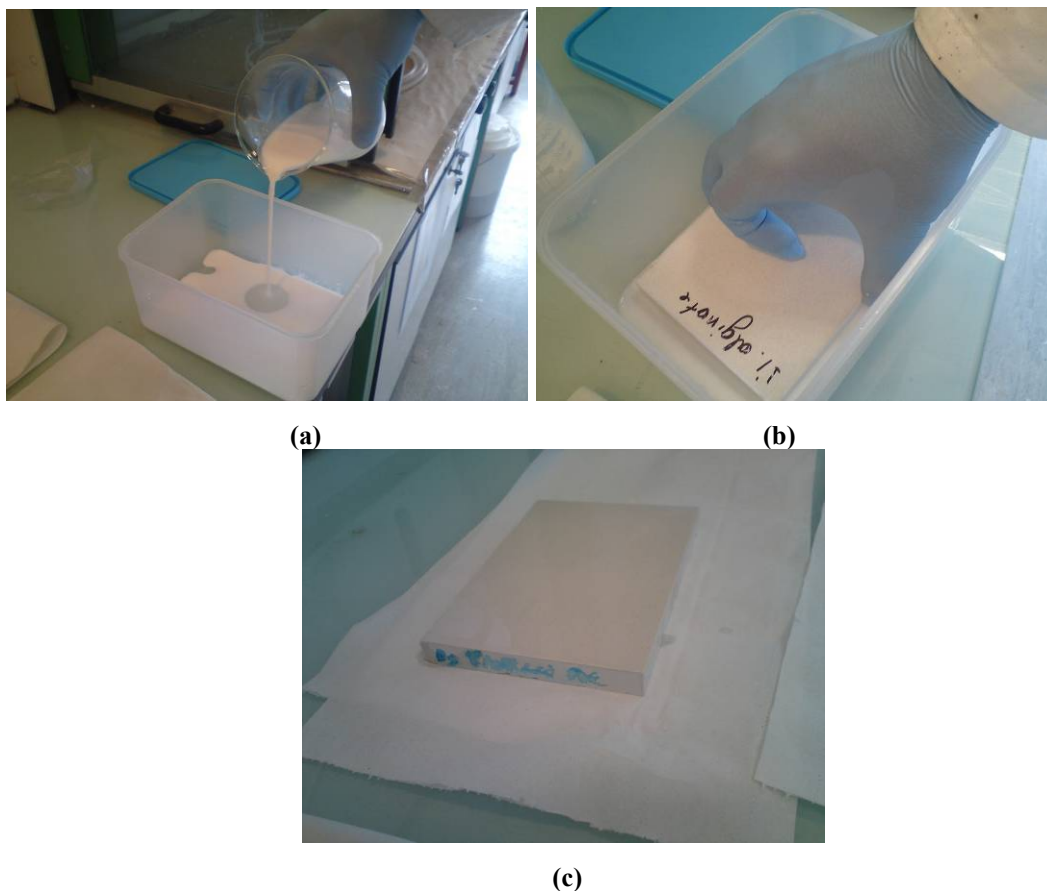


Figure 4.1.1 Different steps followed during the dip-coating method: (a) pour the organic/carbonate solution in a Tupperware container, (b) soak a few seconds the substrate and (c) dry horizontally.

A variety of solutions were prepared in order to achieve the best composition between chitosan and the CR or by mixing them with additive MN. Table 4.1.1 summarizes the solutions prepared.

Reference	Chitosan 652 (%)	Citric Acid (%)	Additives CR ₁ -CR ₂ - CR ₃	Additive MN
DC ¹	1	1	5% CR ₁	X
DC ²	7	2	5% CR ₁	X
DC ³	7	2	5% CR ₂	X
DC ⁴	7	2	4% CR ₂	4% MN
DC ⁵	7	2	2% CR ₃	4% MN
DC ⁶	7	2	4% CR ₂	4% MN ₁

Table 4.1.1 Summary of the solutions prepared for dip-coating method which consist of chitosan 652, citric acid and additives CR individually or in combination with additives MN.

As we can observe from the table, the percentage of concentrations of additives CR and additives MN varied from 2%-5% independent of the reactants. The aim was mainly to obtain the effect of each additives CR, with or without additive MN, in the solution with chitosan 652 and to prepare a stable and well-adhered coating on the UHPC substrate.

In addition to the previous samples performed, chitosan 652 mixed also with acetic acid in order to achieve, as previously mentioned, higher WCA, reduce precipitation, and control and decrease the hydration of concrete induced by the utilization of citric acid. The concentration of chitosan 652 reached values of 7% and that of acetic acid 1%. The preparation of the solution and the deposition of the coating occurred as described previously during the dip-coating method.

Furthermore, different substrates as plaster and ordinary concrete were used for the deposition of coatings made by solutions of 1% or 7% of chitosan 652 mixed with 1% acetic acid to compare the effect of chitosan 652 concentration on the porosity and WCA of the substrates.

4.1.2 Spin-coating method

The spin-coating of a drop is well performed by using a polishing instrument type Mecapol P320 and allows depositing of coating on a UHPC substrate. The solutions were prepared by the same way as described previously and used during the spin coating method and are listed in Table 4.1.2.

Reference	Chitosan 652 (%)	Citric Acid (%)	Additives CR ₁ -CR ₂ - CR ₃	Additive MN
SC ¹	7	2	5% CR ₂	X
SC ²	7	2	5% CR ₁	4% MN
SC ³	7	2	2% CR ₃	4% MN

Table 4.1.2 Summary of the solutions prepared for spin-coating method, which consist of chitosan 652, citric acid, and additives CR individually, or in combination with additives MN.

4.1.3 Storage in bath

The third method used was the bath method. The solutions were prepared again according to the best composition between additives MN and the polysaccharide solution. The samples remained in a bath for 7 days and then dried for 7 more days before they were analyzed by SEM. The solutions prepared are listed in Table 4.1.3.

Reference	Chitosan 652 (%)	Citric Acid (%)	Additives CR ₁ -CR ₂ - CR ₃	Additive MN
SB ¹	1	1	5% CR ₁	X
SB ²	2	1	5% CR ₁	X
SB ³	3	1	5% CR ₁	X
SB ⁴	7	2	5% CR ₁	X
SB ⁵	1	1	5% CR ₂	X
SB ⁶	7	2	4% CR ₂	4% MN
SB ⁷	7	2	2% CR ₃	4% MN
SB ⁸	7	2	2% CR ₁	4% MN
SB ⁹	5	2	1% CR ₁	4% MN

Table 4.1.3 Summary of the solutions prepared for storage in bath which consist of chitosan 652, citric acid and additives CR individually or in combination with additives MN.

4.2 Control of the crystallization of CaCO₃

The formation, control and crystallization of CaCO₃ crystals on an UHPC substrate covered by an organic layer are the main goals of this study. This can be created by mixing CaCl₂ water solution with Na₂CO₃ water solution by the procedure illustrated in Figure 4.2.1

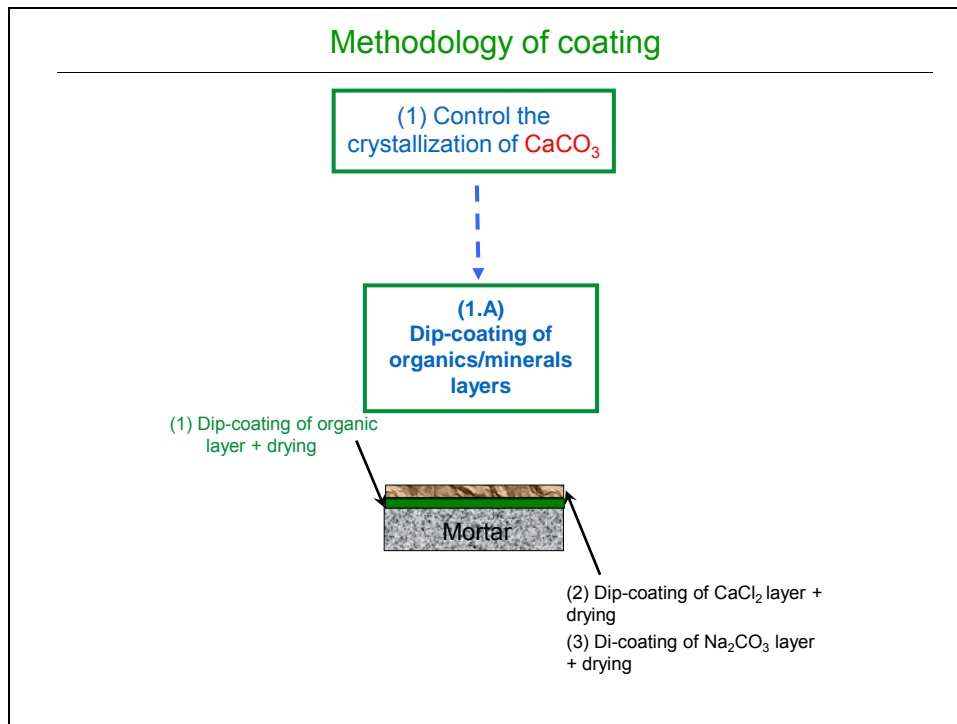


Figure 4.2.1 Methodology of coating the UHPC substrate with the aim to control the crystallization by direct dip-coating of the organics/carbonates.

The organic layer can be formed by using:

- 1) Chitosan 652+ acid (acetic or citric) solubilised in water
- 2) Alginate + water
- 3) Fatty acids (stearic acid) + water
- 4) Carrageenan
- 5) CarboxyMethylCellulose

The ratio between organic compounds and water was selected by checking the viscosity (low viscosity, no gel formation) and by using as few organics as possible (1%).

4.2.1 Dip-coating of organic/carbonates layers

The methodology used to build an organic layer on an UHPC substrate covered by a carbonate layer consists of three different steps. The method followed for the coating deposition was the dip-coating method. The steps that took place during the procedure are:

1) One layer dip-coated, made of organic compounds, well bonded with UHPC substrate.

2) Second layer dip-coated, made of:

a) 10% of CaCl_2 in water, dip-coated on the substrate

b) 10% of Na_2CO_3 in water, dip-coated on the substrate

3) Third (optional) layer, dip-coated, made of organic compounds.

In the first solution prepared, chitosan 652 was used as an organic compound and the experimental procedure follows the steps below:

- 1% of chitosan 652 in distilled water and stirring for 15 min.
- Addition of 1% citric acid and stirring for 20 min. until complete dissolution of chitosan 652. The solution was transparent with yellow colour and very low viscosity.
- After pouring the solution in a Tupperware container as shown in Figure 4.1.1(a), dip-coating of a reference UHPC substrate took place (Figure 4.1.1(b)). The dip-coating lasted for 10sec.
- Drying of the sample in an oven at 45°C for 2h 30min.
- One solution of 10% of CaCl_2 in water prepared and dip-coated on the samples and then dried.
- A solution of 10% Na_2CO_3 in water dip-coated again on the surface of the samples and finally dried.

The same procedure repeated one more time to obtain a multilayer of organics and carbonates.

A second solution was prepared based on alginate as an organic compound. The same procedure as previously followed where instead of chitosan 652 in citric acid solution, a solution of 1% alginate in water was prepared under the same process and conditions. Due to its high viscosity, alginate in water was stirred for 30 min instead of 15 min. In addition, contrary to the use of chitosan 652 where the sample was first dip-coated in CaCl_2 and then in Na_2CO_3 , in alginate a reverse procedure was followed and the sample first dip-coated in Na_2CO_3 and then in CaCl_2 . This is because CaCl_2 on alginate could induce problems of passivation/precipitation. The final solution exhibited moderate viscosity and transparency, and a yellowish colour.

The third organic used was carrageenan. The solution prepared from 1% carrageenan in water showed higher viscosity compared to chitosan 652 and alginate and bubbles appeared inside. The same experimental procedure as previously stated-in the case of alginate though and not in that of chitosan 652 - followed with the difference that the sample remained for 2h 30min in the oven under 45°C and then continued to dry overnight under lab conditions.

Stearic acid, which is a fatty acid, is the fourth organic used. Stearic acid, due to its non-polar property, was dissolved in hexane. Thus, the UHPC substrate dip-coated in 1% of stearic acid in hexane and thereafter in 10% CaCl₂ and 10% Na₂CO₃ like previously.

The final organic compound used was CarboxyMethylCellulose. A solution of 1% of blanose in water was stirred for 3h under 50°C for the first 2h and under 100°C for the last hour. A solution (gel) of high viscosity was obtained where the reference UHPC substrate was dip-coated. The sample was placed in an oven and dried overnight in 45°C. The second layer was made of 10% CaCl₂ in water, where the UHPC substrate was coated as well, and the last dip-coating occurred in a solution of 10% Na₂CO₃ in water.

5 Characterization of the microstructure and surface properties of the coatings (SEM, WCA, XRD, Scratching, Sorptivity)

Chapter 4.1 described the different methodologies for the deposition of layers made of organic and a series of additives. Dip-coating, spin-coating and storage in a bath of the solutions on substrates are the three different methods used in this study. In the following chapters, the characterization will be done for each of the samples, based mainly on the microstructure and surface properties of the coatings in order to identify the best method for the coating deposition (wetting, homogeneity, distribution).

5.1 Deposition of layers made of organo-additive MN

Before displaying the results, it should be mentioned that on the section related to SEM observations, the aim is not only to define the influence of the additives on the coating, but also mainly to end in a conclusion for the best coating method that should be applied for further experiments.

5.1.1 Dip-coating method

Several additives have been added gradually, like CR₁, CR₂, CR₃, CR₂ + additive MN and CR₃ + additive MN.

The solutions prepared for the deposition by dip-coating are listed in Table 4.1.1. A UHPC substrate was dip-coated in each one of them 5 times for 2 sec. After each dip-coating, the weight of the substrates was measured to obtain the mass uptake and the coating mass. SEM analyzed the substrates with well-adhered and well-spread coatings on both the surface and cross-section. Pictures of the views of all the final samples are also taken. All the results are showed below for each sample separately with a description of their composition.

A) Solution of 1% chitosan 652 + 1% citric acid + 5% CR₁ in H₂O



Figure 5.1.1 View of UHPC surface after deposition of coating

The deposition of the coating on the substrate had as a result the formation of a stable but heterogeneously distributed layer on UHPC substrate as can be obtained from Figure 5.1.1. The mass measurement (Table 5.1.1) leads to a result of 0.3% average mass uptake, which means that the contribution and effect of the coating on the total weight is not significant.

B) Solution of 7% chitosan 652 + 2% citric acid + 5% CR₁ in H₂O

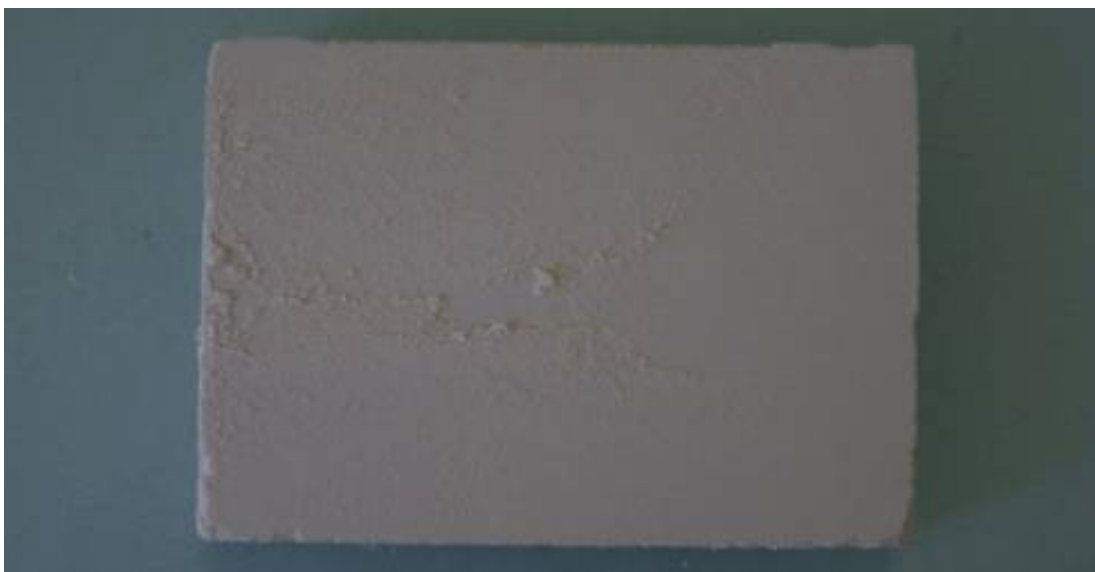


Figure 5.1.2 View of UHPC surface after deposition of coating

The heterogeneous distribution of the coating could result from the heterogeneous incorporation of CR₁ into the organic solution. The coating deposited on the surface formed agglomerations, which could be removed easily after drying (Figure 5.1.2). In addition, the layer formed was not well distributed. The average mass uptake was 0.6% (Table 5.1.1), resulting in the same impact of coating as in the previous sample.

C) Solution of 7% chitosan 652 + 2% citric acid + 5% CR₂ in H₂O

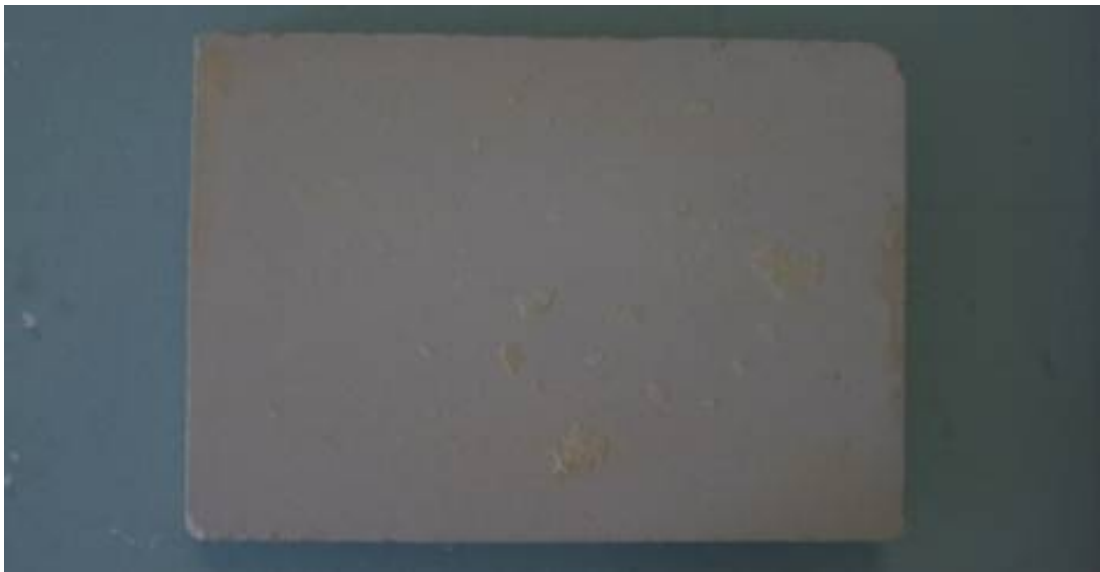


Figure 5.1.3 View of UHPC surface after deposition of coating

The high viscosity of the solution prepared for the coating deposition, which came by the higher chitosan concentration, is the main disadvantage, which leads to agglomerations on the substrate and no layer formation, as can be observed in Figure 5.1.3. The mass uptake (Table 5.1.1) calculation was not necessary due to no coating formation.

D) Solution of 7% chitosan 652 + 2% citric acid + 4% CR₂ + 4% additive MN in H₂O

Figure 5.1.4 View of UHPC surface after deposition of coating

After drying, a coating formed and covered the entire substrate (Figure 5.1.4). Even if the viscosity of the solution was as high as the previous one, the effect of the coating lead in contrast to a better distributed layer well-adhered to the UHPC substrate. The effect on the average mass uptake (Table 5.1.1) was significant and reached a value of 1.6%.

In Figure 5.1.5, the SEM images taken, both on the surface (a), (b) and on the cross-section (c), (d) are obtained. With a mix of CR₂ and additive MN into chitosan 652, no cracks were observed. The UHPC substrate is covered by a coating, made of fine particles linked together by an organic film with thickness around 5 μm . As mentioned, the coating showed very good-adherence and homogeneous distribution. This phenomenon could be linked to the adsorption of chitosan by the additive MN in the solution. Finally, before the coating debond, a stable solution observed during a few hours before precipitation.

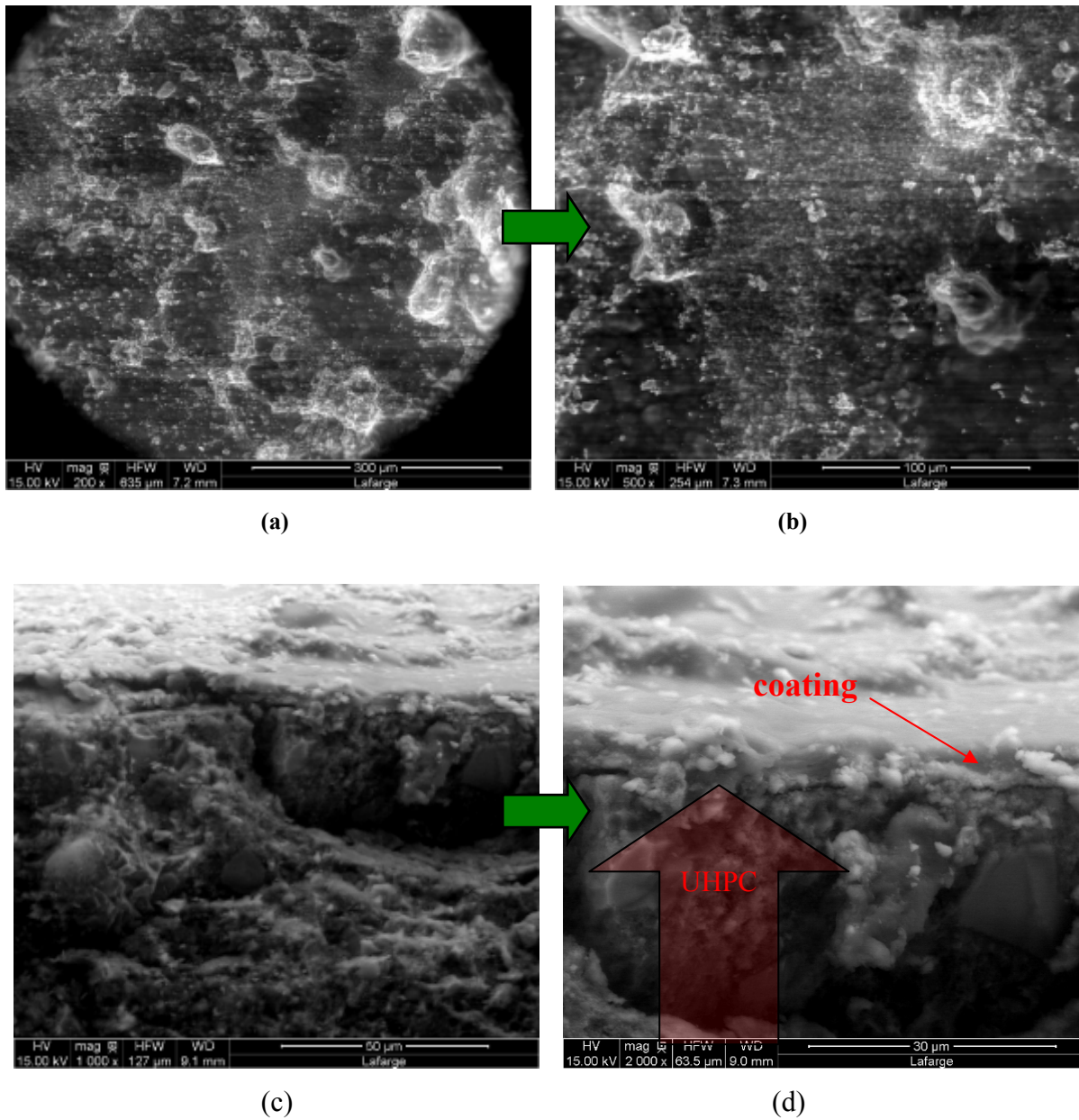


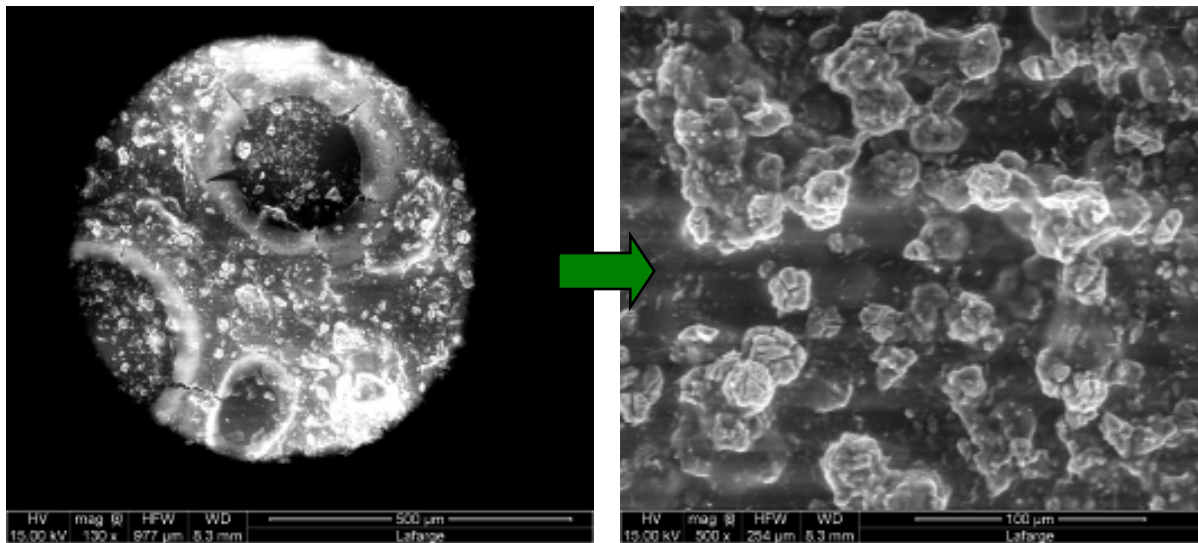
Figure 5.1.5 SEM images of the surface of coating (a) and (b) and cross-section (c) and (d) of a 7% chitosan 652 + 2% citric acid + 4% CR₂ + 4% additive MN.

E) Mixing of an “optimum” solution of 7% chitosan 652 + 2% citric acid + 2 % CR₃ + 4% additive MN in H₂O



Figure 5.1.6 View of UHPC surface after deposition of coating

As in the previous sample, the coating after drying covered the entire surface by forming a film very well adhered on the UHPC surface (Figure 5.1.6). The solution prepared exhibited high viscosity as well. Finally, the average mass uptake (Table 5.1.1) measured 1.1% showing a moderate contribution by the coating on the total weight. This result confirms that additive CR₃ stabilize the solution made of additive MN and chitosan. By the SEM images (Figure 5.1.7), it has been observed that cracks created on the surface and crystals linked together inside the film of chitosan 652.



(a)

(b)

Figure 5.1.7 SEM images of the surface of coating and of a 7% chitosan 652 + 2% citric acid + 4% CR₃ + 4% additive MN in H₂O deposited solution.

Table 5.1.1 lists the results from the mass measurements taken after each dip-coating accompanied by the mass uptake percentage. The first measurement corresponds always to the reference weight of UHPC.

Solution in H ₂ O	Mass Measurements after each dip-coating (gr)					Mass uptake (g/m ²)
	1	2	3	4	5	
1% chit. 652 + 1% c.a + 5% CR ₁	506.84	508.21	508.05	508.75	508.96	1.18
7% chit. 652 + 2% c.a + 5% CR ₁	498.71	502.15	501.46	501.55	502.51	2.11
7% chit. 652 + 2% c.a + 5% CR ₂	449.92	451.80	452.21	452.95	453.35	1.91
7% chit. 652 + 2% c.a + 4% CR ₂ + 4% additive MN	578.64	582.25	586.49	589.85	593.95	8.5
7% chit. 652 + 2% c.a + 2% CR ₃ + 4% additive MN	445.52	449.11	449.89	450.42	451.7	3.4

Table 5.1.1 Mass measurements after each dip-coating and percentage of average mass uptake.

As shown in Table 5.1.1, after each second dip-coating the mass uptake is reduced and, up to the final mass measurement, there is no outstanding change in the weight of the sample. This led us to reduce the dip-coating times for the rest of the samples to 2 times of 10 sec.

F) Solution of 7% chitosan 652 + 2% citric acid + 4% CR₂ + 4% additive MN₁ in H₂O

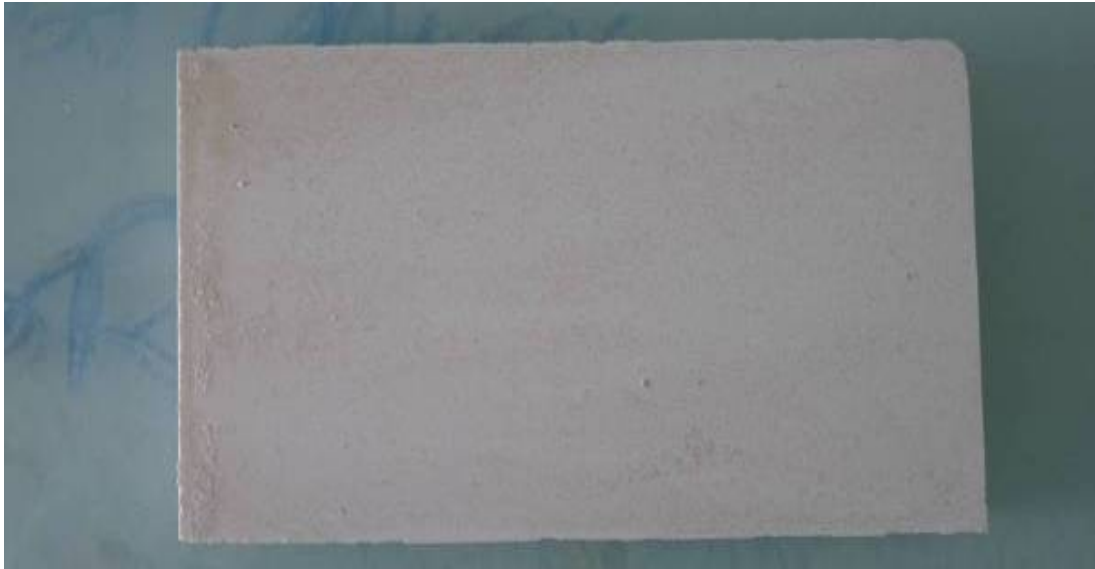


Figure 5.1.8 View of UHPC surface after deposition of coating

After dip-coating of a reference UHPC substrate in the solution, the formation of a stable thin film was obtained (Figure 5.1.8). It has almost the same appearance as the solution of 7% chitosan 652 + 2% citric acid + 4% CR₂ + 4% additive MN.

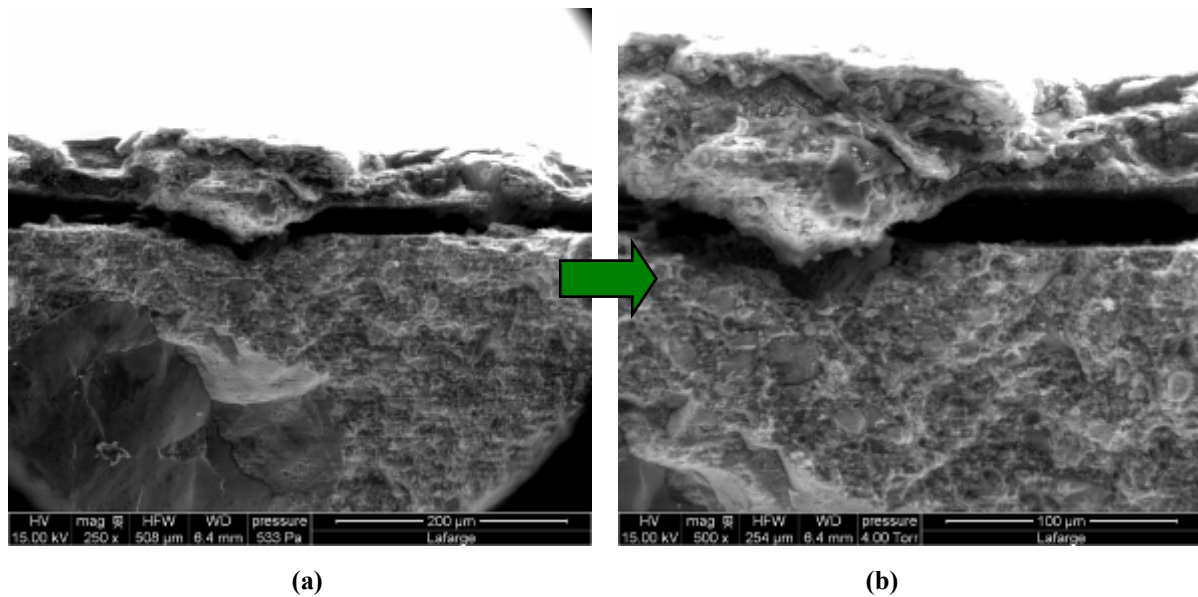


Figure 5.1.9 SEM images of the surface of coating and of a 7% chitosan 652 + 2% citric acid + 4% CR₂ + 4% additive MN₁ in H₂O.

As mentioned in the previous chapter, the replacement of additive MN with additive MN₁ took place due to their different properties. MN₁'s contribution led to debonding of the coating from the substrate, which could be observed from the SEM images (Figure 5.1.9).

Surface Properties

1) Sorptivity

The following method allows measuring the rate of the surface absorption, i.e sorptivity, of different pores materials. The test measures, over time, the mass of water absorbed by the surface of sample, previously conditioned to be constantly dry in an oven at 45° C, to separate the humidity residual. A resin that forbids the permeation of water inside the sample covers the lateral walls of the sample. After applying the resin, the samples should dry for 24h to obtain a constant dry mass. For the measurements of our "best" samples (7% chitosan 652 + 2% citric acid + 4% CR₂ or CR₃+ 4% additive MN), a piece of each sample was cut with specific dimensions to define the surface area which is in contact with the water. In the case of CR₂, the length of each edge was 2.1 cm and 6.4 cm and the surface area is equal to 13.44 cm². In that of CR₃, the sample has the shape of a square with 5.7 cm length and 32.49 cm² surface area. The initial mass of the samples was 36.20 g and

90.94 g, respectively. The samples immersed in water containers with a maximum depth of 3 mm in different terms (Figure 5.1.10).

The absorption can be determined from the following equation,

$$i = (m_0 - m_x)/a \text{ in g/cm}_2,$$

where,

i = Absorption

m_0 = the initial mass of the sample

m_x = the mass of the sample after each immersion

a = surface area of the sample which is in contact with water (cm²).

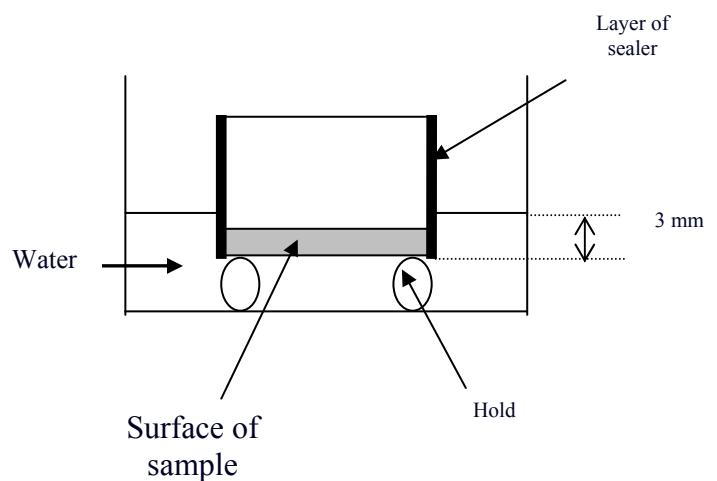
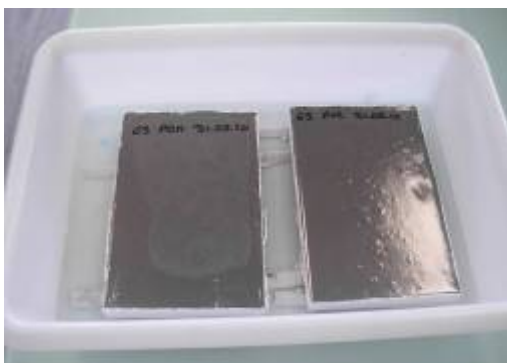


Figure 5.1.10 Virtual description of the sorptivity measurement process.

In the following tables, the results of every immersion for each sample, are presented.

Time (min)	Time in min ^{0,5}	Mass(g)	% water uptake (in mass)*10 ⁻²	water uptake / surface(g/cm ²)*10 ⁻²	Mt(g)	Q/A [mm]*10 ⁻²
0	0	36,2	0	0	0	0
1	1	36,22	5,5	0,15	0,02	0,14
4	2	36,24	11,05	0,29	0,04	0,29
9	3	36,25	13,81	0,37	0,05	0,37
16	4	36,26	16,57	0,45	0,06	0,44
25	5	36,32	33,15	0,89	0,12	0,89
36	6	36,32	33,15	0,89	0,12	0,89
49	7	36,32	33,15	0,89	0,12	0,89
64	8	36,34	38,67	1,05	0,14	1,04
100	10	36,37	46,96	1,26	0,17	1,26

Table 5.1.2 Results of the surface absorption measurements for the UHPC sample with 7% chitosan 652 + 2% citric acid + 4% CR₂ + 4% additive MN coating film.

Time (min)	Time in min ^{0,5}	Mass(g)	water uptake (in mass) *10 ⁻²	water uptake / surface(g/cm ²)*10 ⁻²	Mt(g)	Q/A [mm]*10 ⁻²
0	0	90,94	0	0	0	0
1	1	91,13	20,89	0,58	0,19	0,58
4	2	91,13	20,89	0,58	0,19	0,58
9	3	91,14	21,99	0,61	0,2	0,61
16	4	91,14	21,99	0,61	0,2	0,61
25	5	91,16	24,19	0,67	0,22	0,67
36	6	91,16	24,19	0,67	0,22	0,67
49	7	91,17	25,29	0,70	0,23	0,70
64	8	91,21	29,68	0,83	0,27	0,83
100	10	91,21	29,68	0,83	0,27	0,83

Table 5.1.3 Results of the surface absorption measurements of the UHPC sample with 7% chitosan 652 + 2% citric acid + 2% CR₃ + 4% additive MN coating film.

Additionally, the following graphs show the water absorption of our samples as a function of time.

From graphs 5.1.11, it can be seen that in the case of CR₂-additive MN the water absorption follows almost a linear relationship with $t^{1/2}$, with a very small deviation from the linearity as evidenced by the value of the linear coefficient $R^2=0.9578$. Additionally, the absorption at the beginning is less than that of the UHPC reference leading to protection of the surface from water for a short period until the time exposed in water exceeds 16 min., where the surface absorption increases.

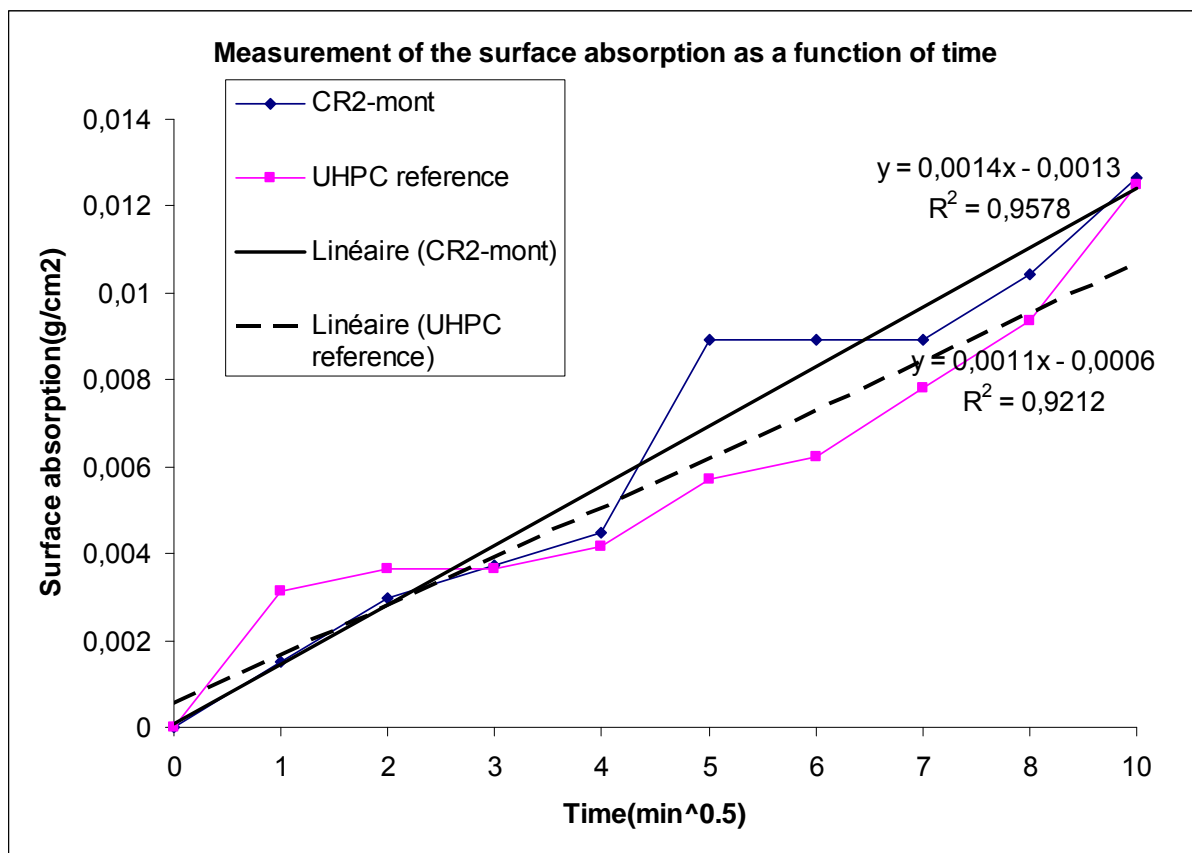


Figure 5.1.11 Surface absorption of UHPC sample with 7% chitosan 652 + 2% citric acid + 4% CR₂ + 4% additive MN coating film as a function of time.

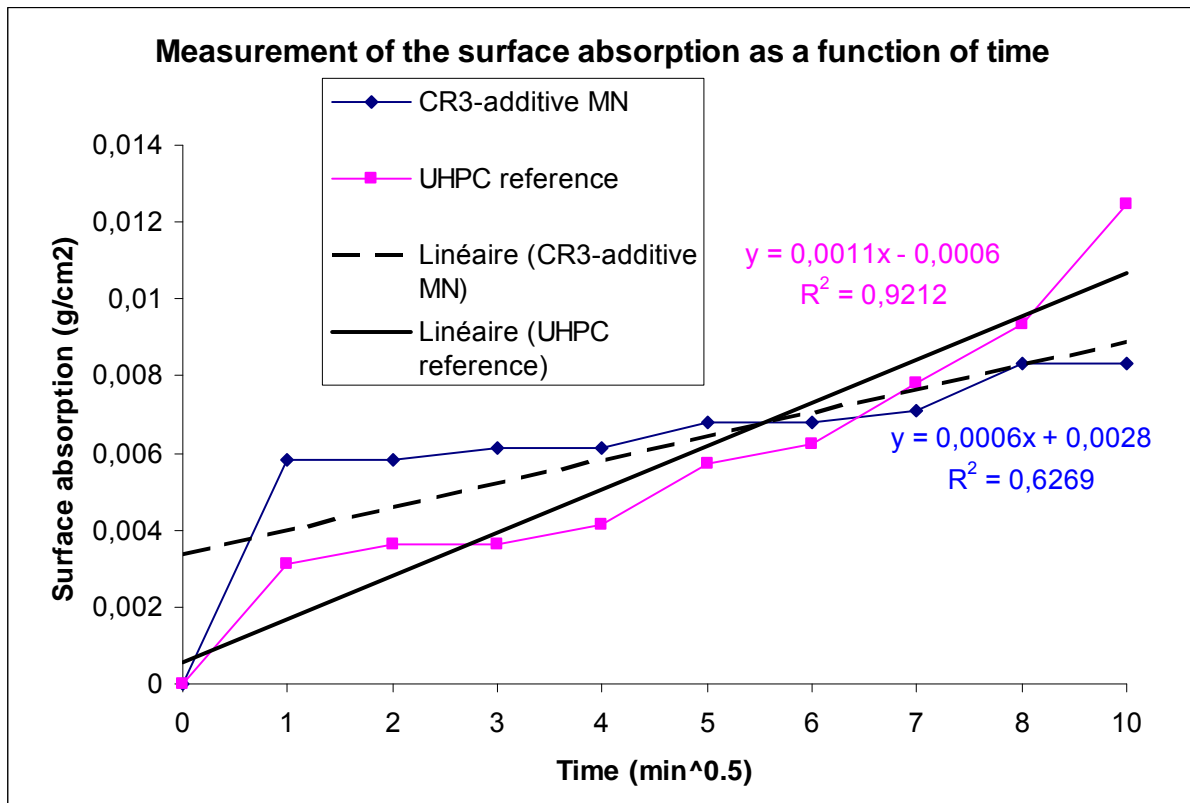


Figure 5.1.12 Surface absorption of UHPC sample with 7% chitosan 652 + 2% citric acid + 2% CR₃ + 4% additive MN coating film as a function of time.

On the other hand, in the case of CR₃-additive MN (Figure 5.1.12) the water absorption deviates from linearity, $R^2 = 0.6269$, due to the high water absorption during the first immersion. After this point, as observed from the graph, the water absorption is very low, less than 0.002 g/cm², until the end of the measurements and the relationship with $t^{1/2}$ is considered linear. In this case, even if the water absorption is higher at the start compared to that of the UHPC reference, after a period above 40 min. the water absorption decreases and becomes less than the UHPC reference.

From the equation, $i = S \cdot t^{0.5} + A$, where S is the sorptivity in mg/cm²/min^{1/2}, T is the elapsed time in min^{1/2} and a is a constant, the sorptivity can be determined, which is equal to 0.0014 and 0.0006 respectively.

2) Mechanical Tests

Mechanical tests were performed in a hydraulic press type Zwick HA 250. The method used was three balls biaxial flexural testing in disks of 50mm diameter and 10mm high. Two disks were dip-coated in solutions of 7% chitosan 652 + 2% citric acid + 4% CR₂ or 2% CR₃ + 4% additive MN, respectively, in order to compare them with a reference one. The comparison ended up in expected results regarding the contribution of the coatings on the UHPC substrate. The three different stress-strain curves (Figure 5.1.13) showed that the treated samples exhibited higher elastic deformation (El. def.) and yield point with the sample containing CR₃ showing better mechanical properties. In addition, the plastic deformation (Pl. def.) is obvious in the case of CR₃ containing coating, in contrast to the rest of the samples that did not show any plastic area. Here should be mentioned that the results have been modified based on the thickness of the samples.

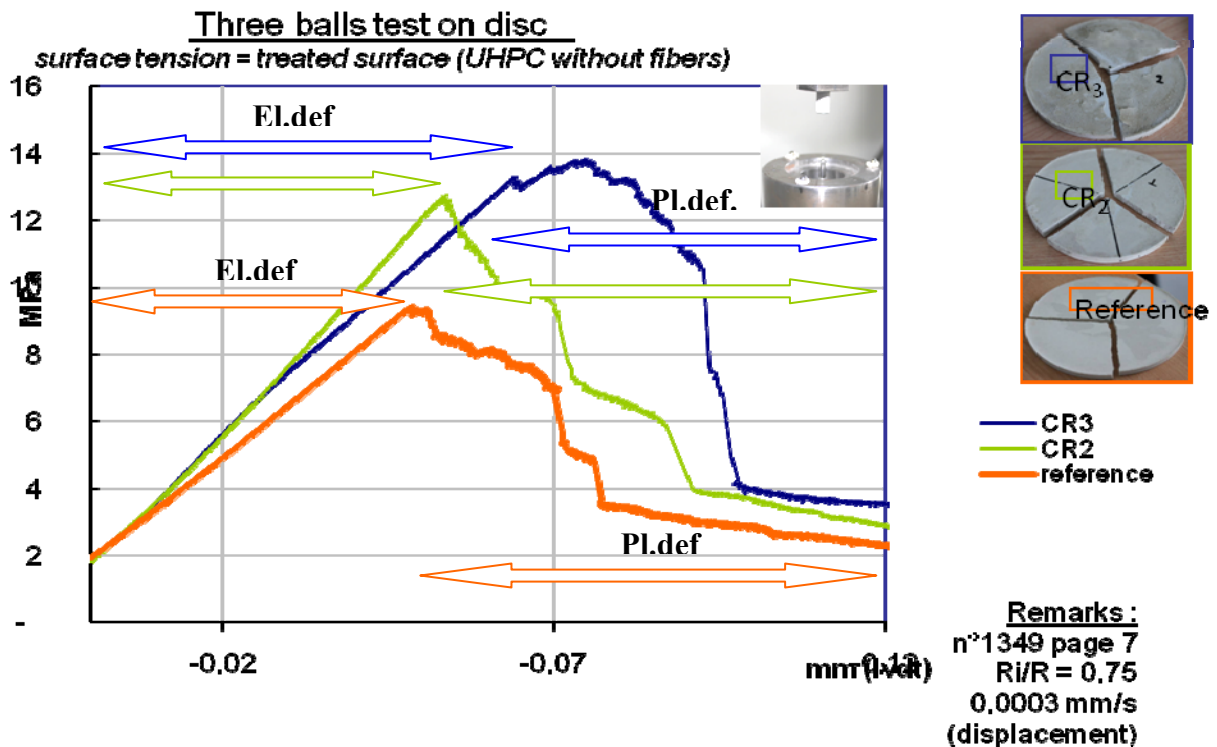


Figure 5.1.13 Three balls test on disk (integral in the graph image) of a reference UHPC (left up), a treated with chitosan 652, additive MN and CR₂ UHPC substrate (left middle) and a treated with chitosan 652, additive MN and CR₃ (left down). The graph shows the behaviour of each coated UHPC substrate in comparison with the reference one.

3) Scratching Tests

The scratching tests were performed with a tool provided by SHEEN Instruments Company. The tool was placed on the surface of a sample with a force applied perpendicular to this. Then, a sharp movement parallel to the surface excoriated the coating. The same procedure was followed with a movement vertically to the lines induced by the first scratching. By this way, conclusion can emerge for the stability and the well-adhesion of the coating on the surface.

For both of our best samples (7% chitosan 652 + 2% citric acid + 2 % CR₃ in water or 4% CR₂ in water + 4% additive MN) almost the same conclusion emerged as it can be observed from Figure 5.1.14. Scratching of the surface did not induce any disorder on the coating leading to the high stability and difficulty to debond from the surface.

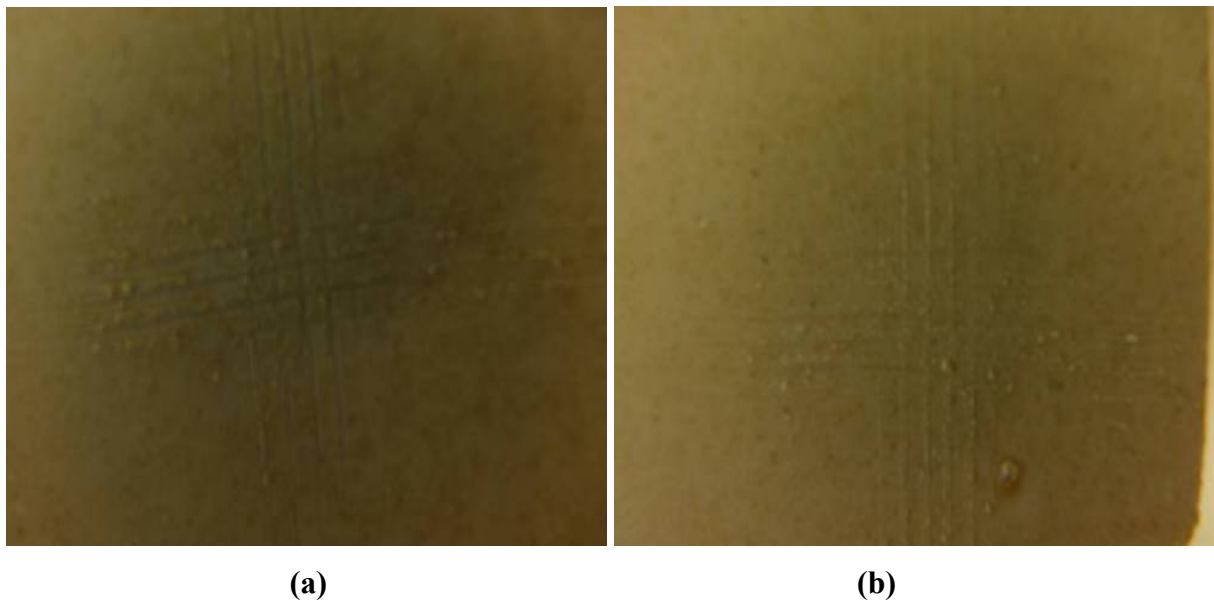


Figure 5.1.14 Scratching tests that were applied in the best of our samples 7% chitosan 652 + 2% citric acid + 2% CR₃ in water + 4% additive MN (a) and in 7% chitosan 652 + 2% citric acid + 4% CR₂ + 4% additive MN in water (b).

4) Water Contact Angle (WCA) Measurements

The WCA values were acquired on a Drop Shape Analysis-DSA 100 contact angle system, provided by Kruss, at room temperature in ambient atmosphere. A drop of 10ml of water was deposited on the coating.

	Water Contact angle
UHPC reference	15-30°
CR ₃ + Additive MN	90°
CR ₂ + Additive MN	77°

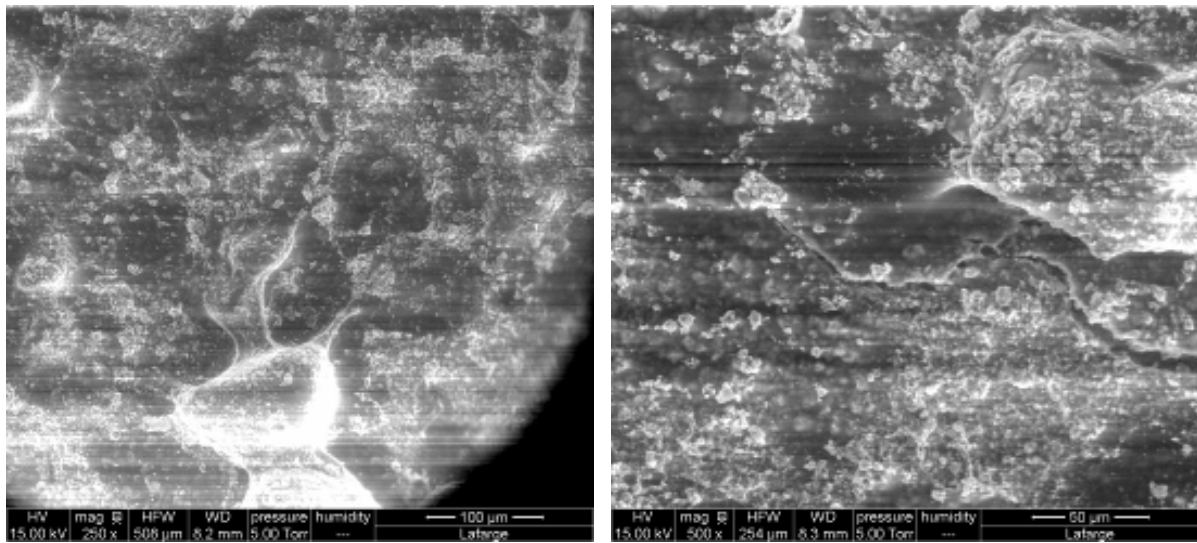
Table 5.1.4 Results of the WCA measurements of the UHPC sample with 7% chitosan 652 + 2% citric acid + 2% CR₃ + 4% additive MN coating film.

Table 5.1.4 shows the results of the tests carried out in reference UHPC substrates and of dip-coated solutions of chitosan 652 and citric acid mixed with additives MN and from the CR series. It can be obtained that the coating, which contains additive MN and CR₃, shows hydrophobic properties and the WCA significantly increased compare to reference UHPC. The latter was also observed in the case of additive MN and CR₂ although without exhibiting high hydrophobic properties.

5.1.2 Spin coating method

The solutions were prepared and used during the spin coating method and listed in Table 4.1.2. Here, the results from Scanning Electron Microscopy of the samples will be demonstrated. SEM images have been taken to determine the surface structure of the coatings. Only the surface analysis has been done but not a cross-section, due to the lack of a complete spread of the droplet on the substrate. The images are sited below each solution's description.

A) Solution of 7% chitosan 652 + 2% citric acid + 5% CR₂ in H₂O



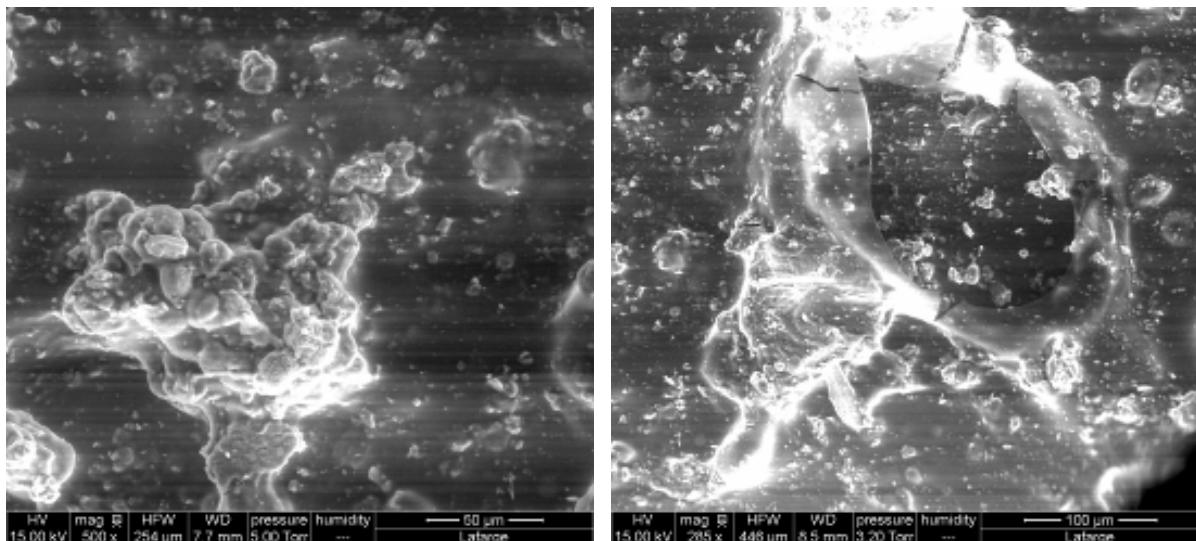
(a)

(b)

Figure 5.1.15 SEM images of the surface of coating and of a 7% chitosan 652 + 2% citric acid + 5% CR₂ in H₂O spin coated solution.

The SEM image illustrated a dispersion of CR₂ additive in chitosan 652 solution over the UHPC substrate where a homogeneously coating formed, although some cracks were observed. The particles of the additives were highly linked into the chitosan 652 film.

B) Solution of 7% chitosan 652 + 2% citric acid + 2% CR₃ + 4% additive MN in H₂O



(a)

(b)

Figure 5.1.16 SEM images of the surface of coating and of a 7% chitosan 652 + 2% citric acid + 2% CR₃ + 4% additive MN in H₂O spin-coated solution.

With a mixture of CR₃ and additive MN into chitosan 652 solution, cracks as well as particle clusters were observed. The areas of the substrate were covered homogeneously by the solution. This result confirms the one obtained after dip-coating.

C) Solution of 7% chitosan 652 + 2% citric acid + 5% CR₁ in H₂O

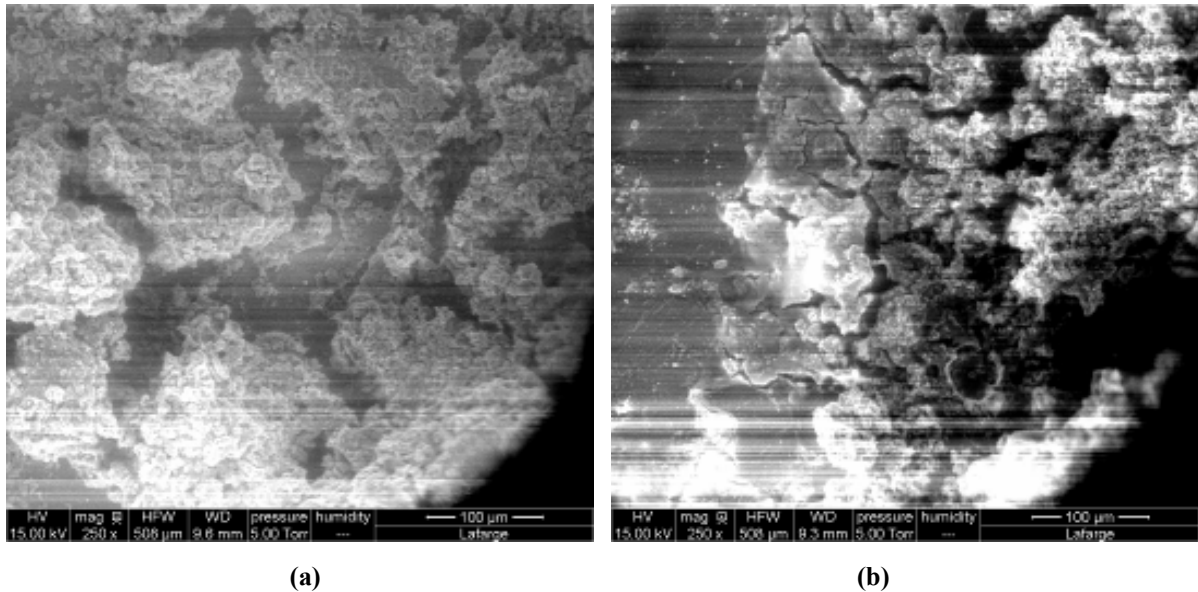


Figure 5.1.17 SEM images of the surface of coating and of a 7% chitosan 652 + 2% citric acid + 5% CR₁ in H₂O spin-coated solution.

The final solution spin coated on the UHPC substrate was a mixture of CR₁ in chitosan 652 solution. The SEM images illustrate cracks and clusters of particles inside a heterogeneous coating. The introduction of CR₁ in the solution did not allow a well-dispersed and uniform coating resulting in the deformation of the additives and incompatible linkage between them.

5.1.3 Storage in bath

As mentioned in chapter 4.1.3 the storage of the coated UHPC substrate in a bath lasted for 7 days and a drying of 7 days followed, to achieve the best environmental conditions on the surface for SEM analysis. All the solutions prepared are mentioned in Table 4.1.2 and the results are demonstrated below. Pictures of viewpoints and SEM images of the samples were taken and showed. The choice of the samples analyzed by SEM was based on the best performance of the coating and its distribution. Viewpoints that are not displayed concern no alteration of the view.

A) Solution of 1% chitosan 652 + 1% citric acid + 5% CR₁ in H₂O

The addition of CR₁ in polyelectrolyte solution and the storage in bath led to no visible formation of layer on the substrate as well as marks of concentrated solution.

B) Solution of 2% chitosan 652 + 1% citric acid + 5% CR₁ in H₂O



Figure 5.1.18 View of UHPC surface after deposition of coating

By addition of a small quantity (1%) of chitosan 652 in the solution, the change at the view of the surface is visible. Even if no mineral film formed, crystallization of CR₁ in the organic was significant and covered the entire UHPC substrate (Figure 5.1.18). The disadvantage of low durability (it could be easily removed by applying force) did not allow further investigation.

C) Solution of 3% chitosan 652 + 1% citric acid + 5% CR₁ in H₂O

The addition of 1% chitosan 652 in contrast to the first increase of chitosan 652 concentration, did not change the view of the surface.

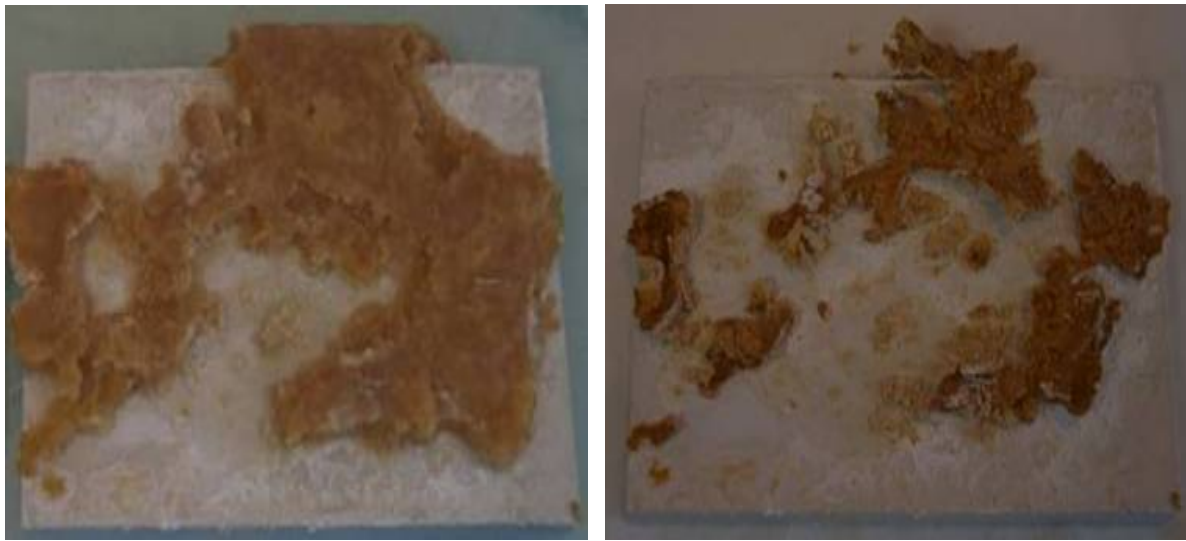
D) Solution of 7% chitosan 652 + 1% citric acid + 5% CR₁ in H₂O

(a)

(b)

Figure 5.1.19 View of UHPC surface after deposition of coating (a) and after drying for 24h (b).

The increase of chitosan 652 concentration led to the formation of a solution with very high viscosity. A thick film covered a part of the sample (Figure 5.1.19(a)), not very well-adhered on the surface with its properties resulting in low durability. The low adherence on the substrate was verified after 24h drying, where the coating totally debonded and the reaction with the atmosphere directed into shrinkage of the film (Figure 5.1.19(b)).

E) Solution of 20% chitosan 652 + 1% citric acid + 5% CR₁ in H₂O

(a)

(b)

Figure 5.1.20 View of UHPC surface after deposition of coating (a) and after drying for 24h (b).

An attempt was made to achieve as high chitosan 652 concentration as possible to define the influence of the organic on film formation. Thus, an increase to 20% of polyelectrolyte was reached, leading to high-viscous gel. Heating of the solution to 45°C during the stirring took place to reduce its viscosity. The solution though, remained very highly viscous with low durability. As before, the sample dried for 24h before again the film debond from the substrate (Figure 5.1.20(b)).

As observed, in the case using CR₁, with the aim to induce crystallization and to form a well-distributed coating on the substrate, the effect of the organic is remarkable. There is a critical range concentration where chitosan 652 acts as a crystallization precursor and where further addition of the organic leads to formation of solution with high viscosity.

Instead of CR₁, CR₂ was used as additive, for the formation of a homogeneous distribution of the coating.

F) Solution of 1% chitosan 652 + 1% citric acid + 5% CR₂ in H₂O



Figure 5.1.21 View of UHPC surface after deposition of coating.

In 1% chitosan 652 concentration, the UHPC substrate was covered by a homogeneous distributed coating very well-adhered and stable which produced a highly viscous solution (Figure 5.1.21).

MN additive acts as a reinforced and structural composer into the solution with the aim to induce a denser film, which will reduce the porosity of the substrate and will facilitate the crystallization. For this reason, a series of samples containing MN additive have been prepared and mixed with additives of CR series.

G) Solution of 7% chitosan 652 + 2% citric acid + 4% CR₂ + 4% additive MN in H₂O

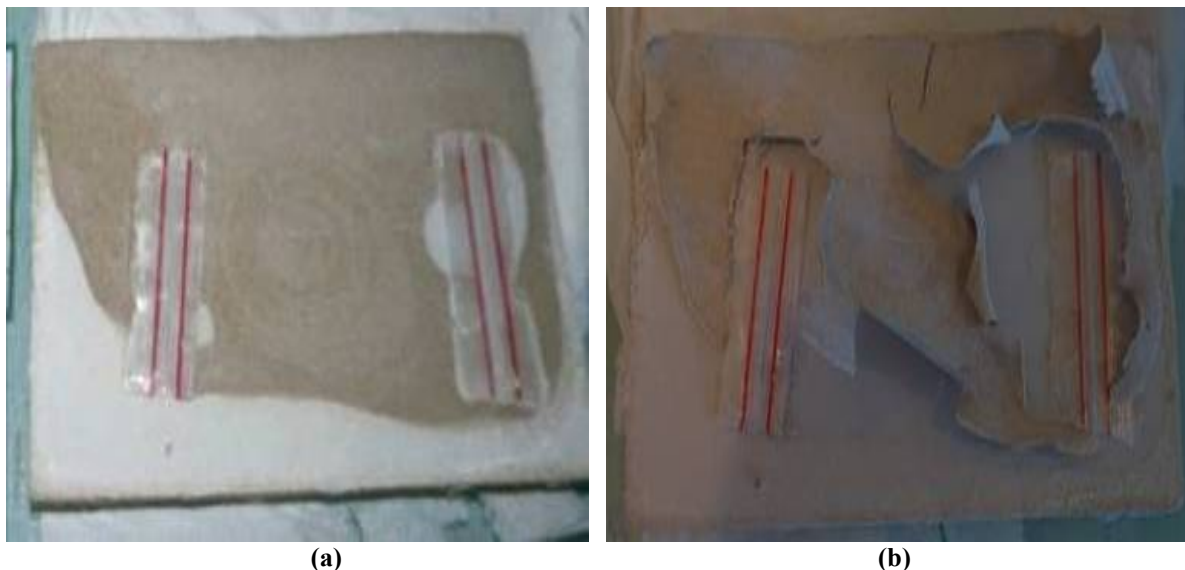


Figure 5.1.22 View of UHPC surface after deposition of coating (a) and after drying for 24h (b).

From Figure 5.1.22, it is observed that the effect of the additive MN in the film formation is notable. First, a better distributed film compared to that containing only additives CR formed. Furthermore, the wettability of the coating on UHPC is lower, which also affects the durability. It is important to notice that the use of additive MN resulted in a less porous film.

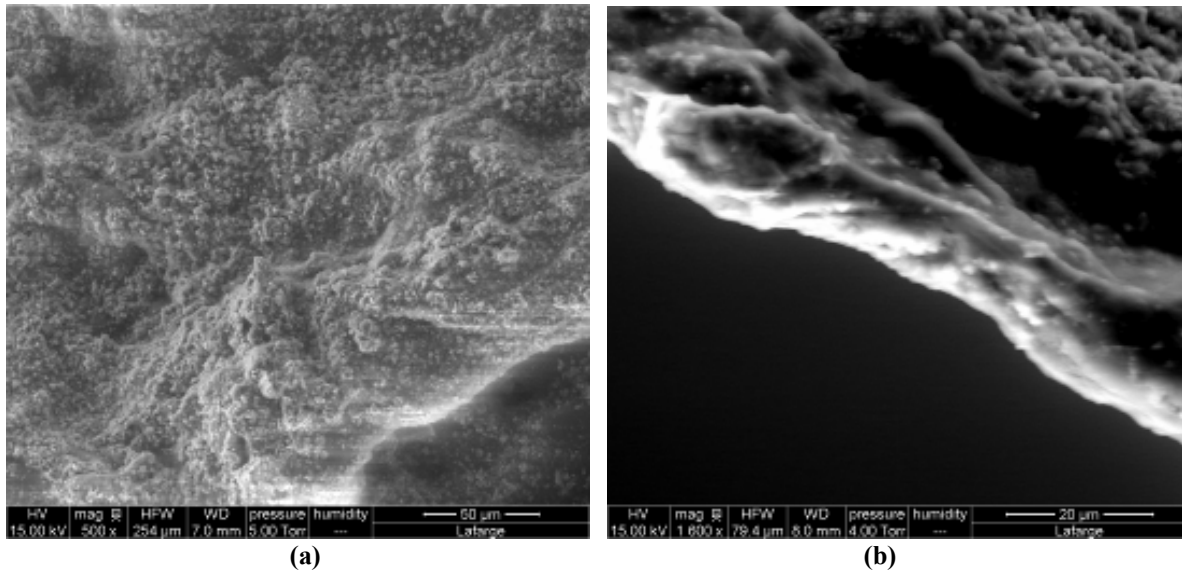
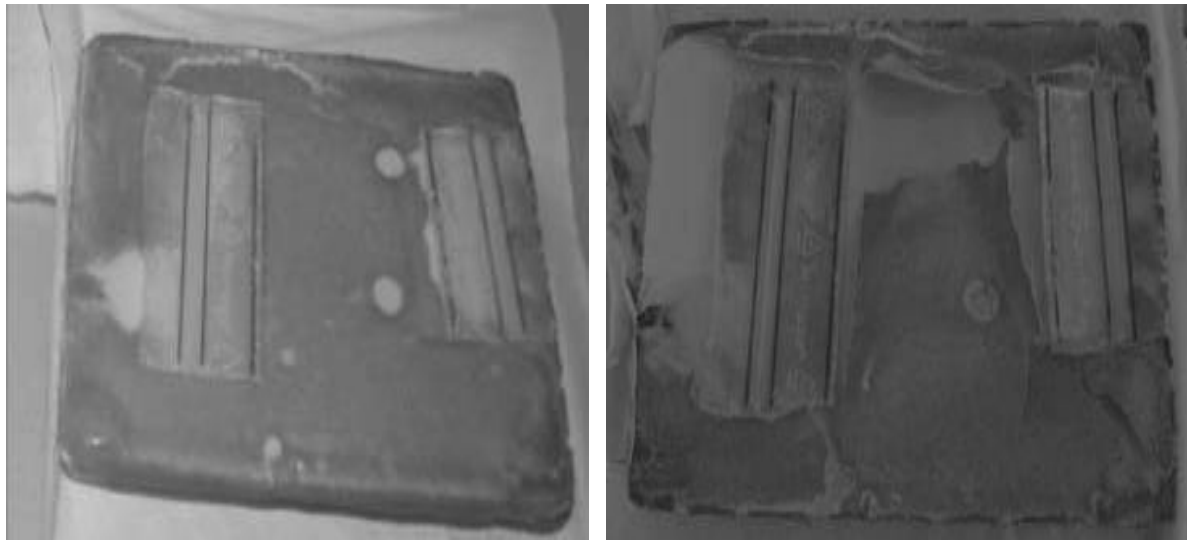


Figure 5.1.23 SEM images of the surface of coating (a) and (b) and cross-section (c) and (d) of a 7% chitosan 652 + 2% citric acid + 4% CR₂ + 4% additive MN in H₂O.

From the SEM images (Figure 5.1.23), the effect of MN additive relevant with the density of the film and the porosity can be observed. Thus, fine particles linked together by an organic film, encouraging the formation of a dense and well-dispersed homogeneous film with just a few cracks present (Figure 5.1.23(a)). The observations of cross-section images showed a homogeneous and cohesive layer (Figure 5.1.23(b)).

H) Solution of 7% chitosan 652 + 2% citric acid + 2% CR₃ + 4% additive MN in H₂O

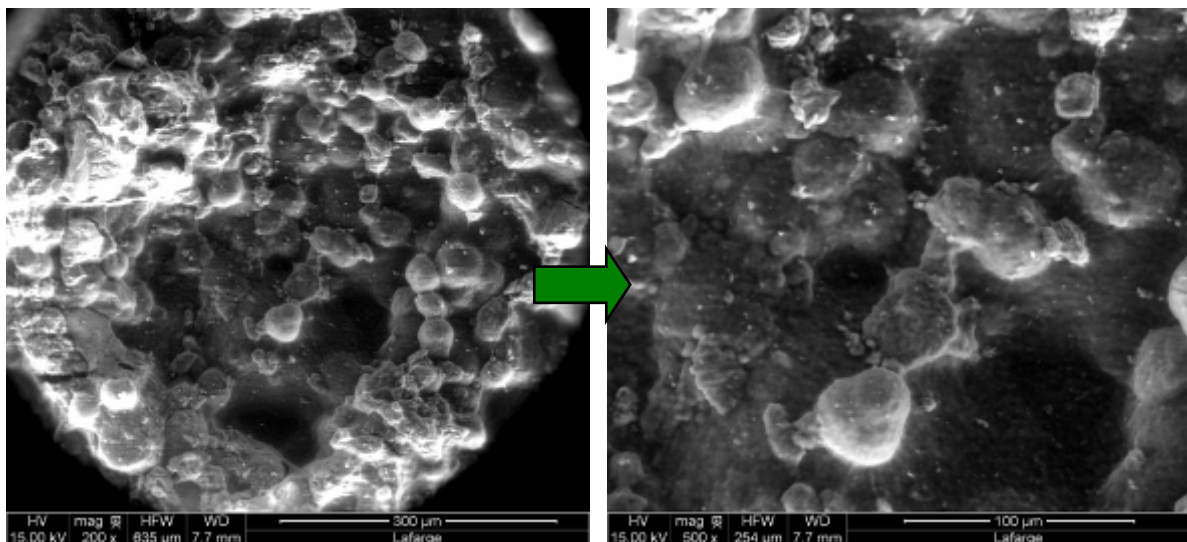


(a)

(b)

Figure 5.1.24 View of UHPC surface after deposition of coating (a) and after drying for 24h (b).

Same results, in terms of the adhesion of the coating on the substrate, were detected in the case of CR₃ as an additive of the CR series. A thick organic layer formed on the UHPC substrate, which covered the entire surface (Figure 5.1.24(a)). After 24h though, debonding of the film from the substrate occurred (Figure 5.1.24(b)) and the cohesive film could be removed easily.



(a)

(b)

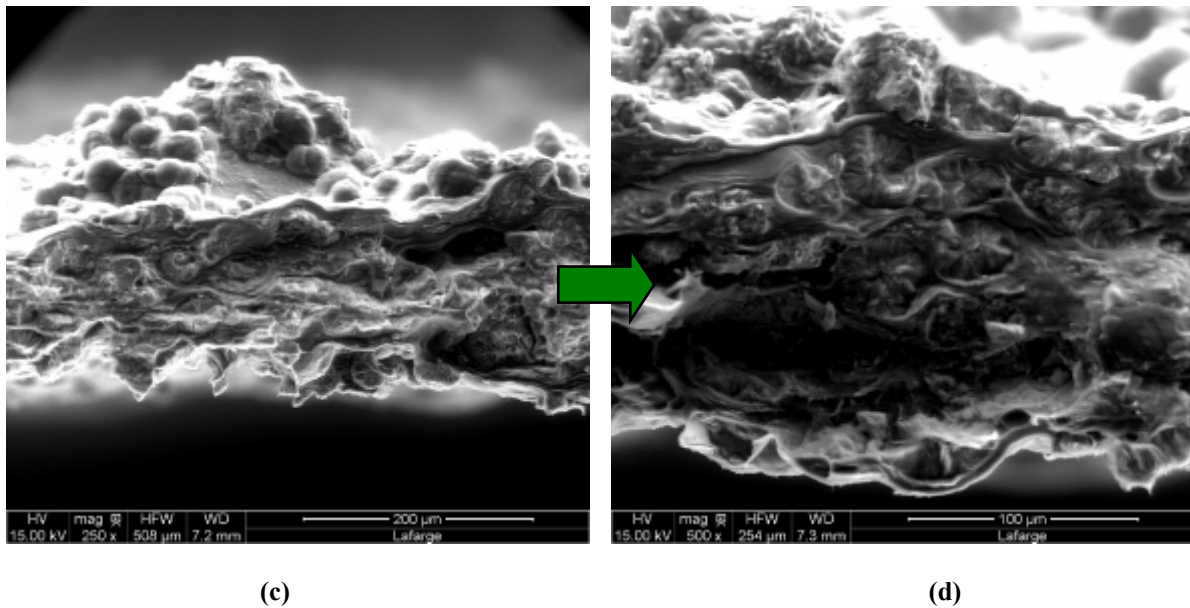


Figure 5.1.25 SEM images of the surface of coating (a) and (b) and cross-section (c) and (d) of a 7% chitosan 652 + 2% citric acid + 2% CR₃ + 4% MN additive in H₂O.

The SEM images show the formation of a rough film consisting of CR and MN additives agglomerations in an organic film (Figure 5.1.25(a)). In the cross-section image, the growth of particles between the organic layers is significant (Figure 5.1.25(b)).

5.2 Control of the crystallization of CaCO₃

5.2.1 Dip-coating of organic/carbonates layers

The solutions prepared for the deposition by this method are described in Chapter 4.2.1. The organics used were a) chitosan 652, b) alginate, c) carageenan, d) stearate, e) CarboxylMethylCellulose. As mentioned during the experimental procedure, the UHPC substrate was dip-coated in a variety of solutions to obtain crystallization of CaCO₃ on the surface. The results related with SEM analysis are listed below.

A) Solution of 1% chitosan 652 + 1% citric acid + (10% CaCl₂+10% Na₂CO₃) in H₂O

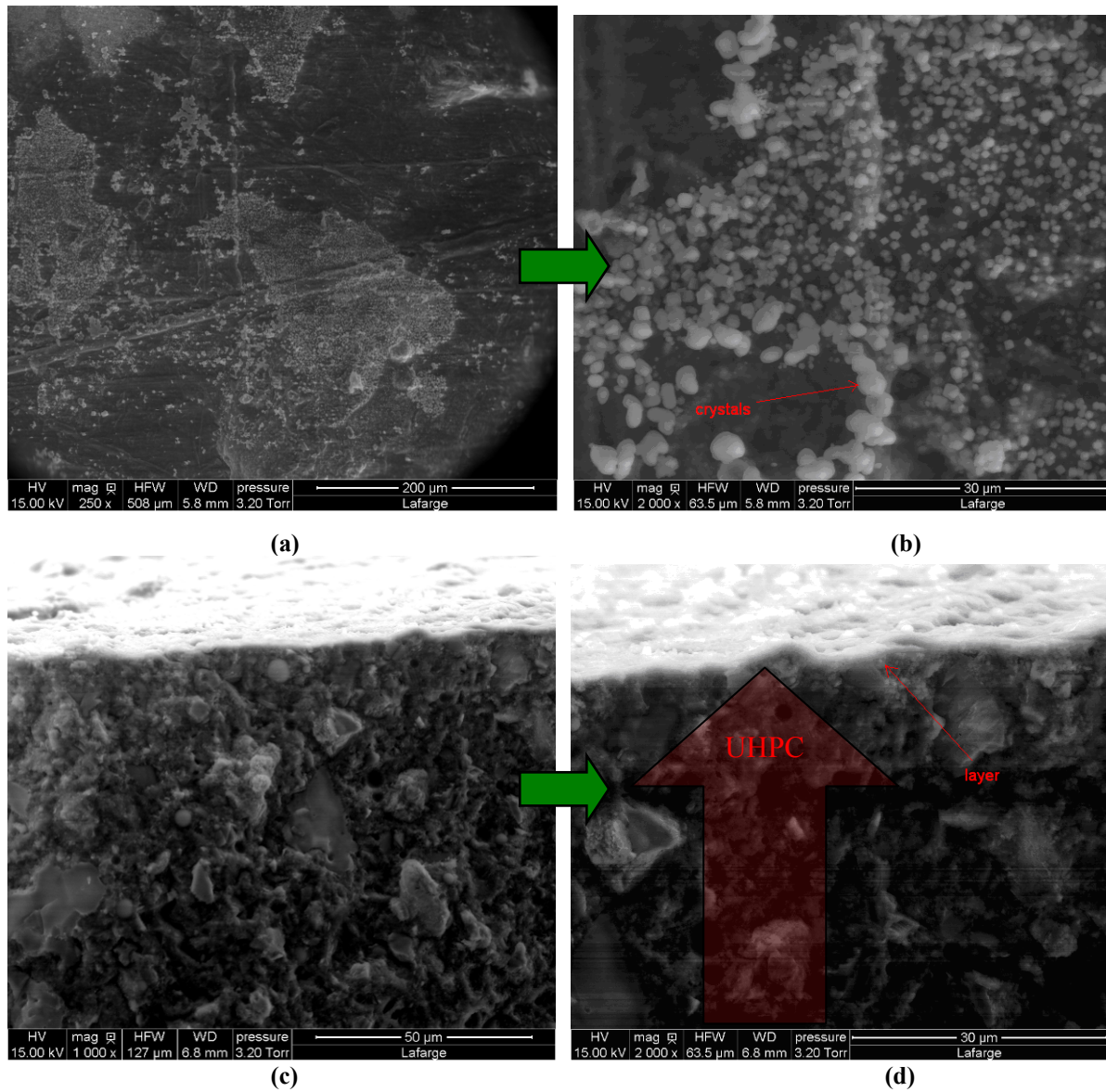


Figure 5.2.1 SEM images of the surface of coating (a) and (b), and cross-section (c) and (d) of a 1% chitosan 652 + 1% citric acid + (10% CaCl₂ + 10% Na₂CO₃) in H₂O.

Calcite crystals are observed on the surface of the sample (Figure 5.2.1(b)). The layer of chitosan 652 formed obtained on the cross-section images very well-bonded on the UHPC substrate (Figure 5.2.1(c, d)). The distribution of the crystals on the organic surface was a drawback but this might refer to the lab procedure used. Under industrial procedure, a better distribution by dip-coating could be achieved.

B) Solution of 1% chitosan 652 + 1% citric acid + (10% CaCl₂+10% Na₂CO₃) (*2) in H₂O

In the above solution two different steps followed to form organic layers. We proceed to:

- 1) First dip-coating of 1% chitosan 652 + 1% citric acid + (10% CaCl₂ + 10% Na₂CO₃) in H₂O.
- 2) Second dip-coating of the first solution.

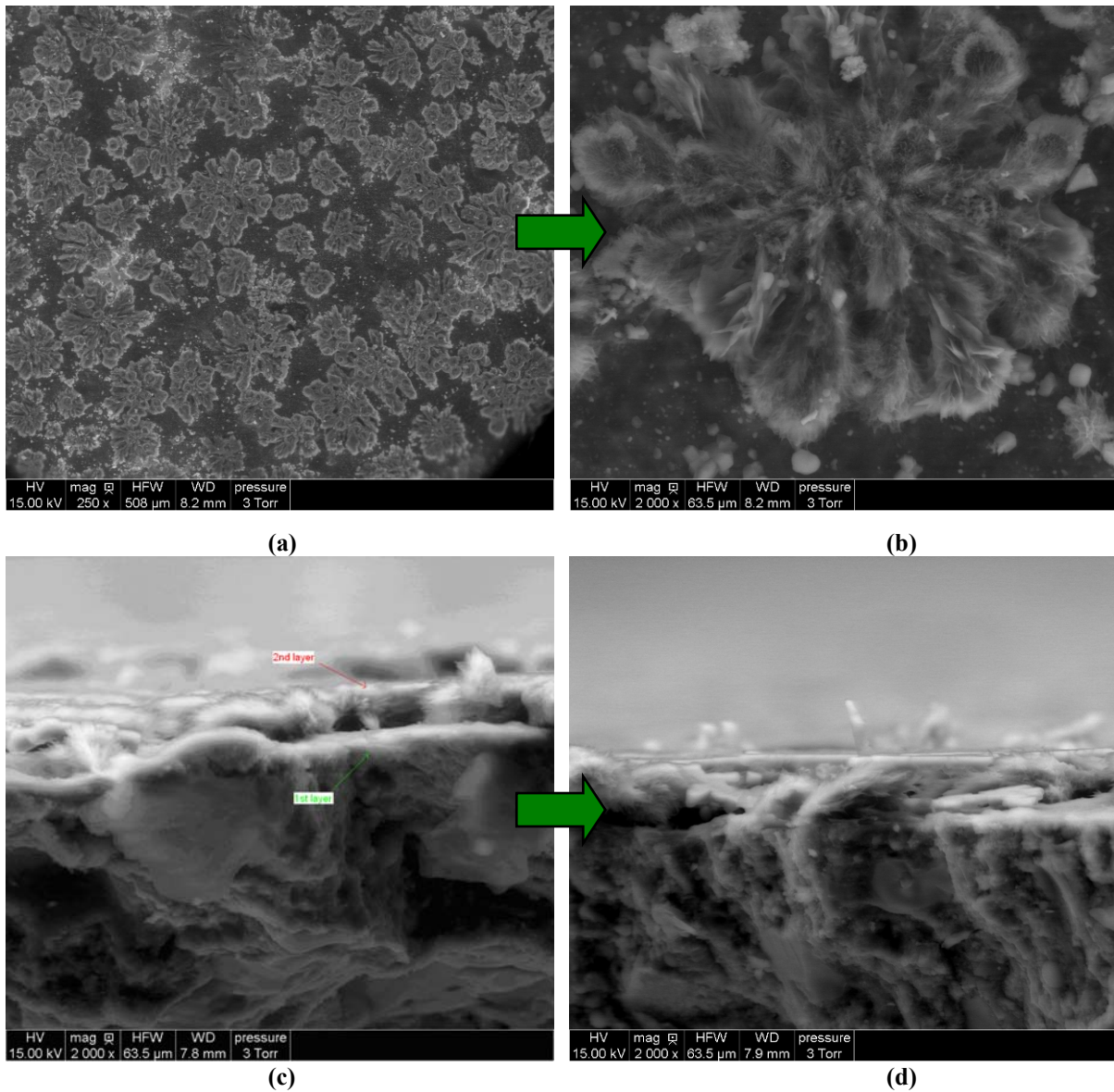


Figure 5.2.2 SEM images of the surface of coating (a) and (b) and cross-section (c) and (d) of a 1% chitosan 652 + 1% citric acid + (10% CaCl₂ + 10% Na₂CO₃) (*2) in H₂O.

From the SEM images of the surface, crystals were observed on the second organic substrate. They were better distributed compared to the previous procedure. The crystals formed on the surface have a flower shape and consist of vertically aligned needles (Figure 5.2.2(a, b)). In some parts of the surface, cubic crystals were observed. In cross-section images, two layers were formed (Figure 5.2.2(c, d)). Moreover, there are parts of the surface where crystals as vertically aligned hairs are observed. It is significant to mention that the good adherence is not only between the UHPC substrate and the first layer but also between the each layer.

Citric acid disturbs the hydration of concrete, thus an effort was made to replace it with another acid like acetic acid. The use of acetic acid not only refers to the influence in the hydration process but it also has effect on the WCA as the results show.

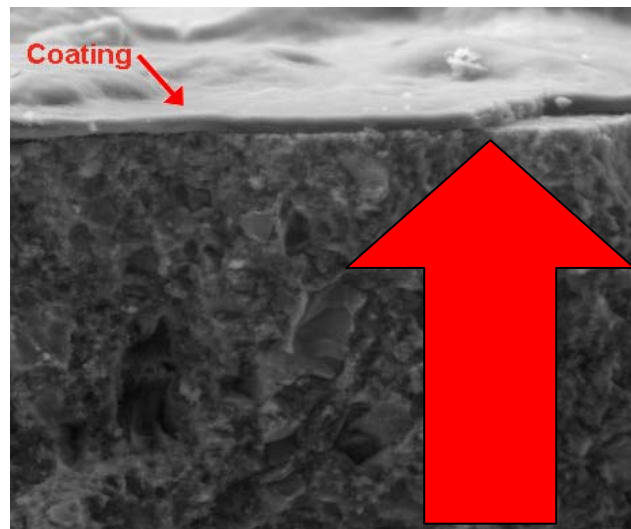


Figure 5.2.3 SEM image of cross-section of the coating from 7% chitosan 652 + 1% acetic acid.

A thin film less than $3\mu\text{m}$ formed, which was very well-adhered on the UHPC substrate (Figure 5.2.3). The WCA angle of the sample measured between 93° and 110° , which shows the highly hydrophobic properties that acetic acid induced. Most of the solution that was prepared afterwards contained acetic acid instead of citric acid.

C) Solution of 1% alginate in H₂O + (10% Na₂CO₃+ 10% CaCl₂) in H₂O

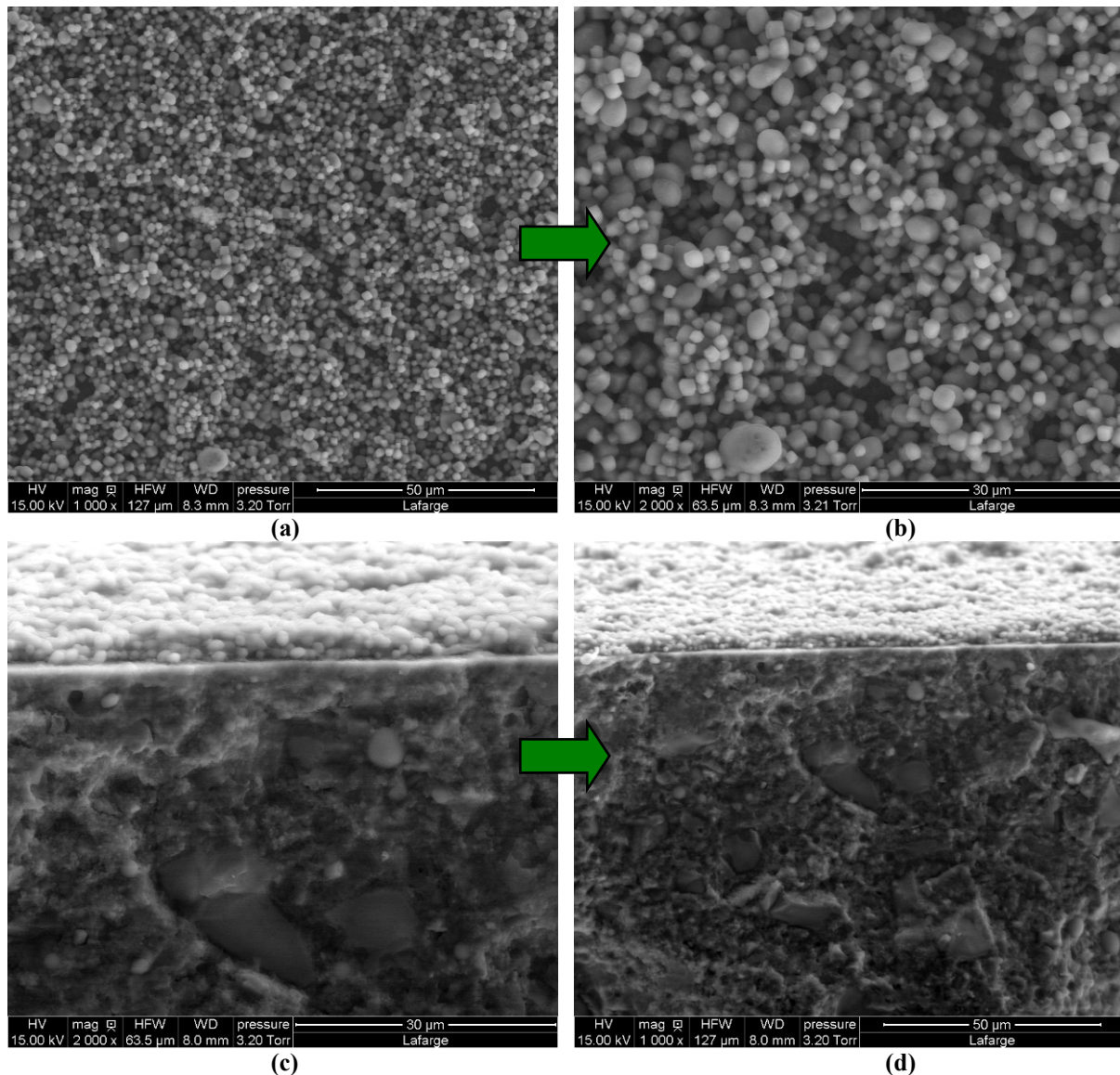


Figure 5.2.4 SEM images of the surface of coating (a) and (b) and cross-section (c) and (d) of a 1% alginate in H₂O + (10% Na₂CO₃ + 10% CaCl₂) in H₂O.

The distribution of the coating with crystals is the best achieved up to now. A film made of calcite crystals was obtained, in the rhombohedral morphology, which covered the entire surface (Figure 5.2.4(a,b)). The coating was very well-adhered to the substrate and the crystals grew inside the organic film (Figure 5.2.4(c,d)).

The existence of calcite crystals could be verified from the XRD results. The tests took place in a DX Anode Copper tool by PANalytical X'Pert with a power of 40 mA * 40 kV, scan angle for 5° to 65° with a step of 0.017 and frequency of 60s/pas while the sample was rotated.

The XRD results (Figure 5.2.5) showed the existence of calcite on the coating by showing several diffraction patterns (red peaks). The rest of the peaks indicate several phases, most appeared to be calcium silicate (Ca_3SiO_5 - green peaks) and the SiO_2 (blue peaks).

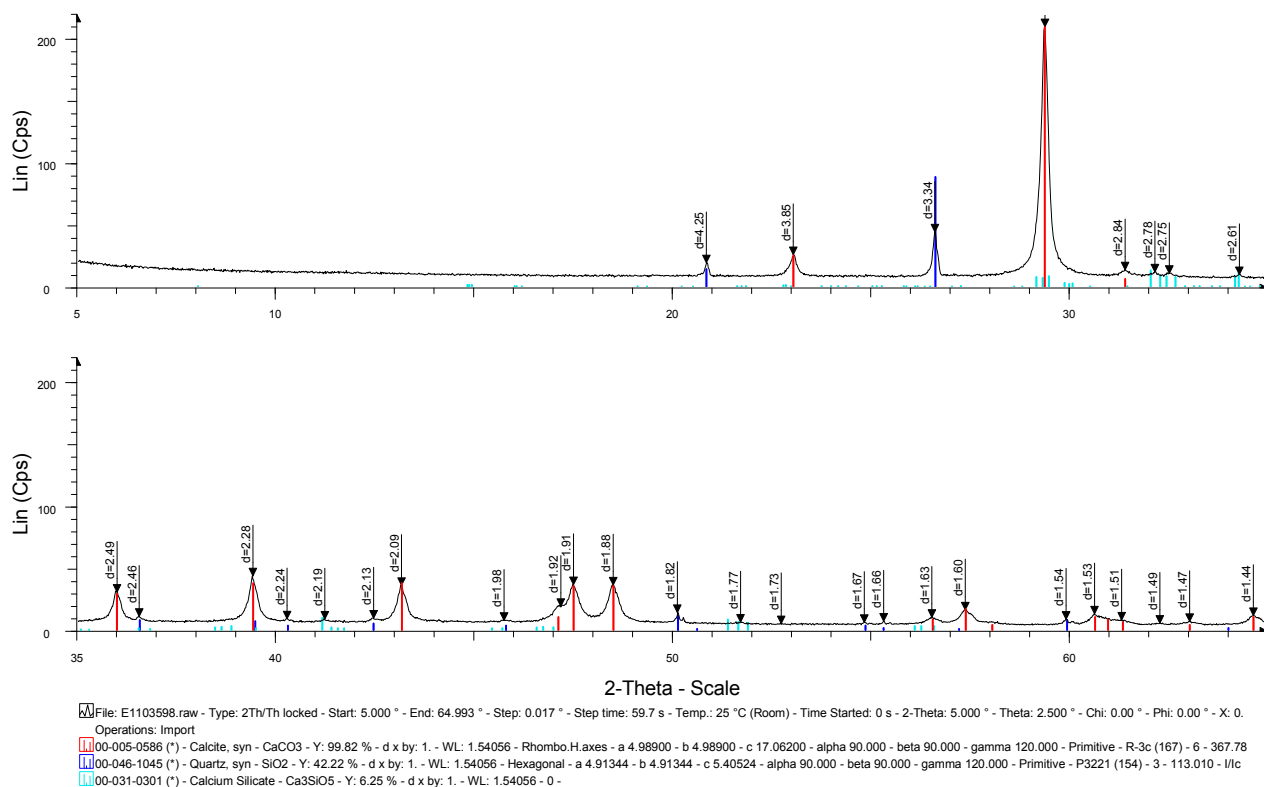


Figure 5.2.5 XRD results of the coating made by 1% alginate in H_2O + (10% Na_2CO_3 + 10% CaCl_2).

D) Solution of 1% carrageenan in H₂O + (10% Na₂CO₃+ 10% CaCl₂) in H₂O

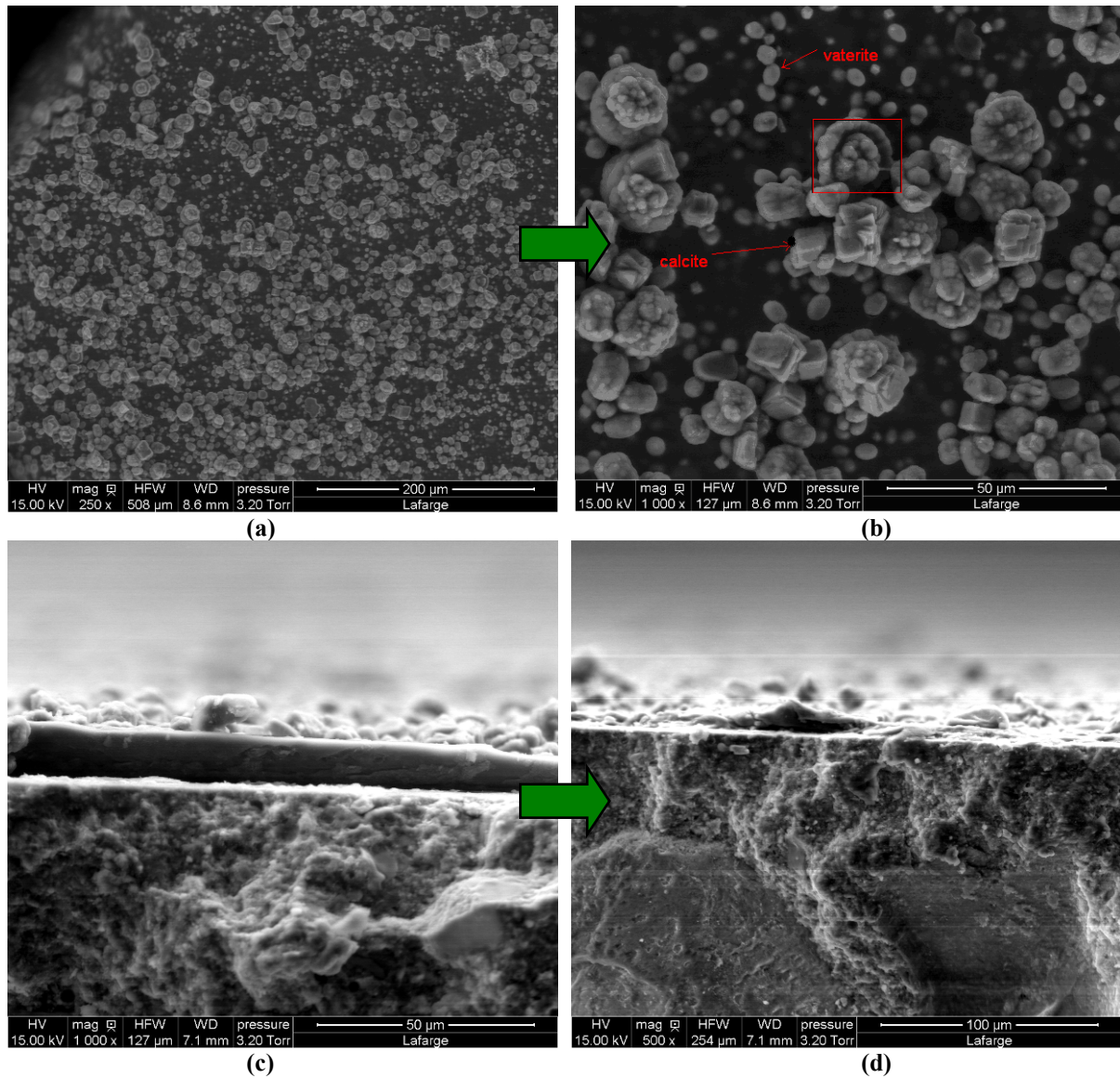


Figure 5.2.6 SEM images of the surface of coating (a) and (b) and cross-section (c) and (d) of a 1% carrageenan in H₂O + (10% Na₂CO₃ + 10% CaCl₂) in H₂O.

As previously mentioned, in the case of alginate, calcite crystals appeared in the same cubic shape. Another CaCO₃ phase, vaterite, came into view at the coating with a circular morphology. The interest here refers to the metastable phase between vaterite and calcite, which is shown in the red inset box in Figure 5.2.6 (b). The cross-section images show parts of the edges of film that debonded (Figure 5.2.6(c)) but further inside, the film was well-adhered to the substrate (Figure 5.2.6(d)). The XRD results (Figure 5.2.7) show diffraction patterns of calcite (red peaks), vaterite (green peaks) and SiO₂ (blue peaks).

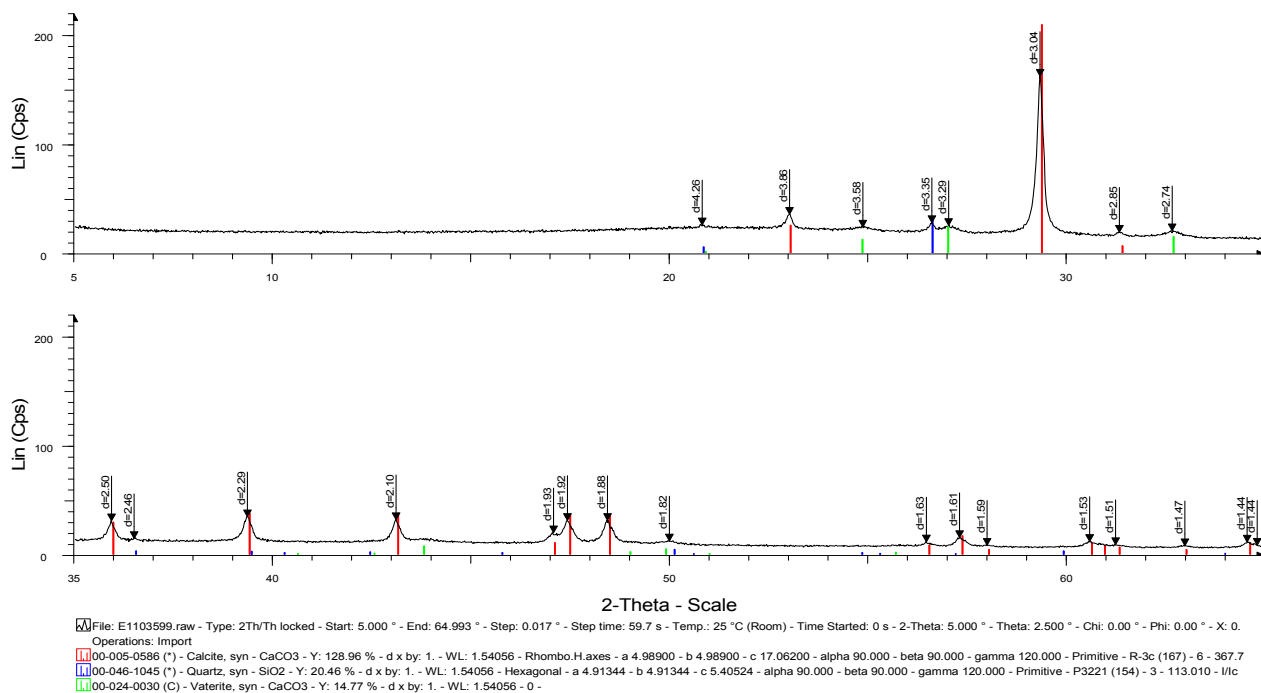
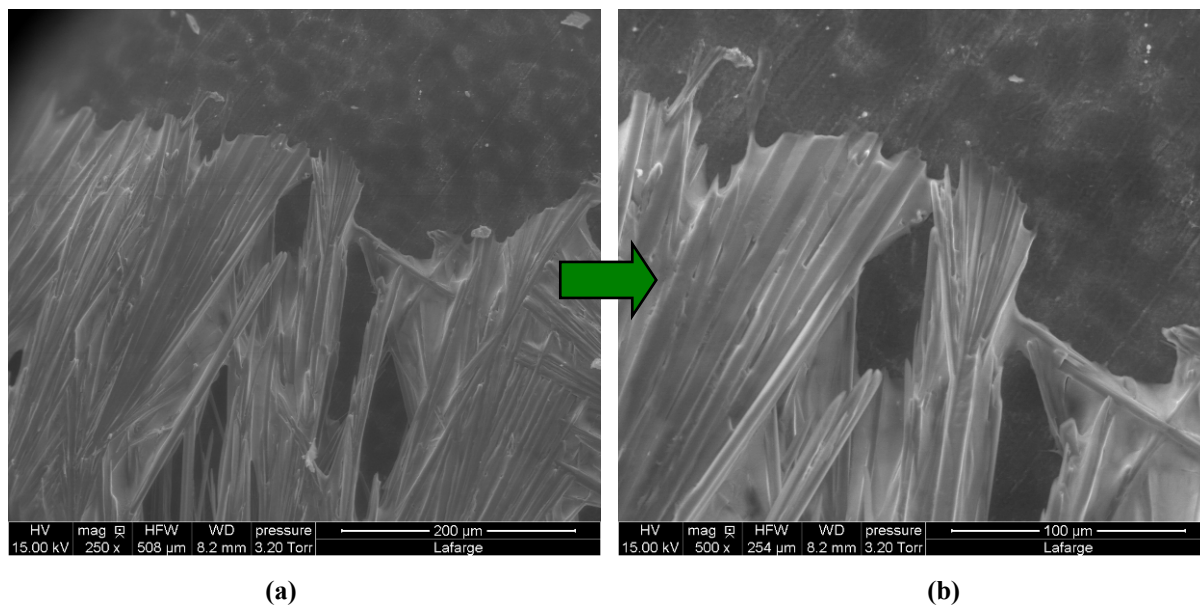


Figure 5.2.7 XRD results of the coating made by 1% carrageenan in H₂O + (10% Na₂CO₃ + 10% CaCl₂).

E) Solution of 1% stearic acid in hexane + (10% CaCl₂+ 10% Na₂CO₃) in H₂O



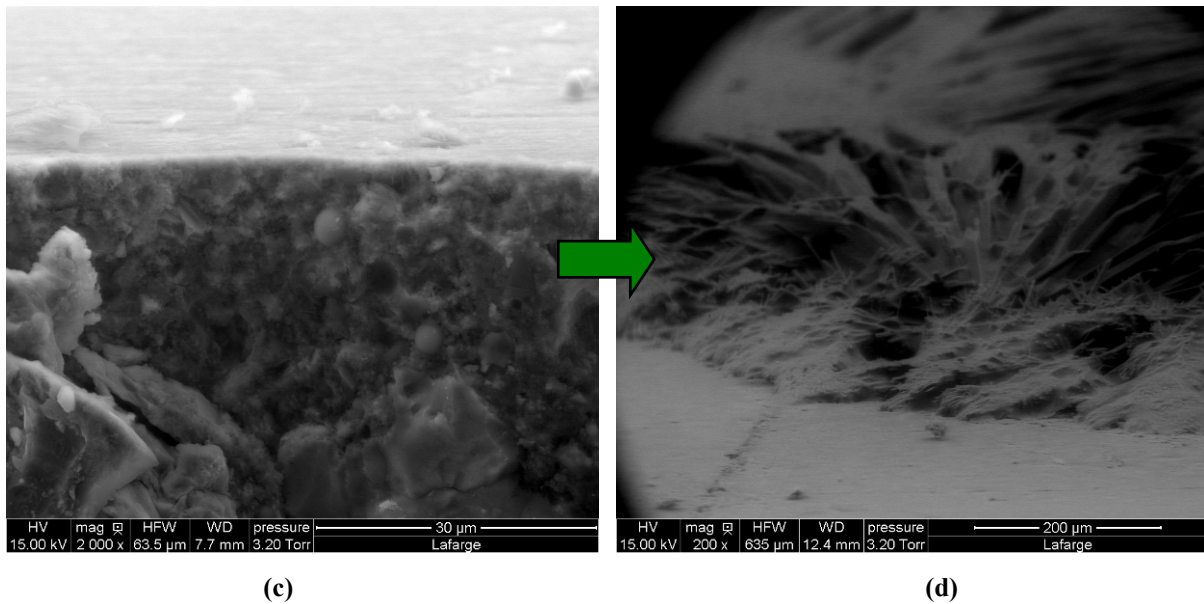


Figure 5.2.8 SEM images of the surface of coating (a) and (b) and cross-section (c) and (d) of a 1% stearic acid in hexane + (10% CaCl_2 + 10% Na_2CO_3) in H_2O deposited solution.

Stearate is one of the fatty acids not soluble in water, hence, hexane was used as solvent. Hexane is a natural non-polar solvent so hydrophobicity is one of the properties of hexane. Due to this property, the solution could not spread on the surface, but only droplets were observed on it (Figure 5.2.8(a, b)). The cross-section images (Figure 5.2.8(c, d)) did not display any specific interest.

F) Solution of 1% CarboxylMethylCellulose in H_2O + (10% CaCl_2 + 10% Na_2CO_3) in H_2O

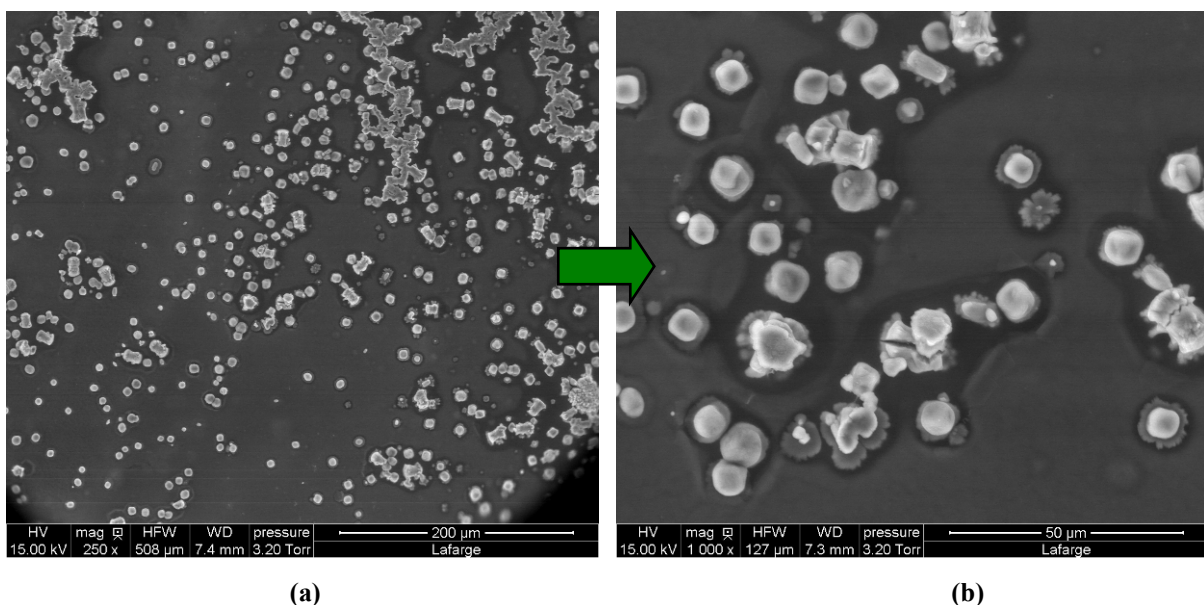


Figure 5.2.9 SEM images of the surface of coating (a) and (b) and cross-section (c) and (d) of a 1% carboxymethylcellulose in H_2O + (10% CaCl_2 + 10% Na_2CO_3) in H_2O .

The high viscosity of CMC solution did not lead to a good distribution of the carbonates on the substrate. The calcite crystals formed, agglomerated but they did not spread well (Figure 5.2.9(a, b)). The coating showed stability and good adherence on the substrate but the random distribution did not allow further investigation.

In order to broaden the study of the samples and the behaviour regarding the crystallization under specific environments, a different approach was taken referring to the change of temperature. Thus, organics as chitosan 652 and alginate were examined with the same experimental procedure, under different temperature conditions.

Organics	Minerals	Homogeneity / Composition	WCA
Chitosan 652 + acetic acid	/	homogenous coating	93-110°
Chitosan 652 + citric acid	CaCl ₂ /Na ₂ CO ₃ => CaCO ₃	heterogeneous crystallization	52°
Chitosan + citric acid (layer by layer)		more homogeneous crystallization	42°
Alginate		Only calcite – highly homogeneous	34°
Stearate		not possible to coat homogeneously	/
Carrageenan		Calcite & Vaterite – highly homogeneous	103°
CarboxyMethylCellulose (CMC)		heterogeneous crystallization	36°

Table 5.2.1 Summary of the properties of each coating related with the WCA results.

The main points that emerge from the results are that the coatings showed good homogeneity and exhibited also good WCA with hydrophobic properties or close to hydrophobicity. Chitosan 652 and carrageenan with highly homogeneous surface, good distribution of crystals and well-adherence also displayed good WCA results as can be observed from the table. On the other hand, alginate, which demonstrated highly homogeneous crystallization, exhibited also hydrophilic properties with low WCA for each different environment.

5.3 Use of substrate made of ordinary concrete and plaster

The organics deposited on the UHPC substrate showed several results and a variety of conclusions emerged from these. A challenge was to obtain how chitosan 652, the organic used the most, will interact with other substrates like ordinary concrete and plaster and how will affect them. In order to observe the influence of the concentration of organic on the surface properties, two different solutions were made based on chitosan 652. The first contains 1% chitosan 652 and the second 7% chitosan 652, both diluted in 1% acetic acid due to its best performance in terms of WCA.



Figure 5.3.1 Dip-coating of chitosan 652 + 1% acetic acid on plaster and ordinary concrete in different chitosan 652 concentrations: (a) and (c) 1% chitosan while (b) and (d) 7% chitosan .

Both of the substrates showed differences when a higher concentration of chitosan 652 was deposited on them. Plaster and ordinary concrete with 1% chitosan 652 exhibited WCA of 0° while the increase up to 7% chitosan 652 showed 98° and 103° WCA respectively with reduced porosity and no droplet absorption (Figure 5.3.1 (a), (b)). Indeed, we can conclude that the first organic layer dip coated on porous substrate, should contain a higher organic concentration to seal the substrate porosity.

6 Discussion

The main idea that this project was based on, was the inspiration by biomineralization and as a result the understanding of biomineralization strategies. Our inspiration was based on the structure of mussels-nacre and an attempt was made to mimic and finally to connect it with the bibliographic review, based on the surface properties and the promotion of hydrophobicity.

For example Aizenberg ^[74], in the work related to biomimicking the structure of echinoderms, came up with a set of new approaches to the synthesis of ordered, oriented crystalline materials at the nanoscale. In the case of echinoderms, entire skeletons are built out of CaCO_3 in the form of calcite and this carbonate structure links it with the structure of nacre. Aizenberg showed us how it is possible to promote the nucleation of crystals by epitaxial growth at specific activated sites of a CaCO_3 substrate. Epitaxy also contributes to the production of anisotropic strain at the organic/inorganic interface, which in turn will contribute to the control of shape and orientation of crystals. Even the movement of actuated spines in sea urchins could be controlled by introducing the spines in hydrogels or patterned confining surfaces. In fabricating such nanospines, Aizenberg brought in a simple two-step soft-lithography process, with the use of elastomeric molds, for creating replicates of nanostructured surfaces with definite geometries and in particulate for tilted or twisted nanospines. By that way, she was capable of mimicking different surfaces associated with echinoderms. As a result, a promising prospect is the manufacture of a substrate, which could mimic the nacre by the use of different organics and by the growth of crystals either on them or at organic/inorganic interface. Moreover, the growth of CaCO_3 crystals in activated sites of artificial nacre could lead to specific arrays that could be modified to achieve and control the wetting properties of nanostructured surfaces and to induce superhydrophobicity.

We have tried to perform different experimental procedures and methods, to find the appropriate way to deposit a coating composed of organics and carbonates on a UHPC substrate, very well adhered and distributed on it, with the aim to close also its porosity. The

best solutions, from which the coatings came by dip-coating method, were those containing high chitosan concentration and moderate amounts of MN additives and carbonates as CR₂ and CR₃ additives. Other deposition methods, such as spin-coating and storage in bath were used, but were less efficient compare to the dip-coating method. In the case of spin-coating method, the coating did not cover the entire surface during its deposition, resulting in heterogeneous distribution. On the other hand, the storage in bath method led to coating of the substrate, but also in debonding of the coating after drying. Concerning dip-coating experiments, for both CR₂ and CR₃ additives, the WCA reached values close to hydrophobicity, 77° and 90° respectively, and enhanced the mechanical properties of the reference substrate with noticeable scratching properties. The positive effect of the organic coatings on the UHPC substrate was verified also by the sorptivity measurements, where noticeable was the protection of the surface when exposed to water. Especially in the case of CR₃, the toughness of the film against the water was remarkable. Interesting results were obtained also by the scratching and mechanical tests related with the durability of the coated substrates. The use of MN additives was interesting to structure the coating and introduction of CR₂ and CR₃ help to stabilize the solution and to avoid any precipitation before its deposition on the substrate surface. In this case, no wetting or dispersive agents were needed to stabilize the solution during a few hours. MN₁ was also used in replacement of MN, but due to its different properties compare to MN additive, it could not induce a thick and stable layer leading finally to debonding of the coating from the substrate.

Secondly, we made an effort to induce CaCO₃ crystallization on the surface by the use of different organics and carbonates. Several solutions were prepared and reactions occurred between inorganic salts, such as Na₂CO₃ and CaCl₂ which led to crystal growth. Chitosan, alginate and carrageenan were the organics that best applied on the substrate, promoted crystallization and exhibited remarkable wetting properties. Especially in the case of carrageenan with Na₂CO₃ and CaCl₂, the surface was highly homogeneous and exhibited a WCA of 103°. Finally, the main CaCO₃ forms that appeared (and were confirmed by XRD), were calcite and vaterite. Each organic could enhance the creation of one of these two forms. In contrast to the organics mentioned previously, stearic acid and carboxymethylcellulose were used as well, but their polar behavior as well as bad wetting of the substrate and high viscosity respectively led to negative effect during the distribution.

Organics in higher concentrations can be used in different substrates as plasters and ordinary concrete, to close the porosity and to increase the wetting properties. Furthermore, chitosan demonstrated better performance when mixed with acetic acid instead of citric acid, but the high viscosity in presence of acetic acid led to unavoidable use of citric acid, due to the induction of cement hydration.

Further experiments will focus mainly on the use of additional organics to observe their influence on the growth of crystals and the surface properties. Such organics are lactic acid, glucono- δ -lactone and adipic acid. Moreover, the use of mussel composed of aragonite and chitosan as a substrate, is interesting due to the flat surface that mussels exhibit. Besides, the formation of multilayer of organics/carbonates to measure anti-scratching, hardness, and sorptivity properties, is another prospect of this project. Finally, Mg ions could be used in order to stabilize the crystallization and to control its kinetics and its morphology ^[4, 17, 75], as well as the use of $(\text{NH}_4)_2\text{CO}_3$ instead of Na_2CO_3 in order to obtain different morphologies.

7 Conclusions

The formation, deposition, and analysis of organic coatings in order to evaluate the influence on the surface properties of a UHPC substrate were carried out. The organic macromolecules influence the nucleation and growth of inorganic minerals by the contribution of additive. That could be used as a first step for the formation of natural biominerals to produce organic-inorganic materials such as shell, bone, and pearl. A series of insoluble organic matrixes as substrates were used for the formation of soluble inorganic matrixes in order to promote heterogeneous nucleation. These natural biomaterials (based on carbonates, natural and organic compounds) are known also for their noticeable mechanical properties. Several methods were used for the deposition of the coating on the UHPC substrate under different environmental conditions to achieve a good distribution of crystals and additives on the surface. The results showed that there are some organics (e.g chitosan, alginate, carrageenan) that could lead to crystal growth.

8 References

- [1] Meyer, H.J. **The influence of impurities on the growth rate of calcite.** Journal of Crystal Growth, 1984, 66 (3), 639–646.
- [2] Rodríguez-Clemente, R., Gómez-Morales, J. **Microwave precipitation of CaCO₃ from homogeneous solutions.** Journal of Crystal Growth, 1996, 169 (2), 339–346.
- [3] Belcher, A.M., Wu, X.H., Christensen, R.J., Hansma, P.K., Stucky, G.D., Morse, D.E. **Control of crystal phase switching and orientation by soluble mollusc-shell proteins.** Nature, 1996, 381 (6577), 56–58.
- [4] Wada, N., Yamashita, K., Umegaki, T. **Effects of carboxylic acids on calcite formation in the presence of Mg²⁺ ions.** Journal of Colloid and Interface, 1999, 212 (2), 357–364.
- [5] Mao, C., Li, H., Cui, F., Feng, Q., Wang, H., Ma, C. **Oriented growth of hydroxyapatite on (0001) textured titanium with functionalized self-assembled silane monolayer as template.** Journal of Materials Chemistry, 1998, 8 (12), 2795–2801.
- [6] Wada, N., Kanamura, K., Umegaki, T. **Effects of carboxylic acids on the crystallization of calcium carbonate.** Journal of Materials Chemistry, 2001, 233 (1), 65–72.
- [7] Xiaodeng, Y.; Guiying, X.; Yigian, C.; Fang, W.; Hongzhi, M.; Weiping, S.; Yan, B.; Houjian, G.; **CaCO₃ crystallization control by poly(ethylene oxide)-poly(propylene oxide)-polyethylene oxide triblock copolymer and O-(hydroxy isopropyl) chitosan.** Journal of Crystal Growth, 2009, 311, 4555–4559.
- [8] Addadi, L., Raz, S., Weiner, S. **Taking advantage of disorder: Amorphous calcium carbonate and its roles in biomineralization.** Advanced Materials, 2003, 15 (12), 959–970.
- [9] Braga, D. **From Amorphous to Crystalline by Design: Bio-Inspired Fabrication of Large Micropatterned Single Crystals.** Angewandte Chemie – International Edition, 2003, 42 (45), 5544–5546.
- [10] Cölfen, H. **Precipitation of carbonates: Recent progress in controlled production of complex shapes.** Current Opinion in Colloid and Interface Science, 2003, 8(1-2), 23–31.
- [11] Ajikumar, P.K., Ling, G.W., Subramanyam, G., Lakshminarayanan, R., Valiyaveetil, S. **Synthesis and characterization of monodispersed spheres of amorphous calcium carbonate and calcite spherules.** Crystal Growth and Design, 2005, 5(3), 1129–1134.
- [12] Szcześ, A., Chibowski, E., Hołysz, L. **Influence of ionic surfactants on the properties of freshly precipitated calcium carbonate.** Colloids and Surfaces A: Physicochemical and Engineering Aspects, 2007, 297 (1-3), 14–18.
- [13] Payne, S.R., Heppenstall-Butler, M., Butler, M.F. **Formation of thin calcium carbonate films on chitosan biopolymer substrates.** Crystal Growth and Design, 2007, 7 (7), 1262–1276.

- [14] Kotachi, A., Miura, T., Imai, H. **Polymorph control of calcium carbonate films in a poly(acrylic acid)-chitosan system.** *Crystal Growth and Design*, 2006, 6 (7), 1636–1641.
- [15] Wada, N., Suda, S., Kanamura, K., Umegaki, T. **Formation of thin calcium carbonate films with aragonite and vaterite forms coexisting with polyacrylic acids and chitosan membranes** *Journal of Colloid and Interface Science*, 2004, 279 (1), 167–174.
- [16] Liang, P., Zhao, Y., Shen, Q., Wang, D., Xu, D. **The effect of carboxymethyl chitosan on the precipitation of calcium carbonate.** *Journal of Crystal Growth*, 2004, 261 (4), 571–576.
- [17] Yang, X., Xu, G. **The influence of xanthan on the crystallization of calcium carbonate.** *Journal of Crystal Growth*, 2011, 314 (1), 231–238.
- [18] Ukrainczyk, M., Kontrec, J., Kralj, D. **Precipitation of different calcite crystal morphologies in the presence of sodium stearate.** *Journal of Colloid and Interface Science*, 2009, 329 (1), 89–96.
- [19] Jayaraman, A., Subramanyam, G., Sindhu, S., Ajikumar, P.K., Valiyaveetil, S. **Biomimetic synthesis of calcium carbonate thin films using hydroxylated poly(methyl methacrylate) (PMMA) template.** *Crystal Growth and Design*, 2007, 7 (1), 142–146.
- [20] He, L., Xue, R. **Formation of calcium carbonate films on chitosan substrates in the presence of polyacrylic acid.** *Journal of Solid State Chemistry*, 2009, 182 (5), 1082–1087.
- [21] Kato, T., Suzuki, T., Amamiya, T., Irie, T., Komiyama, M., Yui, H., **Effects of macromolecules on the crystallization of CaCO₃ the Formation of Organic/Inorganic Composites.** *Supramolecular Science*, 1998, 5 (3-4), 411–415.
- [22] Stempflé, P., Pantalé, O., Rousseau, M., Lopez, E., Bourrat, X. **Mechanical properties of the elemental nanocomponents of nacre structure.** *Material Science and Engineering C*, 2010, 30 (5), 715–721.
- [41] Falini, G., Fermani, S., Gazzano, M., Ripamonti, A. **Oriented crystallization of vaterite in collagenous matrices.** *Chemistry – A European Journal*, 1998, 4 (6), 1048–1052.
- [42] Dalas, E., Koutsoukos, P.G. **The crystallization of vaterite on cholesterol.** *Journal of Colloid and Interface Science*, 1989, 127 (1), 273–280.
- [43] Manoli, F., Dalas, E. **Calcium carbonate overgrowth on elastin substrate.** *Journal of Crystal Growth*, 1999, 204 (3), 369–375.
- [44] Manoli, F., Koutsopoulos, S., Dalas, E. **Crystallization of calcite on chitin.** *Journal of Crystal Growth*, 1997, 182 (1-2), 116–124
- [45] Naoya Hosoda and Takashi Kato. **Thin-Film Formation of Calcium Carbonate Crystals: Effect of Functional Groups of Matrix Polymers.** *Chemistry of Materials*, 2001, 13, 688–693.
- [46] Kuther, J.; Seschadri, R.; Knoll, W.; Tremel, W. **Templated growth of calcite, vaterite and aragonite crystals on self-assembled monolayers of substituted alkylthiols on gold.** *Journal of Materials Chemistry*, 1998, 8, 641-650.

- [47] Ueyama, N.; Hosoi, T.; Yamada, Y.; Doi, M.; Okamura, T.; Nakamura, A.; **Calcium complexes of carboxylate-containing polyamide with sterically disposed NH-O hydrogen bond: Detection of the polyamide in calcium carbonate by ^{13}C cross-polarization/magic angle spinning spectra.** *Macromolecules*, 1998, 31, X-7126.
- [48] Braun, P.V., Osenar, P., Tohver, V., Kennedy, S.B., Stupp, S.I. **Nanostructure templating in inorganic solids with organic lyotropic liquid crystals.** *Journal of the American Chemical Society*, 1999, 121 (32), 7302-7309.
- [49] Darder, M., Colilla, M., Ruiz-Hitzky, E. **Biopolymer-clay nanocomposites based on chitosan intercalated in montmorillonite.** *Chemistry of Materials*, 2003, 15 (20), 3774-3780.
- [50] Domard, A. **In Advances in Chitin Science**; Chen, R. H., Chen, H. C., Eds.; National Taiwan Ocean University Publisher: Tapei, 1998, Vol.III, 24.
- [51] Roberts, G.A.F. **In Chitin Chemistry**; Roberts, G. A. F., Macmilian Press Ltd.: London, 1992, 274.
- [52] Sorlier, P., Denuzière, A., Viton, C., Domard, A. **Relation between the degree of acetylation and the electrostatic properties of chitin and chitosan.** *Biomacromolecules*, 2001, 2 (3), 765-772.
- [53] Draget, K.I., Skjåk-Bræk, G., Smidsrød, O. **Alginate based new materials.** *International Journal of Biological Macromolecules*, 1997, 21 (1-2), 47-55.
- [54] Smidsrød, O. **Molecular basis for some physical properties of alginates in the gel state.** *Faraday Discussions of the Chemical Society*, 1974, 57, 263-274.
- [55] Kohn, R., Larsen, B. **Preparation of water-soluble polyuronic acids and their calcium salts, and the determination of calcium ion activity in relation to the degree of polymerization.** *Acta Chemica Scandinavia*, 1972, 26 (6), 2455-2468.
- [56] Smidsrod, O., Haug, A. **Dependence upon the gel-sol state of the ion-exchange properties of alginates.** *Acta Chemica Scandinavia*, 1972, 26 (5), 2063-2074.
- [57] <http://www.btinternet.com/~martin.chaplin/hycar.html> in 15th June 2011
- [58] MPOB (2003) Malaysian Oil Palm Statistics, 2003, 22, 56. Malaysian Palm Oil Board, Malaysia.
- [59] Killen, B.U., Corrigan, O.I. **Factors influencing drug release from stearic acid based compacts.** *International Journal of Pharmaceutics*, 2001, 228 (1-2), 189-198.
- [60] Heryanto, R., Hasan, M., Abdullah, E.C., Kumoro, A.C. **Solubility of stearic acid in various organic solvents and its prediction using non-ideal solution models.** *Science Asia*, 2007, 33 (4), 469-472.
- [61] Barton, A.F.M. **Solubility parameters.** *Chemical Reviews*, 1975, 75 (6), 731-753.
- [62] Kulicke, W.-M., Kull, A.H., Kull, W., Thielking, H., Engelhardt, J., Pannek, J.-B. **Characterization of aqueous carboxymethylcellulose solutions in terms of their molecular structure and its influence on rheological behaviour.** *Polymer*, 1996, 37 (13), 2723-2731.

- [63] Zhang, L.-N., Zhang, M., Chen, J.-H., Zeng, F.-B. **Solution properties of antitumor carboxymethylated derivatives of α -(1 \rightarrow 3)-D-glucan from *Ganoderma lucidum*.** Chinese Journal of Polymer Science (English Edition), 2001, 19 (3), 283-289.
- [64] Kulicke, W.-M., Reinhardt, U., Fuller, G.G., Arendt, O. **Characterization of the flow properties of sodium carboxymethylcellulose via mechanical and optical techniques.** Rheological Acta, 1999, 38 (1), 26-33.
- [65] Sabitjan Ya. Inagamov, Gafur I. Mukhamedov. **Structure and physical-mechanical properties of interpolymeric complexes based on sodium carboxymethylcellulose.** Journal of Applied Polymer Science, 2011, 122(3), 1749-1757.
- [66] Szcześ, A. **Influence of SDS on particle size and adhesion of precipitating calcium carbonate.** Colloids and Surfaces A: Physicochemical and Engineering Aspects, 2008, 320 (1-3), 98-103.
- [67] Orme, C.A., Noy, A., Wierzbicki, A., McBride, M.T., Grantham, M., Teng, H.H., Dove, P.M., Deyoreo, J.J. **Formation of chiral morphologies through selective binding of amino acids to calcite surface steps.** Nature, 2001, 411 (6839), 775-779.
- [68] Dalas, E., Klepetsanis, P.G., Koutsoukos, P.G. **Calcium carbonate deposition on cellulose.** Journal of Colloid and Interface Science, 2000, 224 (1), 56-62
- [69] Wang, L., Meng, Z., Yu, Y., Meng, Q., Chen, D. **Synthesis of hybrid linear-dendritic block copolymers with carboxylic functional groups for the biomimetic mineralization of calcium carbonate.** Polymer, 2008, 49 (5), 1199-1210.
- [70] Sondi, I., Škapin, S.D., Salopek-Sondi, B. **Biomimetic precipitation of nanostructured colloidal calcite particles by enzyme-catalyzed reaction in the presence of magnesium ions.** Crystal Growth and Design 8 (2), 435-441.
- [71] Oaki, Y., Imai, H. **The hierarchical architecture of nacre and its mimetic material.** Angewandte Chemie - International Edition, 2005 44 (40), 6571-6575.
- [72] Wang, R.Z., Suo, Z., Evans, A.G., Yao, N., Aksay, I.A. **Deformation mechanisms in nacre.** Journal of Materials Research, 2001 16 (9), 2485-2493.
- [73] Aksay, I.A., Trau, M., Manne, S., Honma, I., Yao, N., Zhou, L., Fenter, P., (...), Gruner, S.M. **Biomimetic pathways for assembling inorganic thin films.** Science, 1996, 273 (5277), 892-898.
- [74] Aizenberg, J. **New nanofabrication strategies: Inspired by biomineralization.** MRS Bulletin, 2011, 35 (4), 323-330.
- [75] Falini, G., Fermani, S., Gazzano, M., Ripamonti, A. **Biomimetic crystallization of calcium carbonate polymorphs by means of collagenous matrices.** Chemistry - A European Journal, 1997, 3 (11), 1807-1814.